RIVERINE AND SEDIMENT PROCESSES IN THE YANGTZE RIVER ESTUARY-MODELING AND VALIDATION

A Thesis

by

CHI LU

Submitted to the Office of Graduate and Professional Studies of
Texas A&M University
in partial fulfillment of the requirements for the degree of

MASTER OF SCIENCE

Chair of Committee,	James M. Kaihatu
Committee Members,	Hamn-Ching Chen
	Robert Hetland
Head of Department,	Sharath Girimaji

December 2016

Major Subject: Ocean Engineering

ABSTRACT

The sediment flux from the Yangtze River into the estuary area decreased during the past three decades and the operation of the world's largest hydropower project, Three Gorges Dam (TGD), made this situation much more severe. In the delta area, another project called Deep Water Navigation Channel was also completed in 2011. To investigate hydrodynamic and sediment transport processes, and document the impact of the Three Gorges Dam and the Deep Water Navigation Channel on estuarine hydrodynamics and morphology changes, we used the Delft3D flow module. Several islands and shoals in the Yangtze Estuary region were located near Deep Water Navigation Channel (DNC) and their morphological changes were tightly coupled with the sediment flux from the Yangtze River. The evolution of the geometry and elevation of these islands and shoals in the river are used as metrics to gauge the effect of the manmade changes to the Yangtze River Delta, as well as predict future changes and effects. Parameters such as cumulative erosion/sedimentation, 1-D transect profile, current and sediment mass per area are analyzed. Results show that Jetties built in the DNC project will slow down the current velocity inside the deep navigation channel and will induce a new pattern of local sediment transport, causing more sediment deposition inside the channel. The reduced sediment flux caused by the completion of TGD will decrease the available sediment mass on the bed of the Yangtze River Estuary and lead to coastline erosion of the islands and shoals in the Yangtze River Estuary in the future.

ACKNOWLEDGMENTS

I would like to thank my advisor Dr. James Kaihatu who gave me the opportunity to study and research under his supervise. During my MS research, Dr. Kaiahtu provided me enough space to think and conduct my research independently and whenever I came out with problems, he would offer me vert insightful suggestions. I feel very happy and fortunate to be his student. I also want to thank my two committee members Dr. Chen and Dr. Hetland. Dr. Chen's CFD class helped me a lot to understand the gird and equation calculation in numerical modeling. Dr. Hetland offered me kind help on my model calibration process. My thanks also go to Wonhyun Lee who gave me a lot of help in building the grid and wind data processing and Ying-po Liao who helped me use Latex and Lyx. Last but not least, I would like to thank my family, my wife, my son and my parents. Without their support and encouragement, I cannot go to this level.

TABLE OF CONTENTS

LIST OF FIGURES

Page

LIST OF TABLES

Page

1 INTRODUCTION

River deltas are landforms formed by sediment deposition when rivers flow into a lake, sea or ocean. River deltas are inhabited by over 60 % of the world population, and are, consequently, of paramount agricultural and economical importance. Delta morphology is mainly controlled by several boundary conditions and forcing types such as water discharge, sediment supply from a river's suspended load and bedload, waves, tides and longshore current (Wright and Coleman, 1973; Syvitski and Saito, 2007). With the interaction between these force factors, hydrodynamic and morphodynamic processes in a delta and its estuary are very complex.

Qualitative studies often investigate deltas' surface features and describe the related environmental factors in a qualitative approach(Galloway, 1975). With the development of numerical modeling, an additional, effective method to better understand the hydrodynamic and morphodynamic processes in estuarine areas is available. These numerical models include POM (Blumberg and Mellor, 2013) and FVCOM (Chen et al., 2003) for estuarine circulation; SWAN (Booij et al., 2001) for nearshore wave transformation; ROMS (Shchepetkin and McWilliams, 2005), MIKE by DHI Water and Environment, and Delft3D by WL|Delft Hydraulics, for comprehensive simulations.

The Delft3D model is capable of simulating flow, sediment transport, wave, water quality, morphological development and ecological process in coastal, river and estuarine areas and has been widely used to model these processes in many areas in the world. Lesser et al. (2004) coupled the hydrodynamics with sediment transport and bathymetric evolution together in Delft3D to examine nearshore morphodynamics. Bouma et al. (2007) used Delft3D Flow model to investigate spatial sedimentation and erosion patterns due to biophysical interactions in Southwest Netherlands. van Dongeren et al. (2008) combined video-derived observations and Delft3D model to estimate nearshore bathymetry changes in sites at Duck, NC, USA and Egmond, The Netherlands. Edmonds and Slingerland (2010) conducted several experimental runs with Delft3D to identify roles of sediment properties and vegetation as controls of delta morphodynamics. Xie et al. (2009) used cohesive sediment transport module of Delft3D to analyze the formation and evolution of the tidal channel system in Hagzhou Bay, China. In this study, Delft3D is also utilized to investigate morphodynamics in Yangtze River Estuary, and more details will be presented in the Data and Method section.

1.1 Study area

The Yangtze River originates from the Qinghai-Tibetan Plateau, flowing into East China Sea. It is 6300 km long and its drainage basin area is 1.8×10^6 km^2(Fig.1). It is the largest river in Asia in terms of water discharge (Milliman and Meade, 1983), delivering about 900 km^3/yr freshwater into Yellow Sea and East China Sea (Milliman and Farnsworth., 2010). Sediment discharge of Yangtze River is also very large. The long-term average sediment loads at Datong station, the tidal limit of Yangtze River (Fig.1), are 433 Mt/yr (Xu and Milliman, 2009). The modern Yangtze River discharges most of its annual sediment load between June and September (Chen and Stanley, 1993). Although some sediment is deposited in the midstream of Yangtze River (Yang et al., 2007), about 50 % of the sediment is deposited in the Yangtze River Estuary (Yang et al., 2008) and the remaining sediment is discharged into the East China Sea.

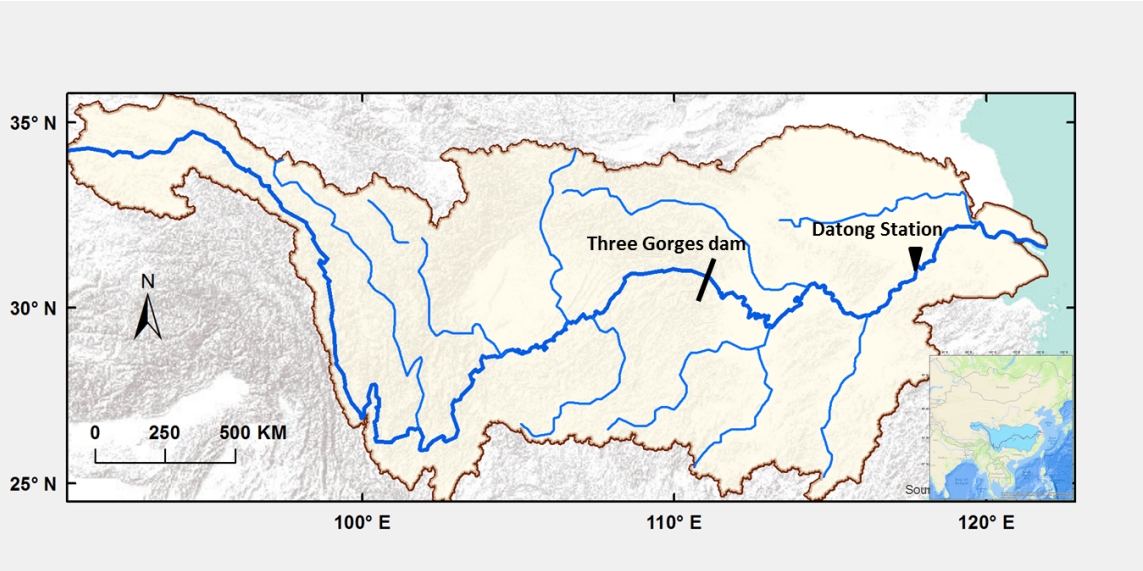

Figure 1: Yangtze River Basin

Yangtze River Estuary is located downstream from Datong Station (Fig.2). The tide in Yangtze River Estuary is mainly semi-diurnal tide, the mean tide range and the spring tide are about 2.66m and 5m respectively and the mean flow velocity is about 1m/s (Gao et al., 2011; Jiang et al., 2012). The mean and maximum wave heights are 1.0 m and 6.2 m respectively (Fan et al., 2006). Although Yangtze River's water flux can reach as high as 900 km^3/yr, the annual tidal prism from the sea into the estuary is even larger with a total volume of 8400 km^3, which is an order of magnitude greater than the annual river flux (Chen et al.,

1988, 2001). Thus the sediment transport in Yangtze River Estuary is strongly influenced by semi-diurnal tidal cycles.

Yangtze River Estuary is a multichannel estuary with several bifurcations separated by islands and shoals (Song et al., 2013). These islands and shoals at the river mouth were formed by sediment accumulation from Yangtze River Basin (Yang et al., 2000), and the present distribution of the islands and shoals in Yangtze River Estuary was caused by a flood event in 1954 which was the largest documented flood in Yangtze River Basin (Shen et al., 2013). Among these islands and shoals, Chongming Island, Hengsha Island, and Changxing Island are inhabited and Jiuduanshasha Shoal is a younger, uninhabited shoal. Jiuduanshasha shoal is a national nature reserve wetland. On the shoal, there is marsh vegetation such as *Scirpus mariquete* and *Scirpus triquier* and the boundary between bare flats and marsh is located about 50cm above mean sea level (Yang et al., 2000) .

Recently, human impacts have played an increasingly important part in Yangtze River Basin and Estuary, including dam construction in the river basin and coastal engineering projects in the estuary. These human impacts will definitely influence the flow, sediment transport and circulation pattern in Yangze River Estuary; one of this research's goal is to identify these influences.

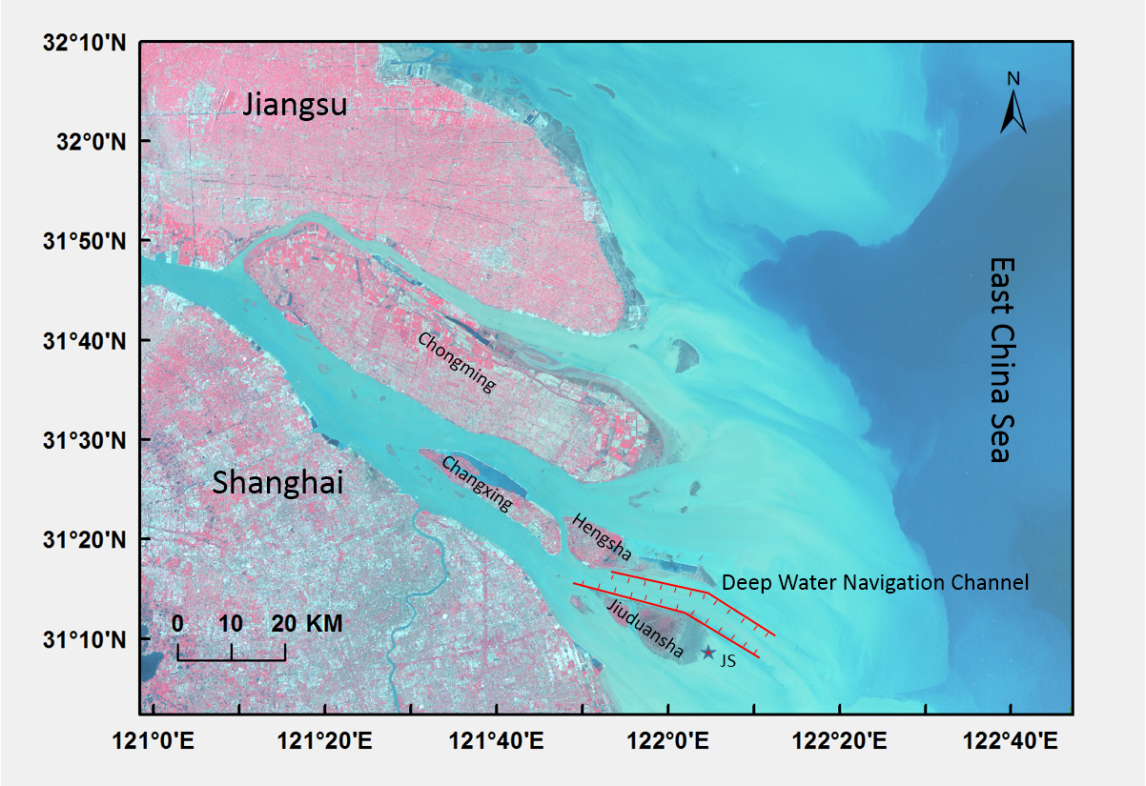

Figure 2: Yangtze River Estuary

1.2 Human impact

1.2.1 Dam construction

A series of dams were built in the Yangtze River basin (Yang et al., 2011), including the world's present largest dam Three Gorges Dam (TGD), which was completed in 2003 (Fig.1). Data from Datong station shows that the sediment load of Yangtze River has been decreasing in the past several decades (Fig.3). Dam construction is the main reason for the decreased sediment load recently (Yang et al. 2011). Dam construction in the Yangtze River Basin started in the 1950s, causing sediment trapping in the reservoirs and reducing the sediment load downstream. From Fig.3, it can be seen that there are three time periods when sediment loads experienced a decreasing trend. The first reduction period was 1969-1985 which was a result of the activation of the Danjiangkou Reservoir on the Hangjiang tributary of Yangtze River. The second period was 1986-2002 which was caused mainly by a large number of dams and reservoirs completed during this time period, as well as the Changzhi Water and Soil Conservation Project on the Jialingjiang tributary in the upper reaches (Yang et al., 2006). After 2002, the decrease in sediment load accelerated after the

commissioning of the TGD. During its first stage of TGD's deployment (2003–2005), 64 % of sediment entering the Three Gorges Reservoir was trapped (Yang et al., 2007). As a result, the sediment loads at Datong station reduced from about 400Mt/yr pre-TGD to less than 200Mt/yr post-TGD (Fig.3).

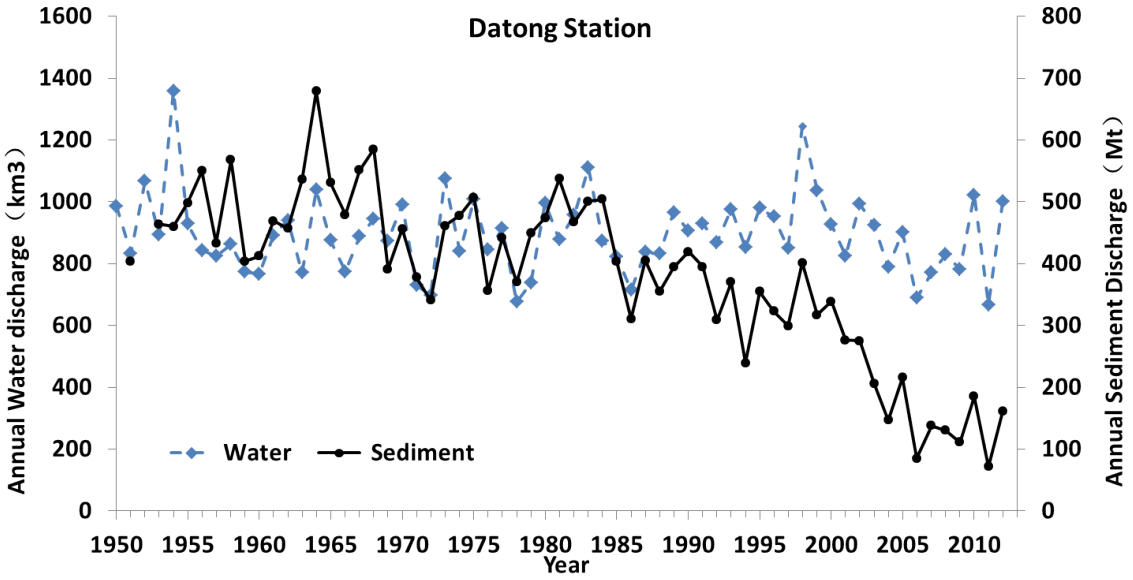

Figure 3: Annual water and sediment discharge in Datong station

1.2.2 Deep water navigation channel

In addition to the effects of the dam construction, coastal engineering construction is another factor influencing the sediment transport and morphodynamic changes of Yangtze River Delta. The largest of these projects is one called the Deepwater Navigation Channel (DNC).. This project started in 1998 and was completed in 2011, creating a 92 km long channel with a water depth of 12.5 m below the mean lowest low water(MLLW). The length of the two dikes is 48.1 km to the north of Jiuduansha Shoal and 49.2 km to the south of Hengsha Island respectively, and total length of the 19 groins is 30 km (Fig.2). The original purpose to build dikes and groins was to increase current speed and decrease sediment deposition in the channel (Song et al., 2013). However, since the completion of DNC, the annual amount of dredged sediment deposit was much larger than the original estimate and there has been a severe silting issue(Liu et al., 2011).

1.3 Research objective

Under the circumstance of the two major human interference discussed above, this study will focus on Jiuduansha shoal's morphological evolution using the Delft3D flow module. Specific goals of this research are:

1. document impacts of TGD and DNC on estuarine hydrodynamics and morphology changes
2. predict the future state of these islands and shoals, especailly national nature reserve wetland Jiuduansha shoal

2 DATA AND METHOD

2.1 Model description

2.1.1 Hydrodynamic module

Delft3D-FLOW is a 2D or 3D hydrodynamic and sediment transport simulation program capable of calculating non-steady flow and transport phenomena that result from forces such as tidal and meteorological forces on a rectilinear or a curvilinear, boundary fitted grid. In this study, the depth averaged 2D flow option in Delft3D is used by assuming the fluid is vertically homogeneous, thus solving the unsteady shallow water equations. The system of equations consists of the horizontal equations of motion, the continuity equation, and the transport equations for conservative constituents. The equations are formulated in both orthogonal curvilinear coordinates and spherical coordinates, each of which is an option in the model. In curvilinear coordinates, the free surface level and bathymetry are related to a flat horizontal plane of reference, whereas in spherical coordinates the reference plane follows the Earth's curvature. In this study, spherical coordinates are used. (Delft3D-FLOW-Manual, 2014)

- Cartesian coordinates (ξ, η)
- Spherical co-ordinates (λ, Φ)

Spherical co-ordinates are a special case of orthogonal curvilinear co-ordinates with:

$$\begin{aligned} \xi &= \lambda, \\ \eta &= \Phi, \\ \sqrt{G_{\xi\xi}} &= R\cos\Phi, \\ \sqrt{G_{\eta\eta}} &= R, \end{aligned} \tag{1}$$

where λ is the longitude, Φ is the latitude, R is the radius of the Earth (6378.137 km, WGS84) and $\sqrt{G_{\xi\xi}}, \sqrt{G_{\eta\eta}}$are coefficients used to transform curvilinear to rectangular co-ordinates.

The flow is forced by tide at the open boundaries, wind stress at the free surface, pressure gradients due to free surface gradients (barotropic) or density gradients (baroclinic). Source and sink terms are included in the equations to model the discharge and withdrawal of water. The governing equations such as continuity equation and momentum equations are listed below:

The continuity equation for incompressible fluids solved by the model is:

$$\frac{\partial\zeta}{\partial t} + \frac{1}{\sqrt{G_{\xi\xi}}\sqrt{G_{\eta\eta}}}\frac{\partial((d+\zeta)U\sqrt{G_{\eta\eta}}}{\partial\xi} + \frac{1}{\sqrt{G_{\xi\xi}}\sqrt{G_{\eta\eta}}}\frac{\partial((d+\zeta)V\sqrt{G_{\xi\xi}}}{\partial\eta} = (d+\zeta)Q \tag{2}$$

where ζ is water level, d is water depth U and V are depth averaged velocities and Q representing the contributions per unit area due to the discharge or withdrawal of water.

The momentum equations solved by the model are:

For the ξ-direction:

$$\frac{\partial u}{\partial t} + \frac{u}{\sqrt{G_{\xi\xi}}}\frac{\partial u}{\partial\xi} + \frac{v}{\sqrt{G_{\eta\eta}}}\frac{\partial u}{\partial\eta} + \frac{w}{d+\zeta}\frac{\partial u}{\partial\sigma} - \frac{v^2}{\sqrt{G_{\xi\xi}}\sqrt{G_{\eta\eta}}}\frac{\partial\sqrt{G_{\eta\eta}}}{\partial\xi} + \frac{uv}{\sqrt{G_{\xi\xi}}\sqrt{G_{\eta\eta}}}\frac{\partial\sqrt{G_{\xi\xi}}}{\partial\eta} - fv = -\frac{1}{\rho_0\sqrt{G_{\xi\xi}}}P_\xi + F_\xi + \frac{1}{(d+\zeta)^2}\frac{\partial}{\partial\sigma}\left(\nu\frac{\partial u}{\partial\sigma}\right) + M_\xi, \tag{3}$$

and for the η-direction:

$$\frac{\partial v}{\partial t}+\frac{u}{\sqrt{G_{\xi\xi}}}\frac{\partial v}{\partial \xi}+\frac{v}{\sqrt{G_{\eta\eta}}}\frac{\partial v}{\partial \eta}+\frac{w}{d+\zeta}\frac{\partial v}{\partial \sigma}+\frac{uv}{\sqrt{G_{\xi\xi}}\sqrt{G_{\eta\eta}}}\frac{\partial \sqrt{G_{\eta\eta}}}{\partial \xi}-$$
$$\frac{u^2}{\sqrt{G_{\xi\xi}}\sqrt{G_{\eta\eta}}}\frac{\partial \sqrt{G_{\xi\xi}}}{\partial \eta}+fu=-\frac{1}{\rho_0\sqrt{G_{\eta\eta}}}P_\eta+F_\eta+\frac{1}{(d+\zeta)^2}\frac{\partial}{\partial \sigma}\left(\nu\frac{\partial v}{\partial \sigma}\right)+M_\eta. \quad (4)$$

where f is Coriolis parameter, ν is the vertical eddy viscosity coefficient, and P_ξ and P_η represent the pressure gradients. The forces F_ξ and F_η represent the imbalance of horizontal Reynold's stresses. The momentum terms M_ξ and M_η represent the contributions due to external sources or sinks of momentum.

2.1.2 Sediment transport module

Both bedload and suspended load transport of non-cohesive sediments and suspended load of cohesive sediments are supported by the sediment transport and morphology module. Inside the module, we can define three sediment fractions mud (cohesive suspended load transport), sand (non-cohesive bedload and suspended load transport) and bedload (non-cohesive bedload only or total load transport). For bedload fraction the suspended load advection-diffusion equation is not solved, which is the only difference from sand fraction. (Delft3D-FLOW-Manual, 2014)

Suspended transport

$$\frac{\partial c^{(l)}}{\partial t}+\frac{\partial uc^{(l)}}{\partial x}+\frac{\partial vc^{(l)}}{\partial y}+\frac{\partial (w-w_s{}^{(l)})c^{(l)}}{\partial z}-$$
$$\frac{\partial}{\partial x}\left(\varepsilon_{s,x}^{(l)}\frac{\partial c^{(l)}}{\partial x}\right)-\frac{\partial}{\partial y}\left(\varepsilon_{s,y}^{(l)}\frac{\partial c^{(l)}}{\partial y}\right)-\frac{\partial}{\partial z}\left(\varepsilon_{s,z}^{(l)}\frac{\partial c^{(l)}}{\partial z}\right) = 0 \quad (5)$$

where:

$c^{(l)}$: mass concentration of sediment fraction (l) (kg/m^3)

u, v and w: low velocity components (m/s)

$\varepsilon_{s,x}{}^{(l)}$, $\varepsilon_{s,y}{}^{(l)}$, $\varepsilon_{s,z}{}^{(l)}$: eddy diffusivities of sediment fraction (l) (m^2/s)

$w_s{}^{(l)}$: sediment settling velocity of sediment fraction (l) (m/s)

2.1.3 Morphology change

The elevation of the bed is updated at each computational time step which guarantees that hydrodynamic flow are always calculated using the most recent bathymetry. At each time-step, the mass change of the bed material as a result of the sediment sink and source terms and transport gradients is calculated. This change

in mass is then translated into a bed level change based on the dry bed densities of the various sediment fractions.

Usually morphological changes take place over much longer time scales than typical flow changes. For instance, tidal flows change significantly in the order of hours, while the morphology of a coastline will often take weeks, months, or years to change accordingly (Delft3D-FLOW-Manual, 2014). In Deflt3D morphology module, one approach to solve this problem is to introduce a "morphological time scale factor" by specifying a value for the variable `MorFac` in the morphology input file.This factor is then implemented by multiplying the erosion and deposition fluxes from the bed to the flow and vice versa by the factor `MorFac`, at each time step. This allows accelerated bed level changes to be incorporated into flow calculations. For example, during a tidal cycle the hydrodynamics is not significantly affected by the bed level changes and the morphological variations are often small. If the morphological factor is set to 10 for instance, the morphological changes will be increased by this factor. From a hydrodynamical perspective this increase in morphological change rate is allowed if the hydrodynamics are not significantly influenced by the morphology change. In that case the morphological development in one tidal cycle can approximately represent the morphological development in 10 tidal cycles. This can reduce the simulation time dramatically. However, it should be noted that some problems may occur such as limited sediment availability due to changing the event order.(Delft3D-FLOW-Manual, 2014)

2.2 Model domain and grid

The model domain is shown in Fig.4. It covers the whole Yangtze Estuary and East China Sea, longitude from 120°E to 123°E and latitude from 30°N to 33°N. Because there is a significant water and sediment exchange between Yangtze River and Hangzhou Bay, Hangzhou Bay is also included in the domain. The upstream boundary of Yangtze River is at Jiangyin which is the upper limit of tidal current (Hu et al., 2009). Three open sea boundaries lie on 123°E, 33°N and 30°N respectively. Two sets of bathymetry data are used in the model. Digitized data from nautical charts are used in shallow water area and for the remainder, GEBCO gridded data are used (`http://www.gebco.net/`). The vertical datum of the two datasets are referred to mean sea level (MSL).

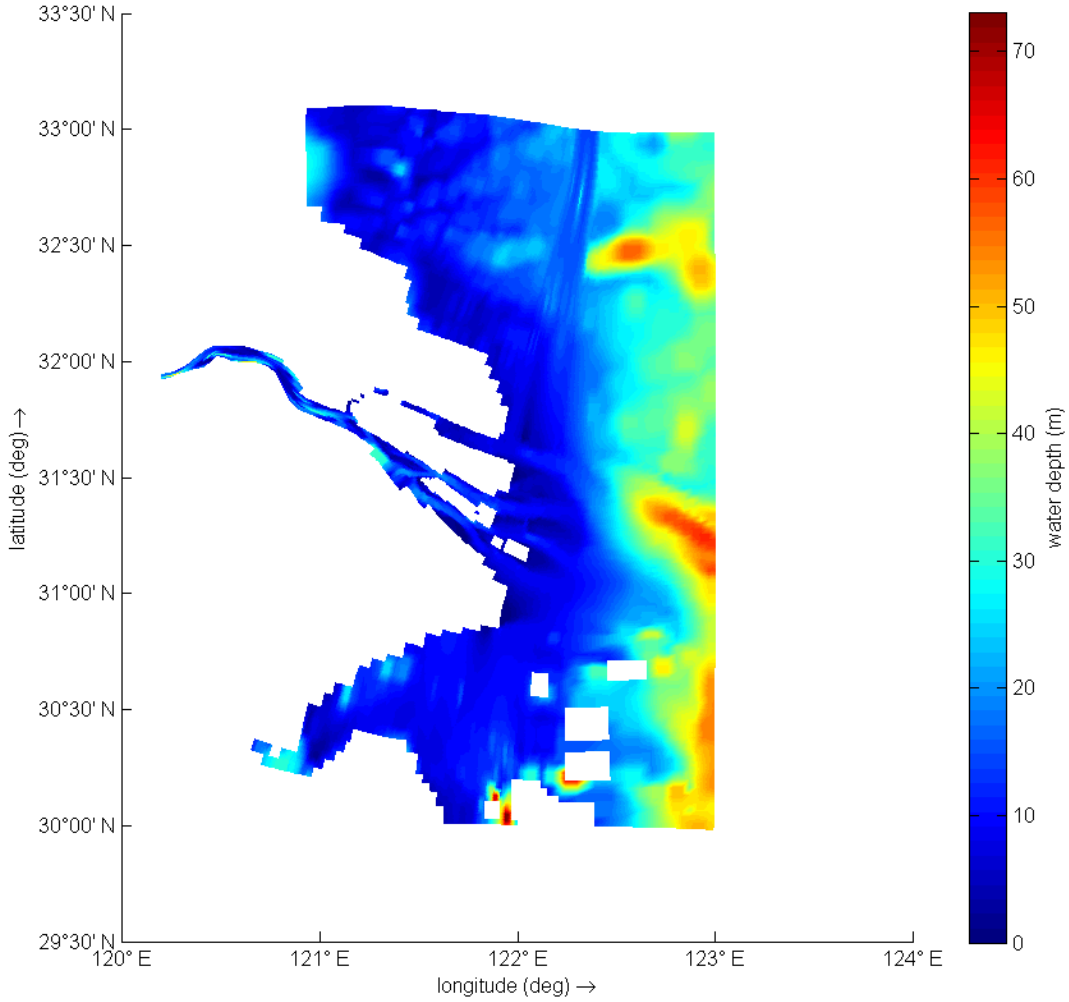

Figure 4: Model domain ad baythymetry

A curvilinear grid (Fig.5) was generated by Delft3D-RGFGRID. The total number of grids is 155×121. Grids with coarser resolution are located in deep offshore area and the grid size is about 4.5 km×4.5 km. In he river mouth region (the area of interest) the grid resolution is higher: about 0.7 km× 0.7 km. Due to the meander property of the river channel, grid lines are fitted along the land boundaries and channels to reduce artificial diffusion as much as possible.

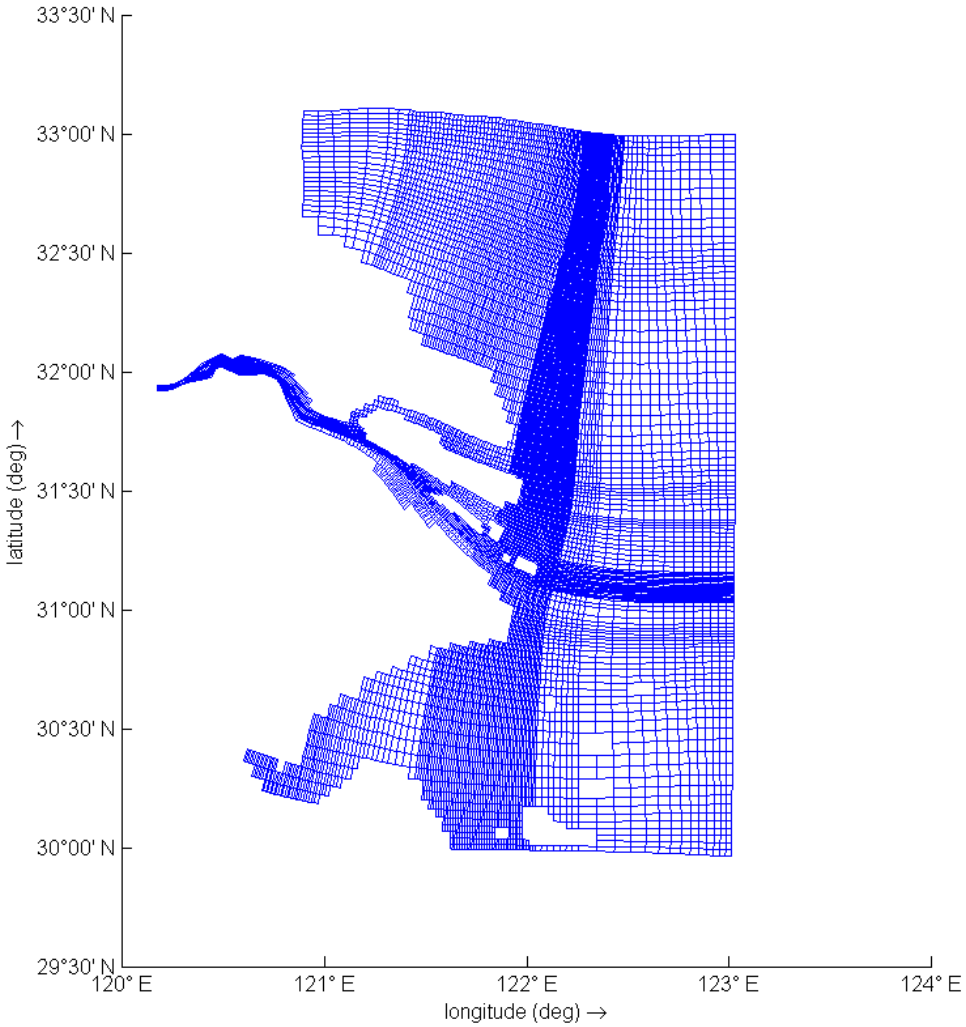

Figure 5: Model grid

2.3 Parameter settings

The major parameters in the model are listed in Table.1. Physical processes including flow, salinity and sediment transport are conducted in the model. According to Hu et al. (2009) and van Maren et al. (2013), five fractions of cohesive sediment including a clay fraction (sediment diameter D_{50}=2 μm), four silt fractions (D_{50}=10, 20, 30 and 40 μm) and one very fine sand fraction (D_{50}=64 μm) are selected in the sediment transport for Yangtze River Estuary. The sediment flocculation is considered for cohesive sediment in the settling velocity (Table.2). Wind process is taken into account, and wind data are downloaded

from National Centers for Environmental Prediction (NCEP) (http://rda.ucar.edu/datasets/ds093.1/). The wind data are NCEP six-hourly reanalysis products with a spatial resolution 0.5°×0.5° covering the whole model domain, and all wind data are converted to 10m elevation using wind profile power law. Wave impact is not considered because the wave height in this area is usually small under normal weather conditions (Hu et al., 2009).

Table 1: Model major parameters

Parameter	value
Time step	0.5 min
Specific density for cohesive and non-cohesive sediment	2650 kg/m^3
Dry bed density for cohesive sediment	500 kg/m^3
Dry bed density for non-cohesive sediment	1600 kg/m^3
Critical erosion stress	0.1 N/m^2
Critical deposition stress	0.05 N/m^2
Erosion rate	2.5×10^{-6} kg/m^2/s

Table 2: Sediment parameters

Sediment diameter D_{50}	Settling velocity in fresh water(mm/s)	Settling velocity in salt water(mm/s)
2 μm	0.25	0.5
10 μm	0.5	1
20 μm	1.5	0.75
30 μm	2	1
40 μm	2.5	1.25

2.4 Initial and boundary conditions

A cold start is used for initial condition and uniform values are assigned for parameters such as sediment concentration, water level, and salinity. At three offshore open boundaries, water level boundary forced by astronomical tide is adopted. The tidal constituents for astronomical tide are extracted from OSU Tide-OTIS Regional Tide Solutions (http://volkov.oce.orst.edu/tides/YS.html), including four semidiurnal constituents (M2, S2, N2, and K2); four diurnal constituents (K1, O1, P1, and Q1); and one shallow water constituents (M4). At upstream boundary of Yangtze River and Hangzhou Bay, yearly averaged water discharges are input to simulate river flow. More details will be discussed in "Model set up" section, to follow.

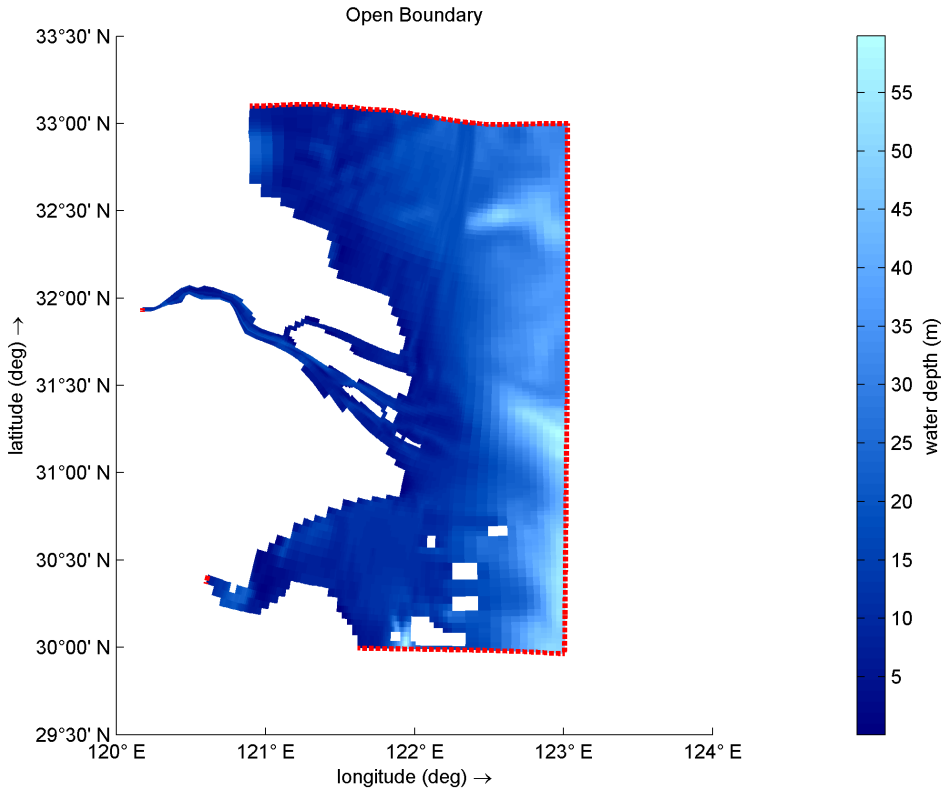

Figure 6: Boundary conditions

3 MODEL SET UP

3.1 Model spin up

As mentioned in section 2.4, the model uses uniform values to spin up before outputting results of morphology changes. Time period for spinning up is from 01/01/1996 to 08/15/1996 and during this period parameters such as sediment concentration, water level, and salinity will run to reach an equilibrium state while the bathymetry is not updated during the flow simulation. Then, the restart file generated from this spin up simulation will be used for the following case's initial condition.

3.2 Model calibration

Water level from 09/01/1996 to 09/30/1996 at JS station (shown in Fig.2) is used to calibrate the model. The calibration result is shown in Fig.7 where the observation data are from Hu et al. (2009). The magnitude and phase are fitted overall, except some phase mismatch during spring tide which may due to the accuracy of the bathymetry and tide constituent data.

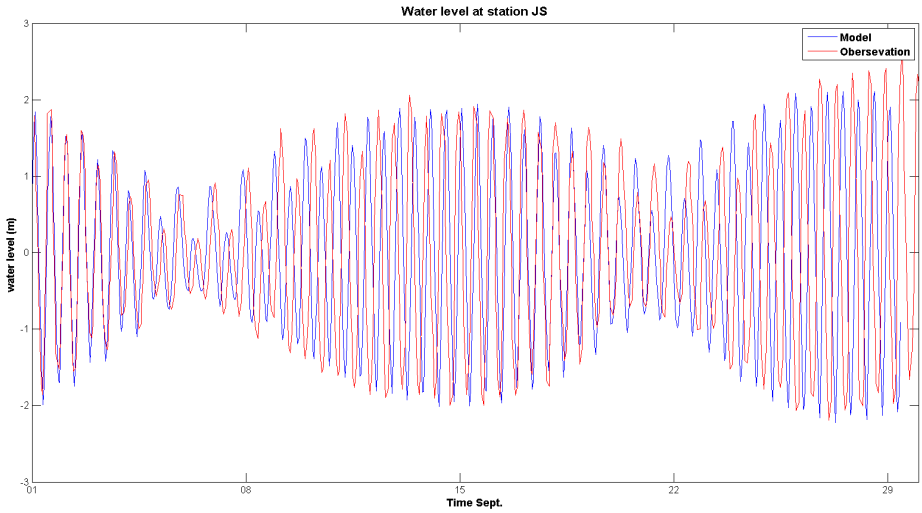

Figure 7: Water level calibration

3.3 Running cases

Based on the research objective, two main factors are considered when setting up the cases. One is the sediment flux from Yangtze River with and without the effect of the TGD and the other is the configuration in Yangtze River Estuary with and without the effects of the DNC. In order to analyze these two factors,

cases are prepared to perform the simulation Table.3.

In Table.3, the `Mor` time means overall model time (morphology factor times simulation time), accounting for a morphology factor of 10; "Y" stands for "yes" ; "N" stands for "no"; and "P" denotes the future prediction with the sediment flux of 75 Mt/yr. Case p11 are used for spinning up and results in case p21 start to output for verification. Case p3, case p4, case p5 and their subsets are used for analyzing the effects of DNC and TGD and their detailed information is listed below.

Case p3: short term simulation (6 years) with jetties built in DNC project

- p31: subsets of p3 with sediment flux 300 Mt/yr before TGD was completed
- p32: subsets of p3 with sediment flux 150 Mt/yr after TGD was completed
- p33: subsets of p3 with sediment flux 75 Mt/yr for future prediction

Case p4: short term simulation (6 years) without jetties

- p41: subsets of p3 with sediment flux 300 Mt/yr before TGD was completed
- p42: subsets of p3 with sediment flux 150 Mt/yr after TGD was completed
- p43: subsets of p3 with sediment flux 75 Mt/yr for future prediction

Case p5: long term simulation (18 years) with jetties built in DNC project

- p51: subsets of p3 with sediment flux 300 Mt/yr before TGD was completed
- p52: subsets of p3 with sediment flux 150 Mt/yr after TGD was completed
- p53: subsets of p3 with sediment flux 75 Mt/yr for future prediction

Table 3: Model cases

Case	Restart File	Mor Time	DNC	TGD	Sediment Flux
p11	spin up	19960815-19980101	N	N	300 Mt/yr
p21	p11	19980101-20040101	Y	N	300 Mt/yr
p3					
p31	p21	20040101-20100101	Y	N	300 Mt/yr
p32	p21	-	Y	Y	150 Mt/yr
p33	p21	-	Y	P	75 Mt/yr
p4					
p41	p21	20040101-20100101	N	N	300 Mt/yr
p42	p21	-	N	Y	150 Mt/yr
p43	p21	-	N	P	75 Mt/yr
p5					
p51	p21	20040101-20220101	Y	N	300 Mt/yr
p52	p21	-	Y	Y	150 Mt/yr
p53	p21	-	Y	P	75 Mt/yr

According to the sediment flux data in Fig.3, three values of annual sediment flux are selected for the cases investigating the TGD's effect. In the simulation, sediment flux of 300 Mt/yr represents the level before TGD was built. Sediment flux of 150 Mt/yr represents the level nowadays after TGD was built. And Sediment flux of 75Mt/yr represents the future level due to the effect of TGD.

The jetties and groins for the deep waterway project (Fig.8) are represented in the model as Current Deflection Walls (CDW) as shown in Fig.9, which allow the water flow over when the water level is sufficiently high.

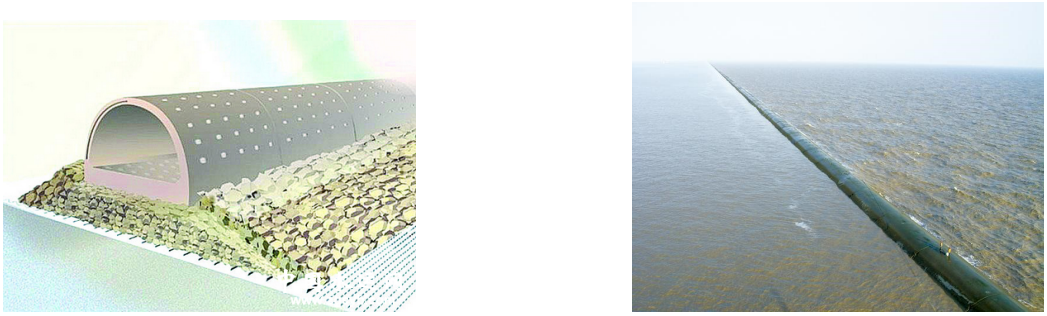

Figure 8: Jetty structure (left) and top view (right) (http://www.cjkhd.com/)

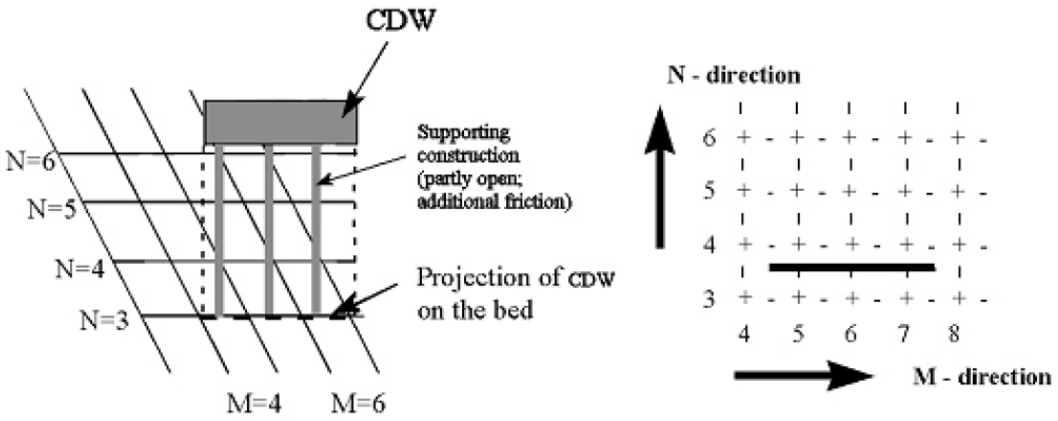

Figure 9: Example of CDW in perspective view (left) and top view (right) from Delft3D-FLOW-Manual (2014)

4 RESULTS

4.1 TGD effect

To analyze the impact of TGD on Yangtze Estuary's morphology, results from cases p31, p32 and p33 (p3) with the jetties and from cases p41, p42 and p43 (p4) without the jetties are used. As shown in Table3, among all these cases, p31 and p41 are cases with 300 Mt/yr sediment flux, p32 and p42 are cases with 150 Mt/yr sediment flux, and p33 and p43 are cases with 75 Mt/yr sediment flux.

4.1.1 Cumulative erosion/sedimentation map

The cumulative erosion/sedimentation module calculates the cumulative value of erosion and deposition during the simulation time period, which is an effective method for uncovering the cumulative morphological changes. Fig.10 shows the cumulative erosion/sedimentation results for the cases listed above.

The left panel in each figure are results for cases p31, p32 and p33. As shown in the contour maps, distribution of erosion or sedimentation seems identical among p31, p32 and p33. The only difference is the amount of erosion or sedimentation in these cases. With the reduction of sediment flux upstream from p31 to p33, the estuary area receives less sediment, and the eroded places undergo additional erosion while the deposited places experience less sedimentation. More results about the erosion or deposition amount will be discussed in section 4.1.2. The right panel in each figure are results for cases p41, p42 and p43. Similar to the left panel, distribution of erosion or sedimentation also seems identical among p41 , p42 and p43 and the only difference is their erosion or deposition quantity. The differences between left and right panel will be discussed in section 4.2.

In addition to the comparison in the DNC region, results north of the DNC (box3 and box4 in Fig.12) are shown in Fig.11a. In the region of box3, distribution of erosion or sedimentation is not significantly affected by the change of the sediment flux just like that in the DNC region. However, in the region of box4, most parts in Fig.11a(right panel) are in the state of deposition, but this scenario changes to much less deposition in Fig.11b(right panel), and dominated by erosion in Fig.11c(right panel). The jetty will accelerate the erosion process (left panel) and more details will be discussed in section 4.2.

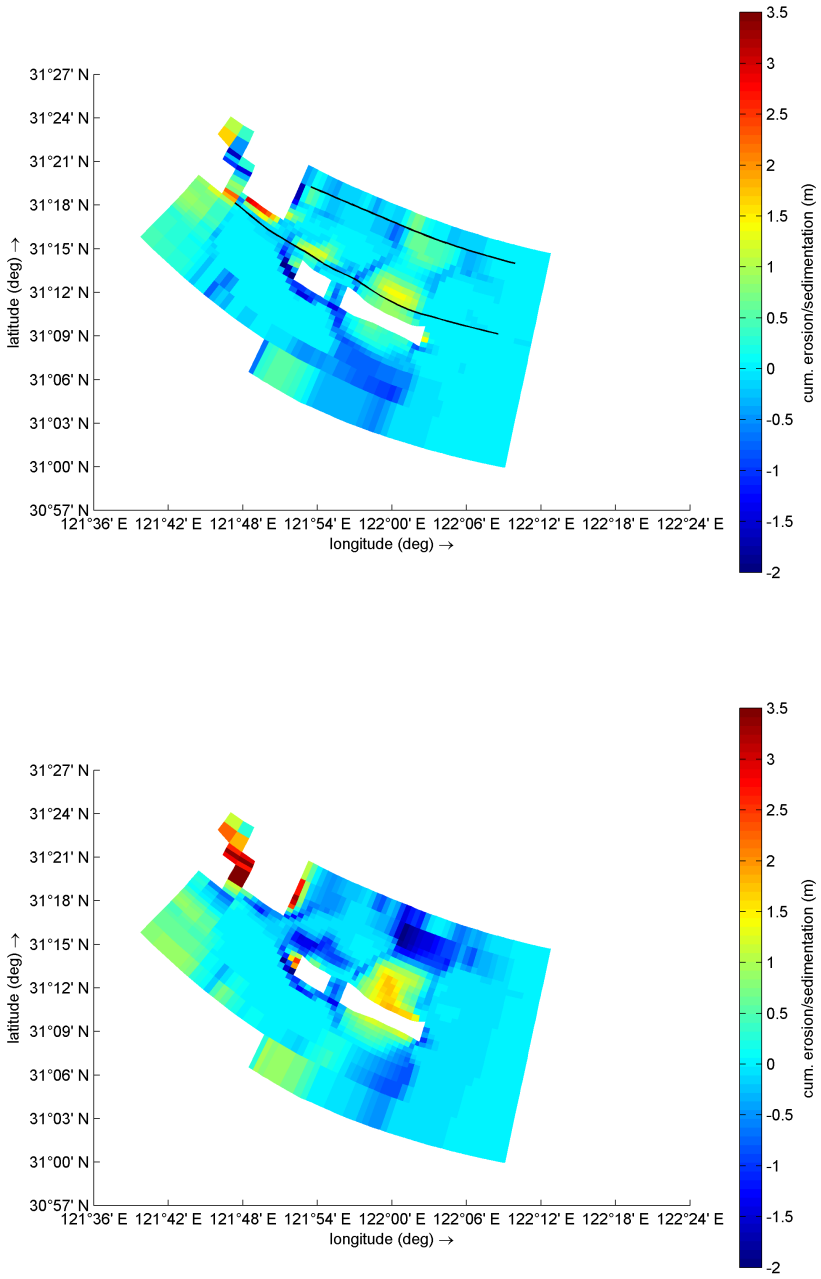

(a) p31(top) and p41(bottom)

Figure 10: Cumulative erosion/sedimentation map in DNC

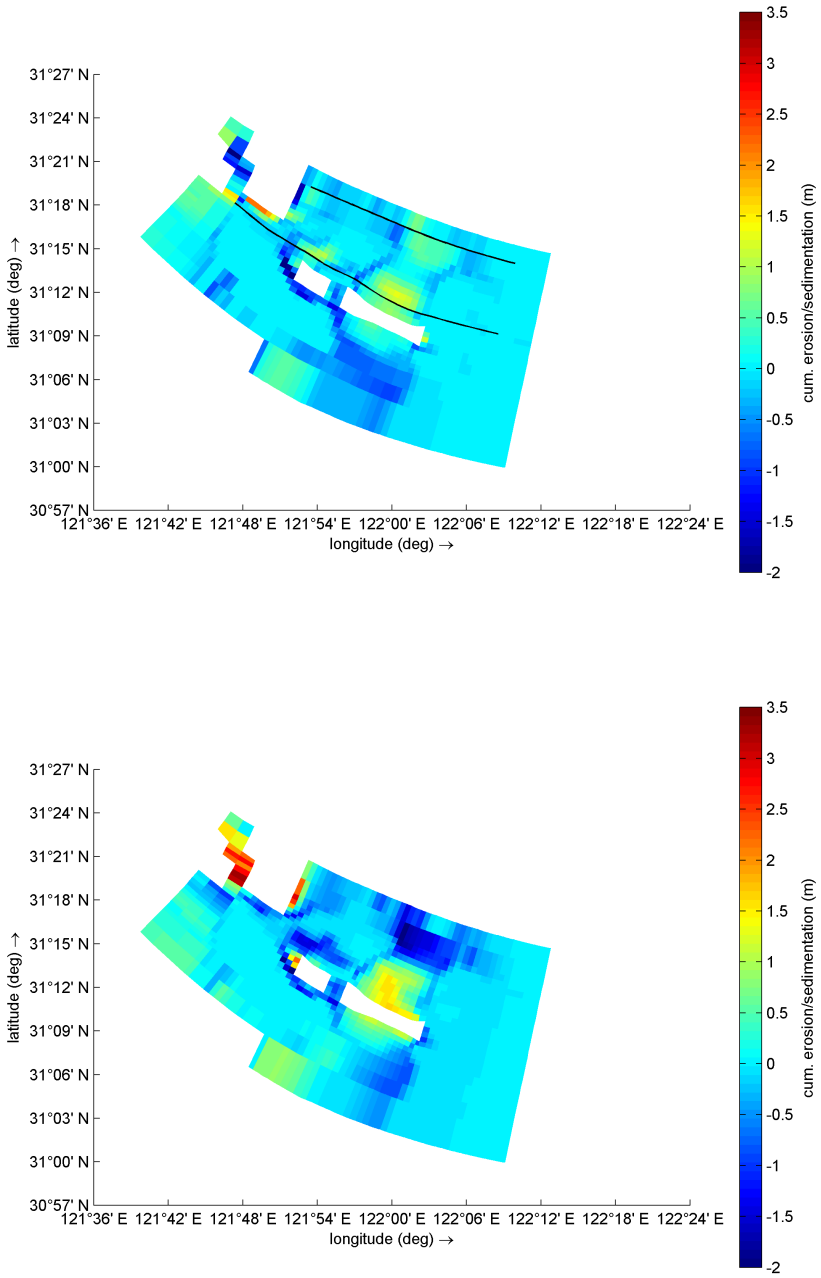

(b) p32(top) and p42(bottom)

Figure 10: Cumulative erosion/sedimentation map in DNC

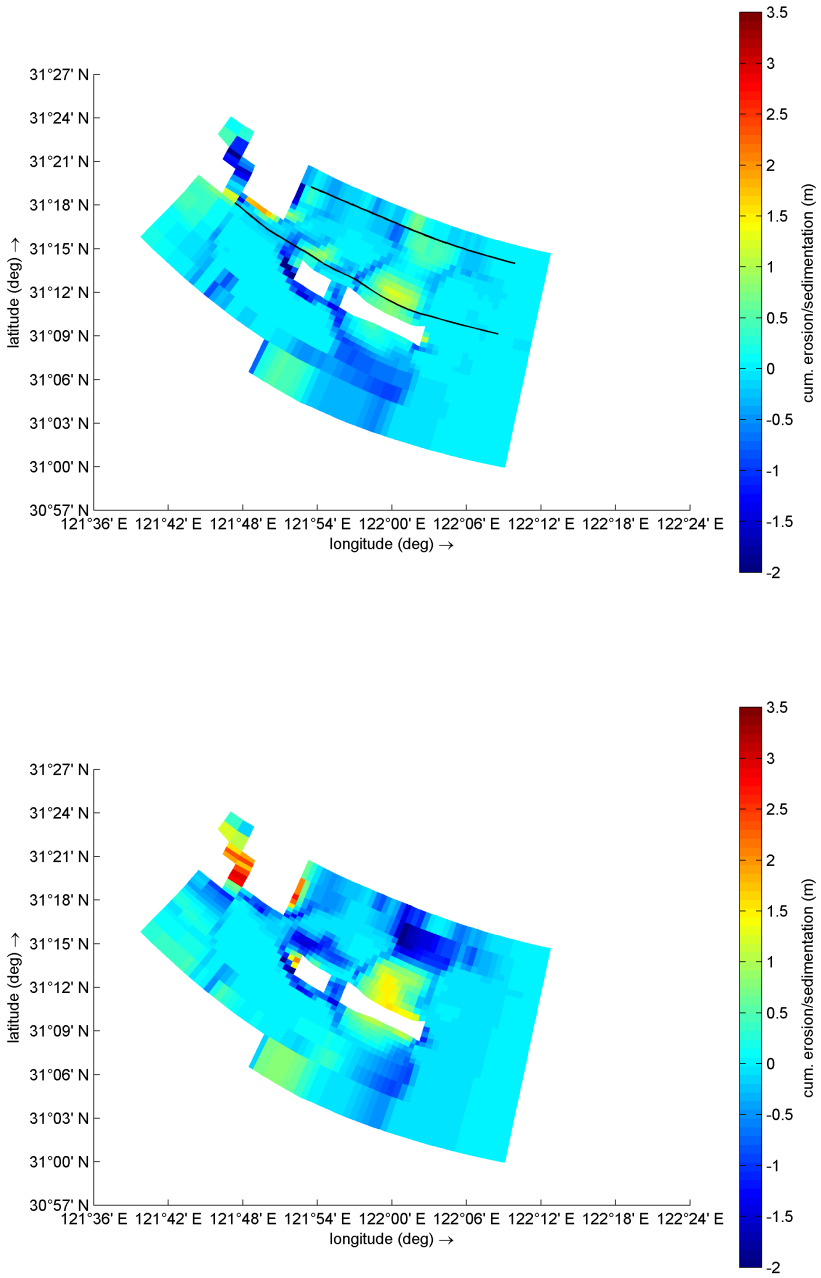

(c) p33(left) and p43(right)

Figure 10: Cumulative erosion/sedimentation map in DNC

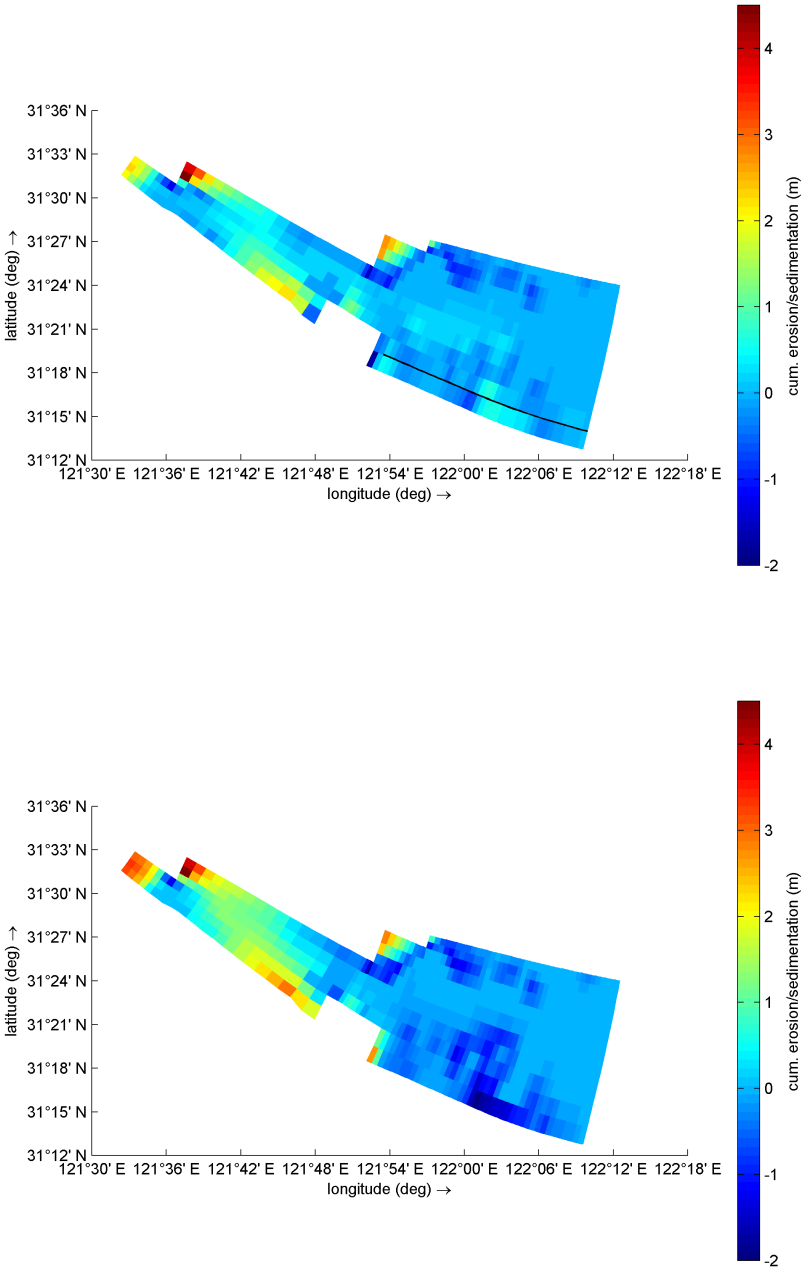

(a) p31(top) and p41(bottom)

Figure 11: Cumulative erosion/sedimentation map north to DNC

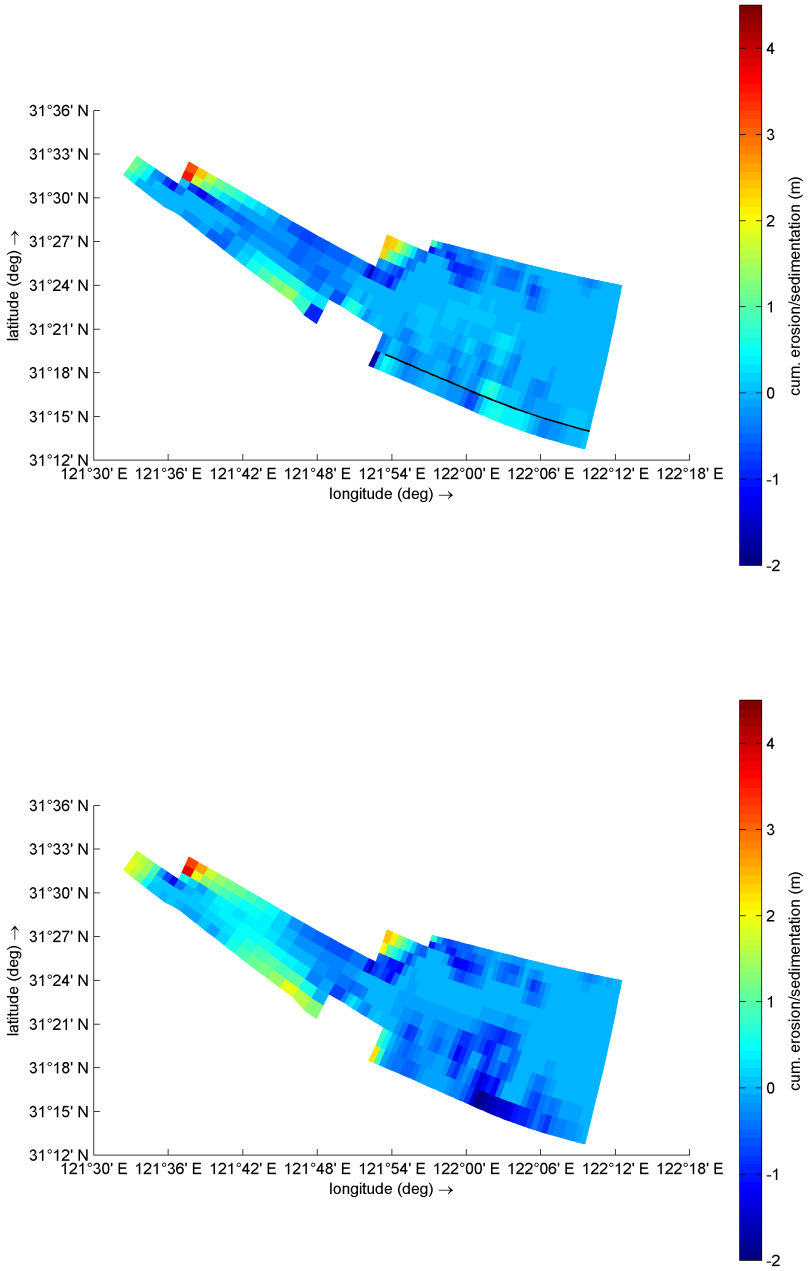

(b) p32(top) and p42(bottom)

Figure 11: Cumulative erosion/sedimentation map north to DNC

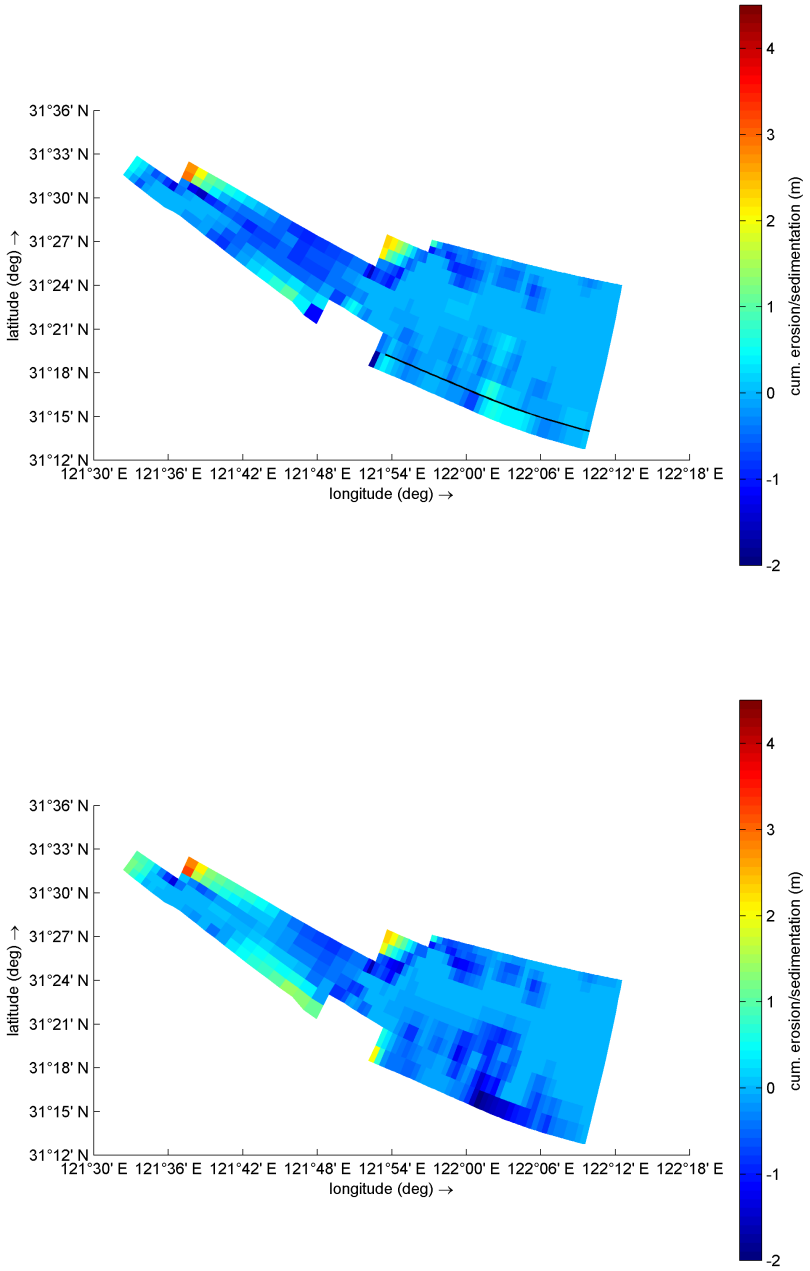

(c) p33(top) and p43(bottom)

Figure 11: Cumulative erosion/sedimentation map north to DNC

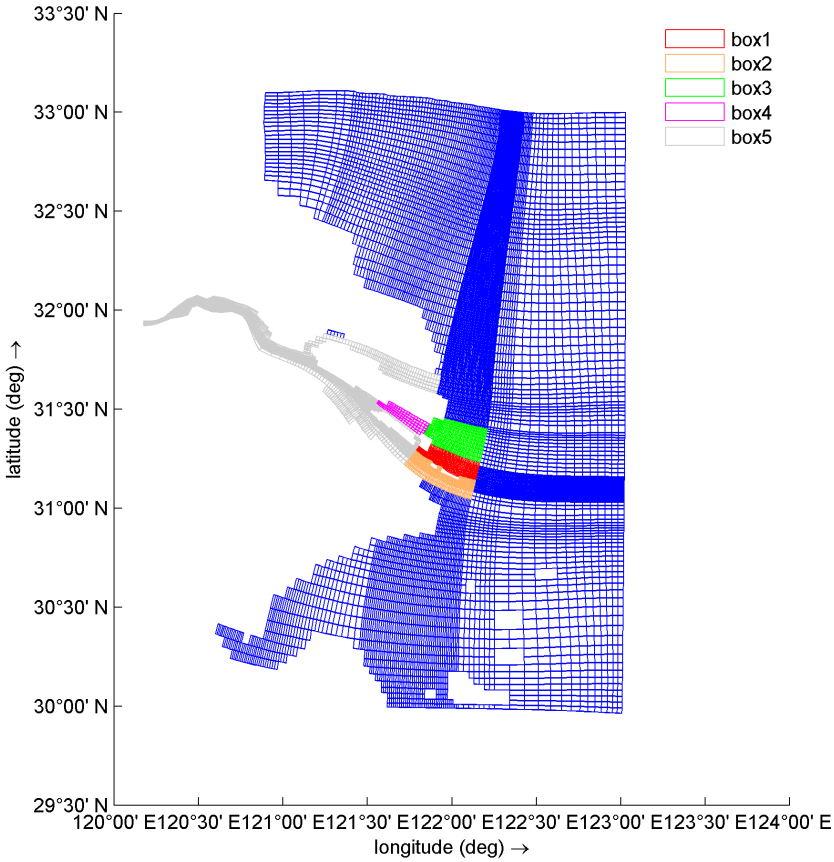

Figure 12: Box locations

4.1.2 Sediment mass per area in given boxes

In order to quantify the morphological changes, the sediment mass per area in a given box is defined so that the amount of sediment changes can be calculated to reflect the overall erosion or deposition in the specific areas. In Fig.12, several boxes of limited area are defined. Total sediment mass divided by the area is calculated for each box in each time step so that the time series of sediment mass per area for each box can be constructed.

Fig.13-Fig.17 show the sediment mass per area results in each box for p3 and the change values of sediment mass per area between initial condition to the end are listed in Table.4. In Fig.13, sediment mass per area all increases for p31, p32 and p33, while in Fig.14 and Fig.15, sediment mass per area all increases for p31, p32 and p33. The quantity differences can be seen in Table.4 which agrees with Cumulative erosion/sedimentation map (Fig.10) that with the decreasing of sediment flux upstream, less deposition or severe erosion takes place. In Fig.16 and 17, the scenariosare neither monotonically increasing nor decreasing. For

p31 in both figures, deposition dominates. For p32, deposition and erosion is nearly balanced. For p33, erosion takes control in both box4 and box5. The erosion and sedimentation patterns for box4 and box5 are more sensitive to the value of sediment flux upstream than the other boxes.

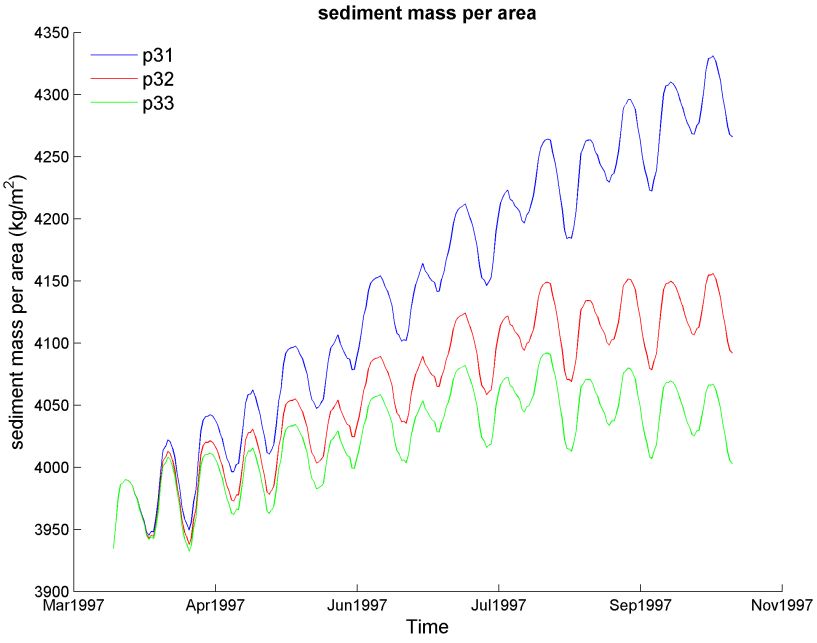

Figure 13: Sediment mass per area in box1 for p3

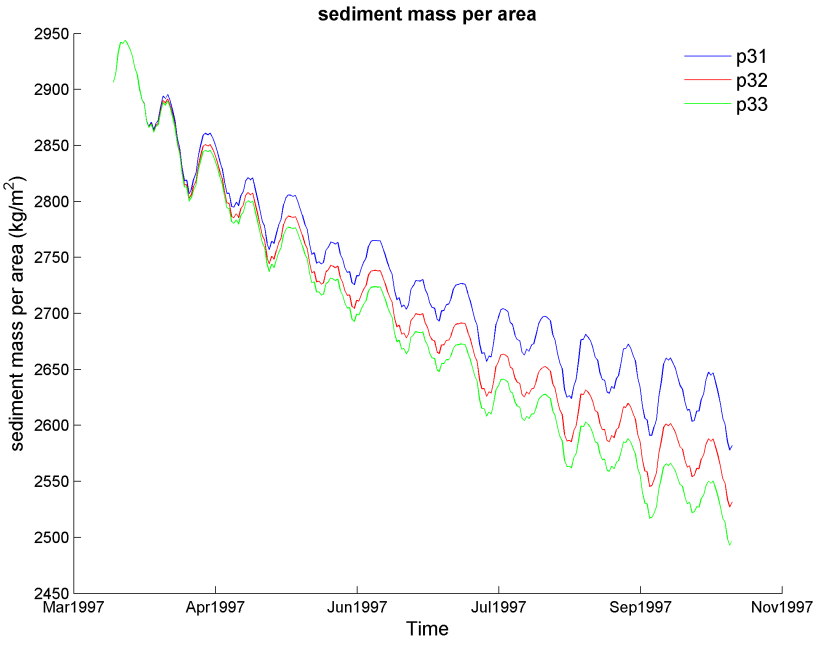

Figure 14: Sediment mass per area in box2 for p3

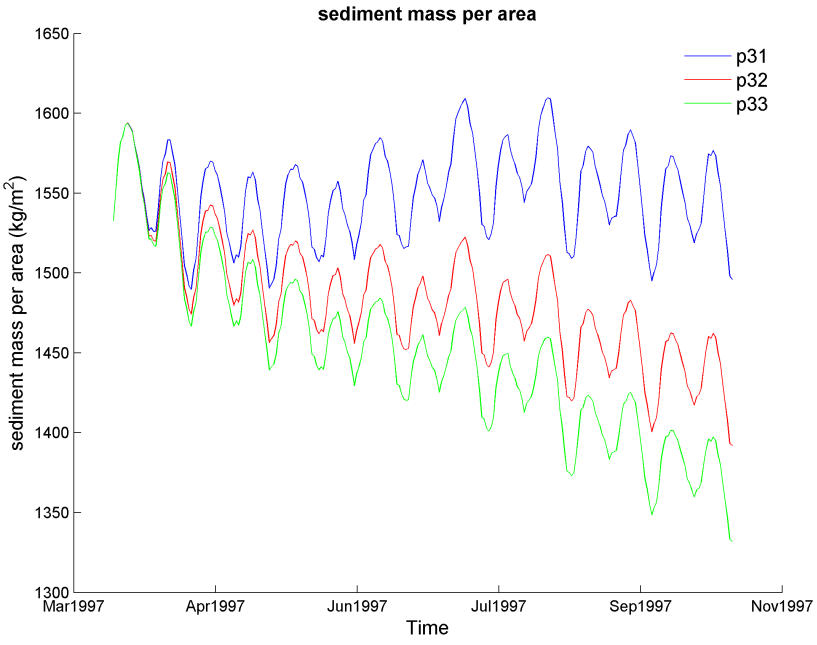

Figure 15: Sediment mass per area in box3 for p3

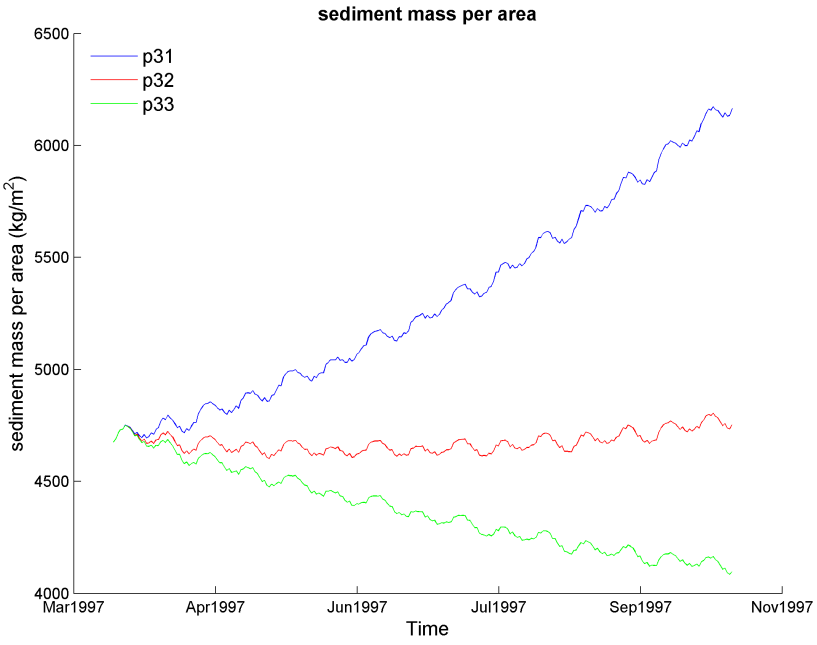

Figure 16: Sediment mass per area in box4 for p3

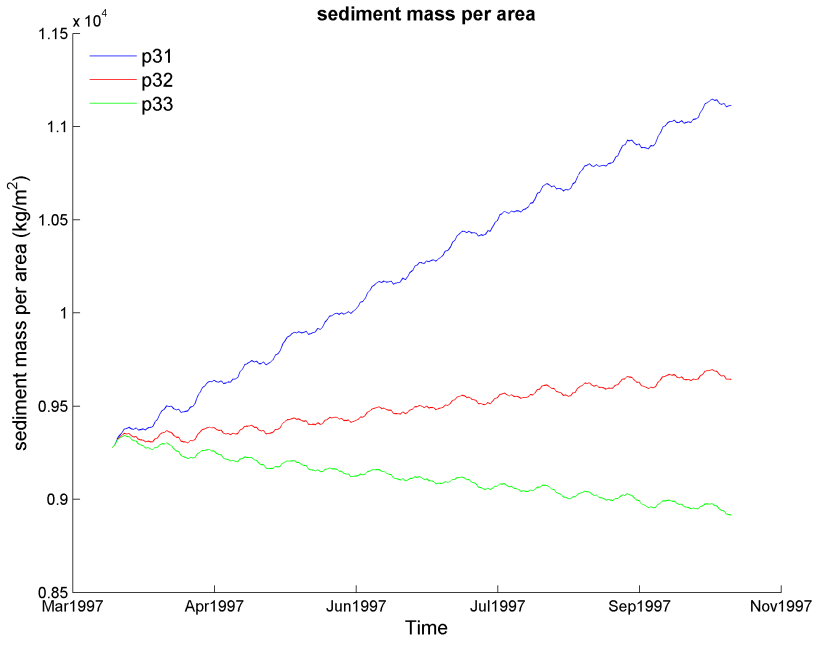

Figure 17: Sediment mass per area in box5 for p3

Table 4: Change values of sediment mass per area for p3

	p31 (kg/m^2)	p32 (kg/m^2)	p33 (kg/m^2)
box1	331	157	68
box2	-324	-357	-410
box3	-37	-141	-201
box4	1489	75	-581
box5	1834	365	-364

Fig.18-Fig.22 show the sediment mass per area results in each box for p4 and the change values of sediment mass per area between initial condition to the end are listed in Table.5. Overall the sensitivity of erosion and sedimentation to the sediment flux upstream is similar to what is discussed for p3, although in p4 the erosion or sedimentation pattern is different from that in p3. More details about the differences between p3 and p4 will be discussed in section 4.2.

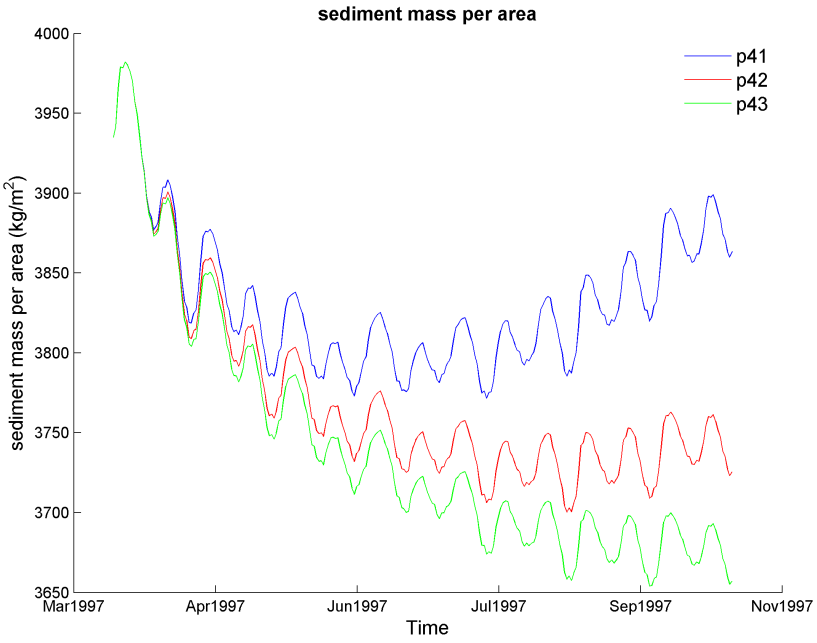

Figure 18: Sediment mass per area in box1 for p4

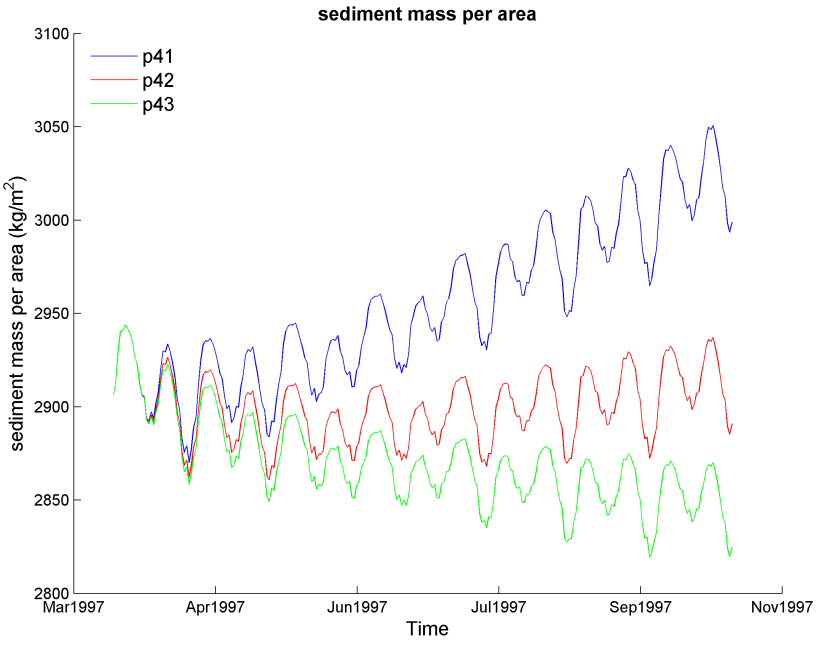

Figure 19: Sediment mass per area in box2 for p4

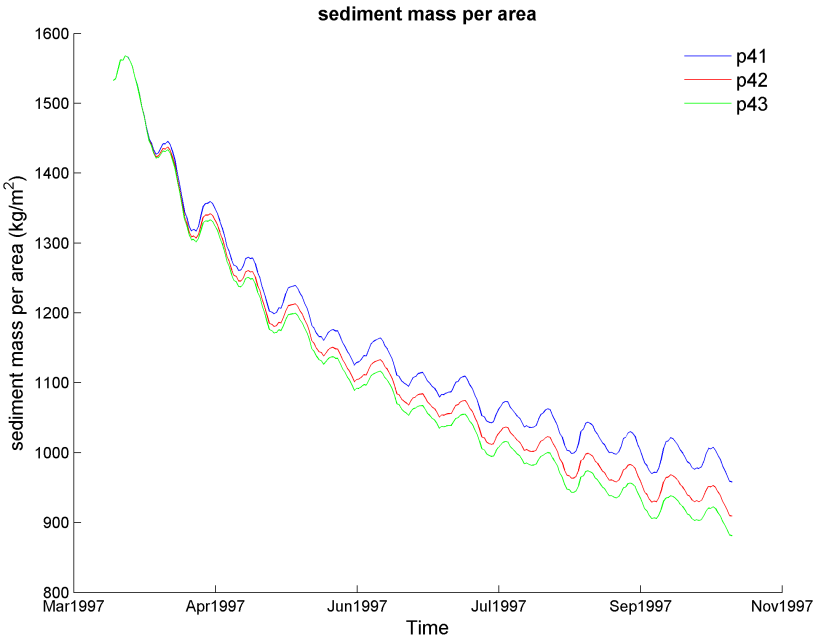

Figure 20: Sediment mass per area in box3 for p4

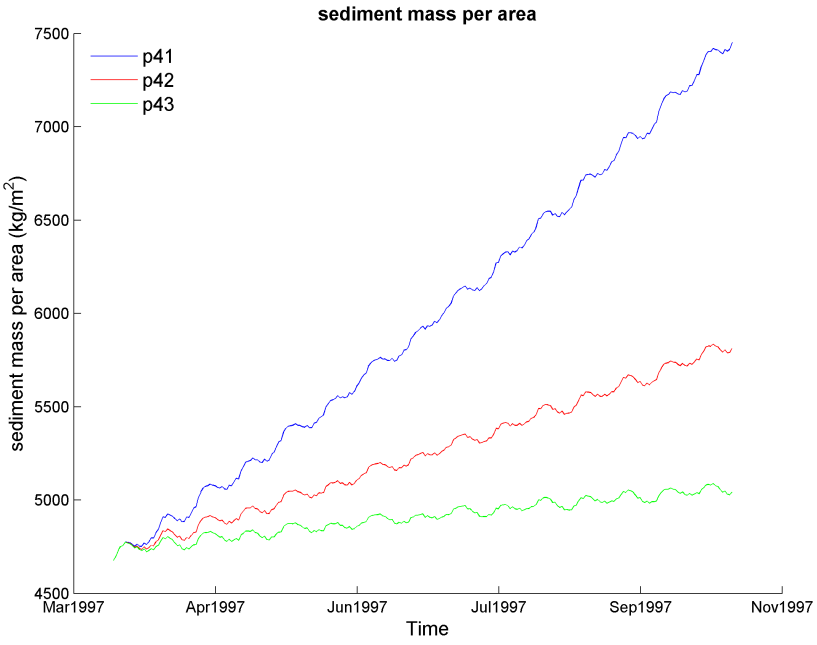

Figure 21: Sediment mass per area in box4 for p4

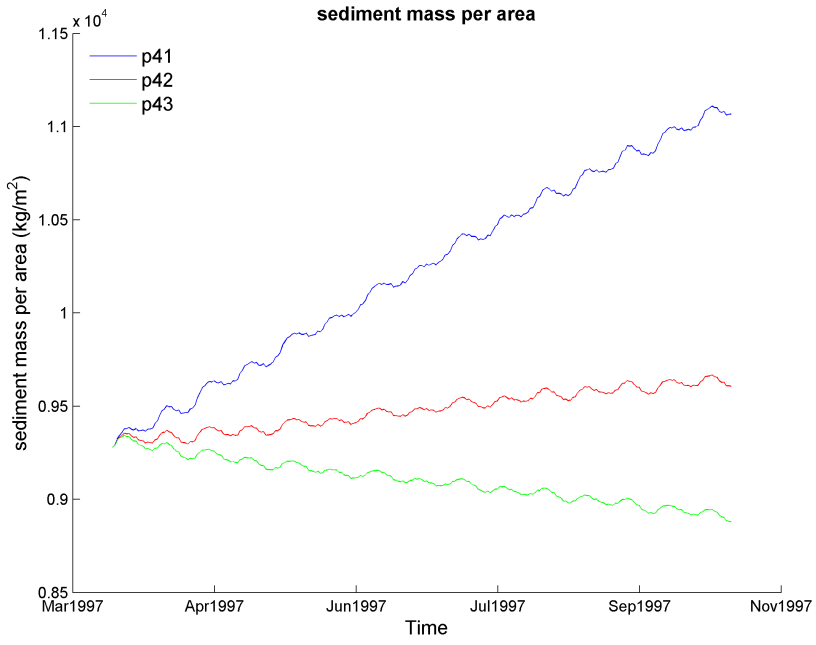

Figure 22: Sediment mass per area in box5 for p4

Table 5: Change values of sediment mass per area for p4

	p41 (kg/m^2)	p42 (kg/m^2)	p43 (kg/m^2)
box1	-71	-209	-278
box2	92	-16	-81
box3	-574	-623	-651
box4	2775	1135	365
box5	1788	328	-400

4.1.3 1-D profile

To get more details about the erosion and sedimentation, transects across the channel and south to the channel are chosen to analyze the bed level elevation (Fig.23). The direction of the transect profile is from southwest to northeast.

Fig.24 compares the initial bed level along with p3 and p4's bed level after the simulation for the transects across the channel. It can be seen from these figures that for most cases there are no major differences among 300 Mt/yr, 150 Mt/yr and 75 Mt/yr and the profiles are almost the same inside each figure. Only in Fig.24a and 24c, there are slight differences among three lines.

Fig.25 shows the transect profile changes south to the channel. Similar to Fig.24, inside each figure three cases almost overlap with each other except a little gap along transect m115S in Fig.25c.

4.2 DNC project effect

To study the influence of DNC, cases p3 and p4 used in "TGD effect" are also used here, but from different perspectives focusing on the jetties effect. As shown in Table.3 among all these cases, p31, p32 and p33 are cases with jetties, while p41, p42 and p43 are cases without jetties. And all the other conditions are the same for p31 and p41, p32 and p42, p33 and p43 respectively.

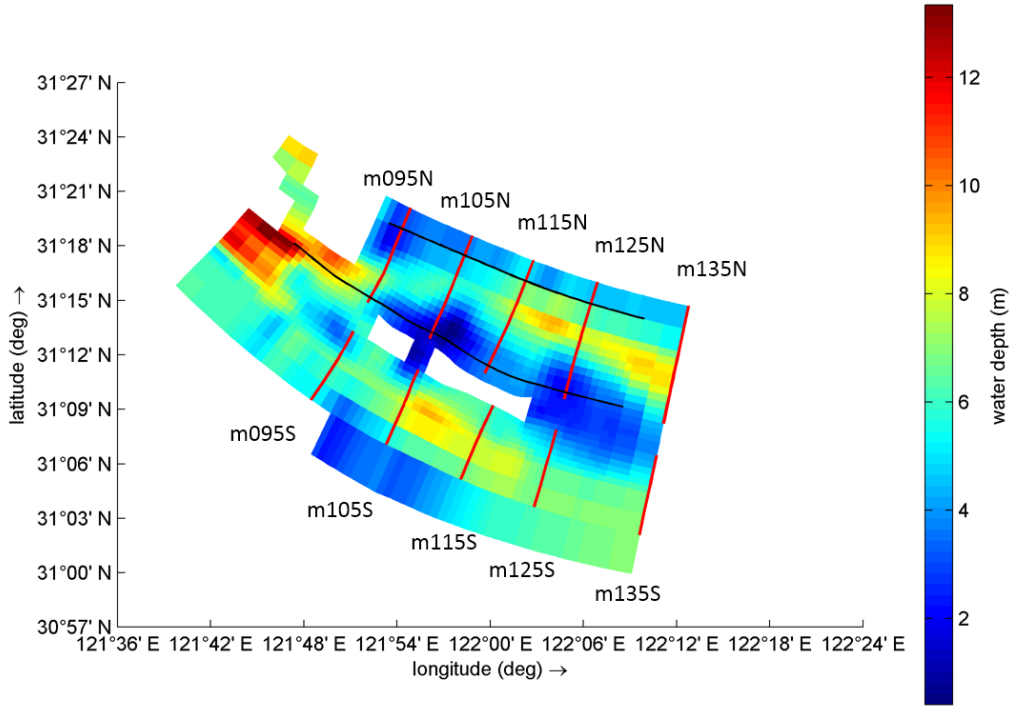

Figure 23: Location of transect profiles

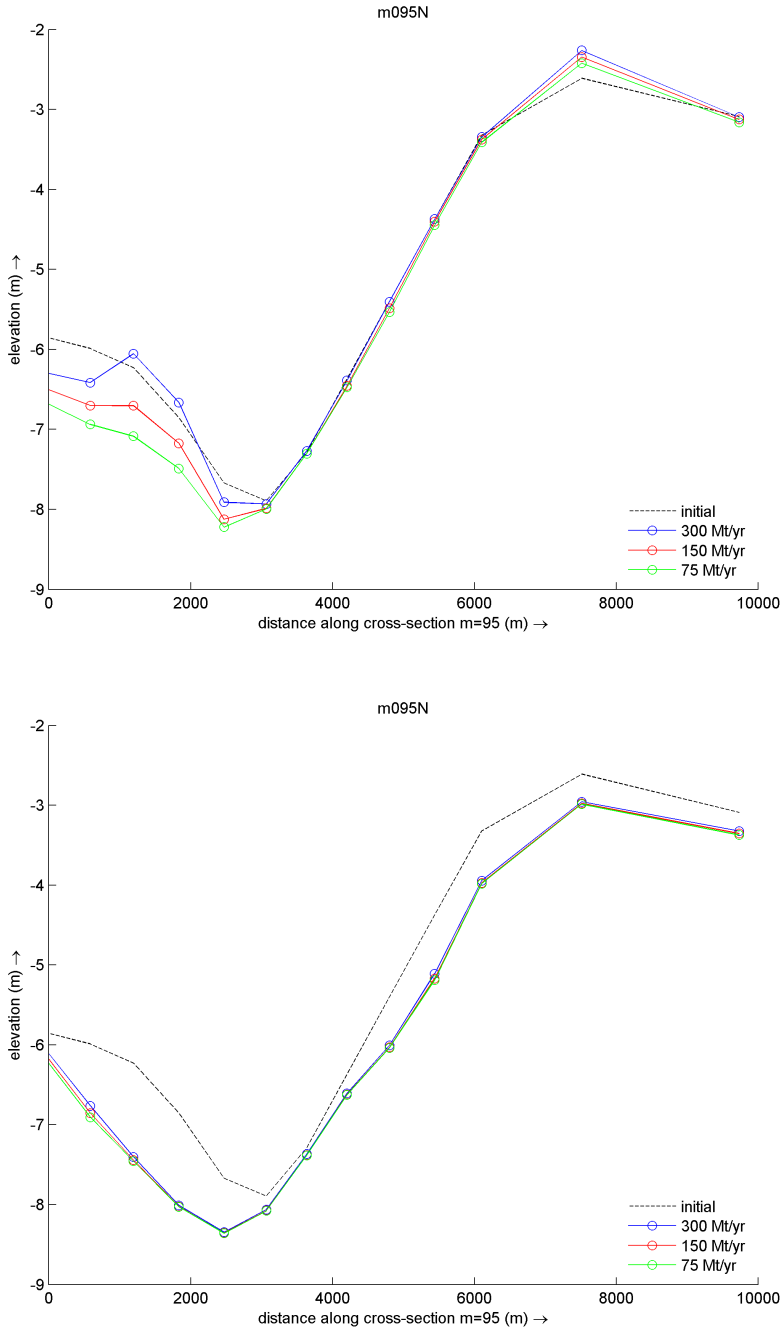

(a)

Figure 24: 1-D transect profile across the channel p3(top panel) and p4(bottom panel)

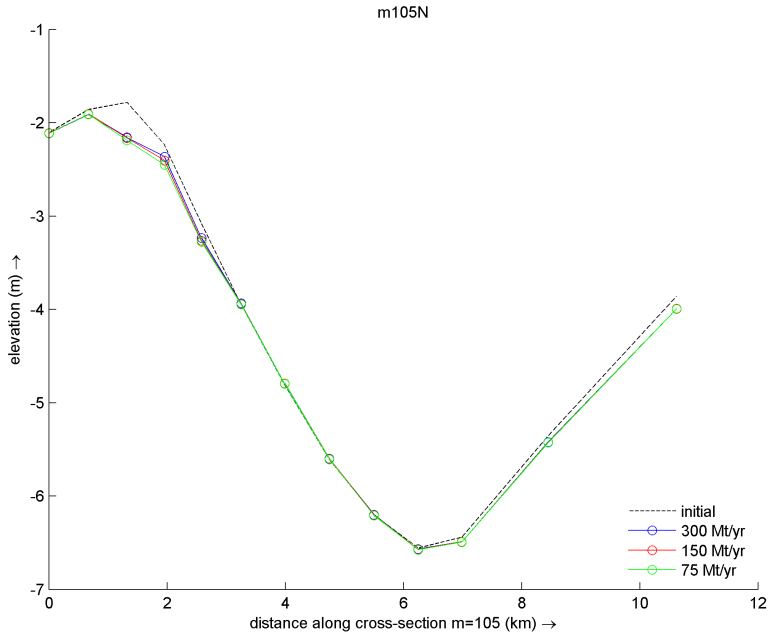

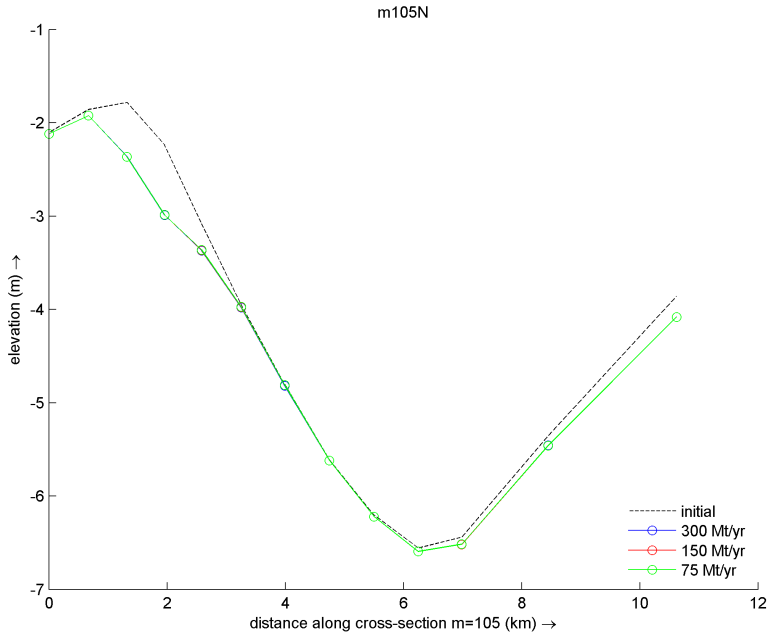

(b)

Figure 24: 1-D transect profile across the channel p3(top panel) and p4(bottom panel)

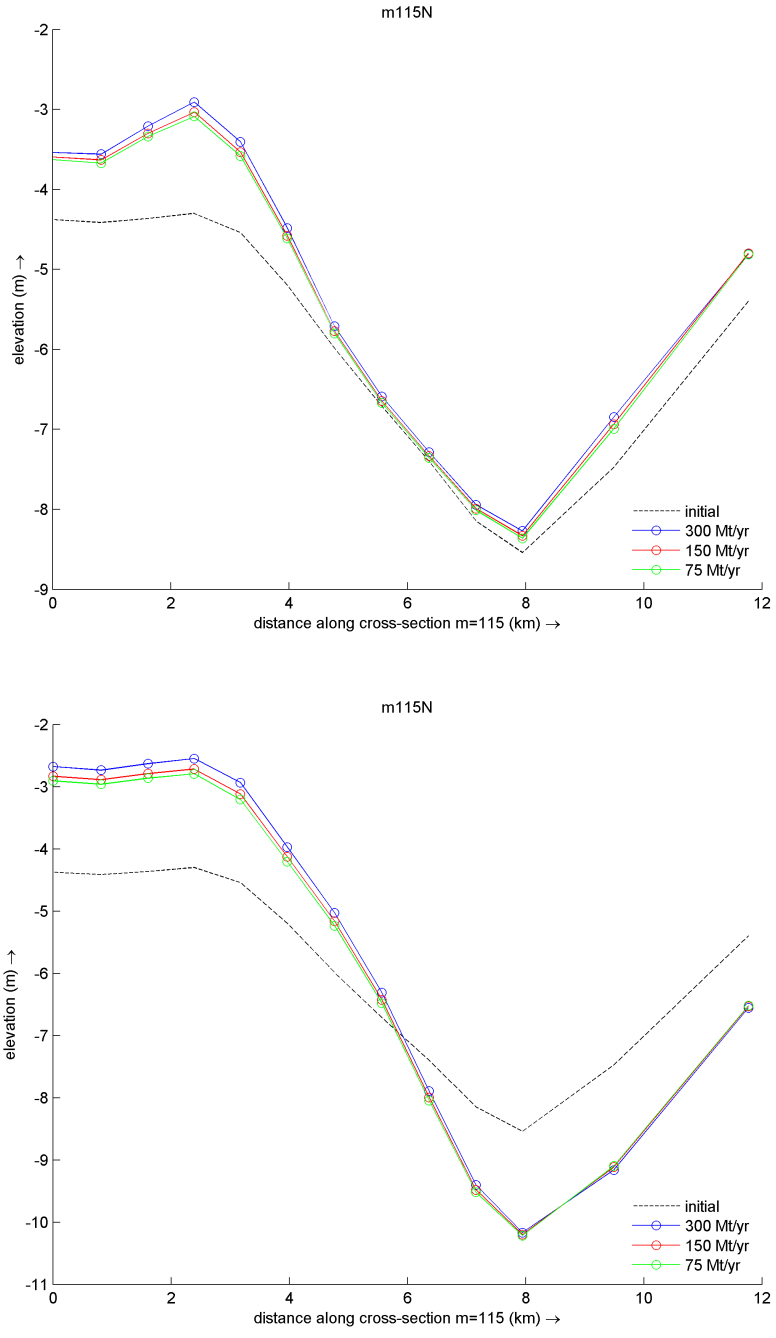

(c)

Figure 24: 1-D transect profile across the channel p3(top panel) and p4(bottom panel)

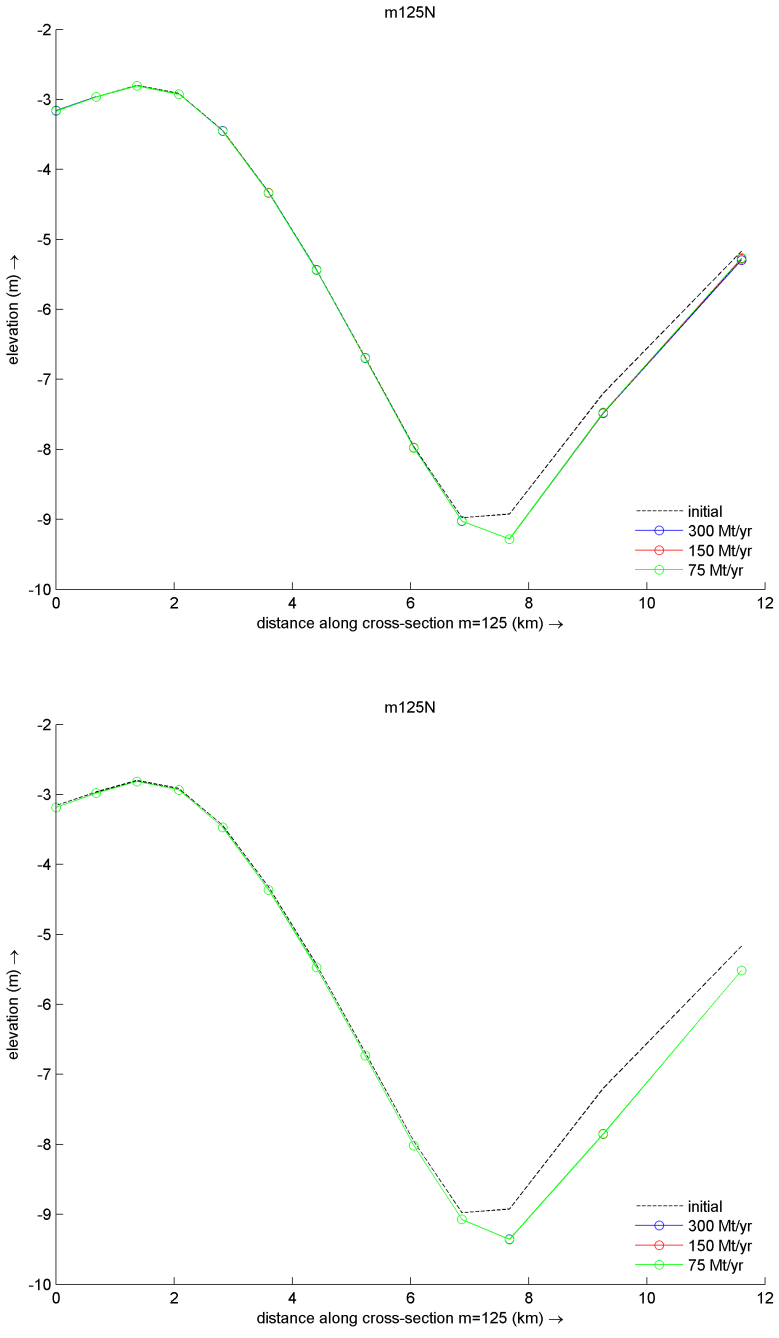

(d)

Figure 24: 1-D transect profile across the channel p3(top panel) and p4(bottom panel)

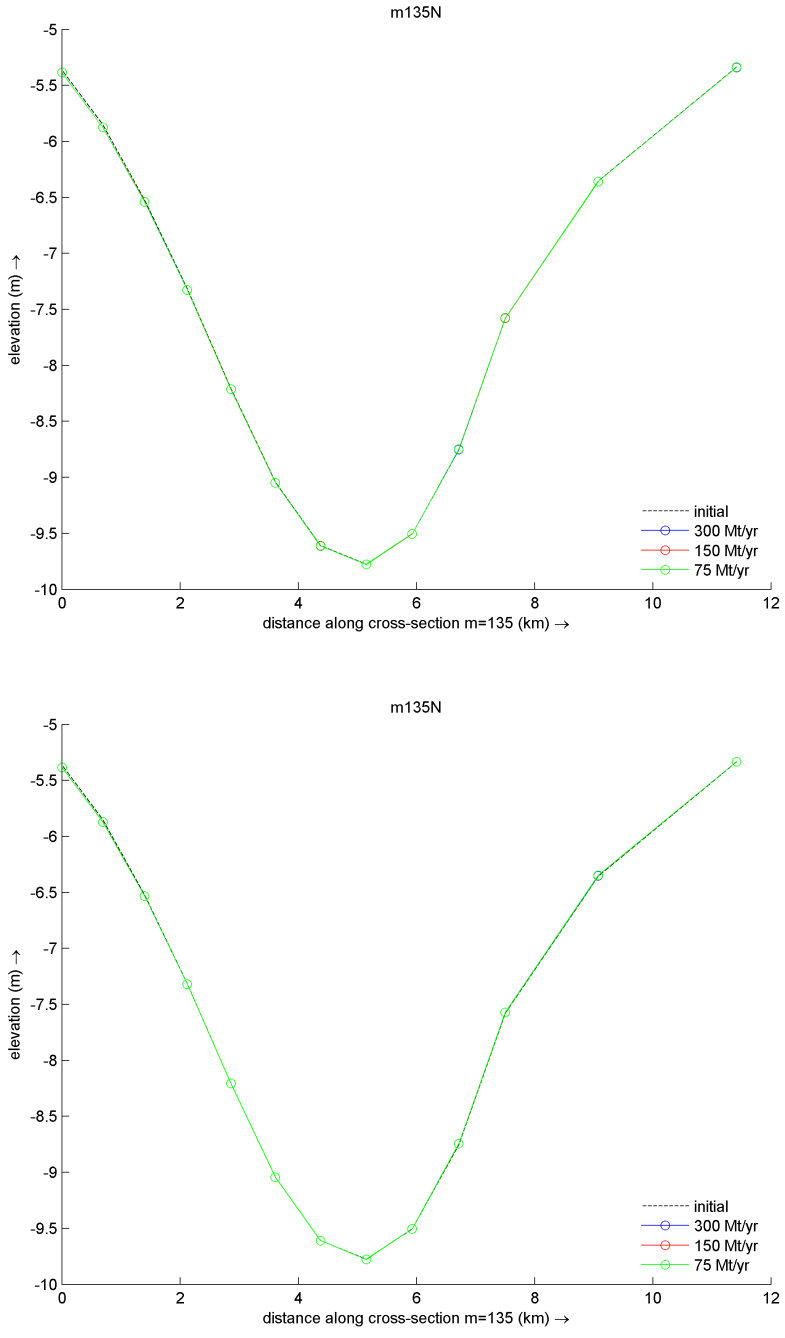

(e)

Figure 24: 1-D transect profile across the channel p3(top panel) and p4(bottom panel)

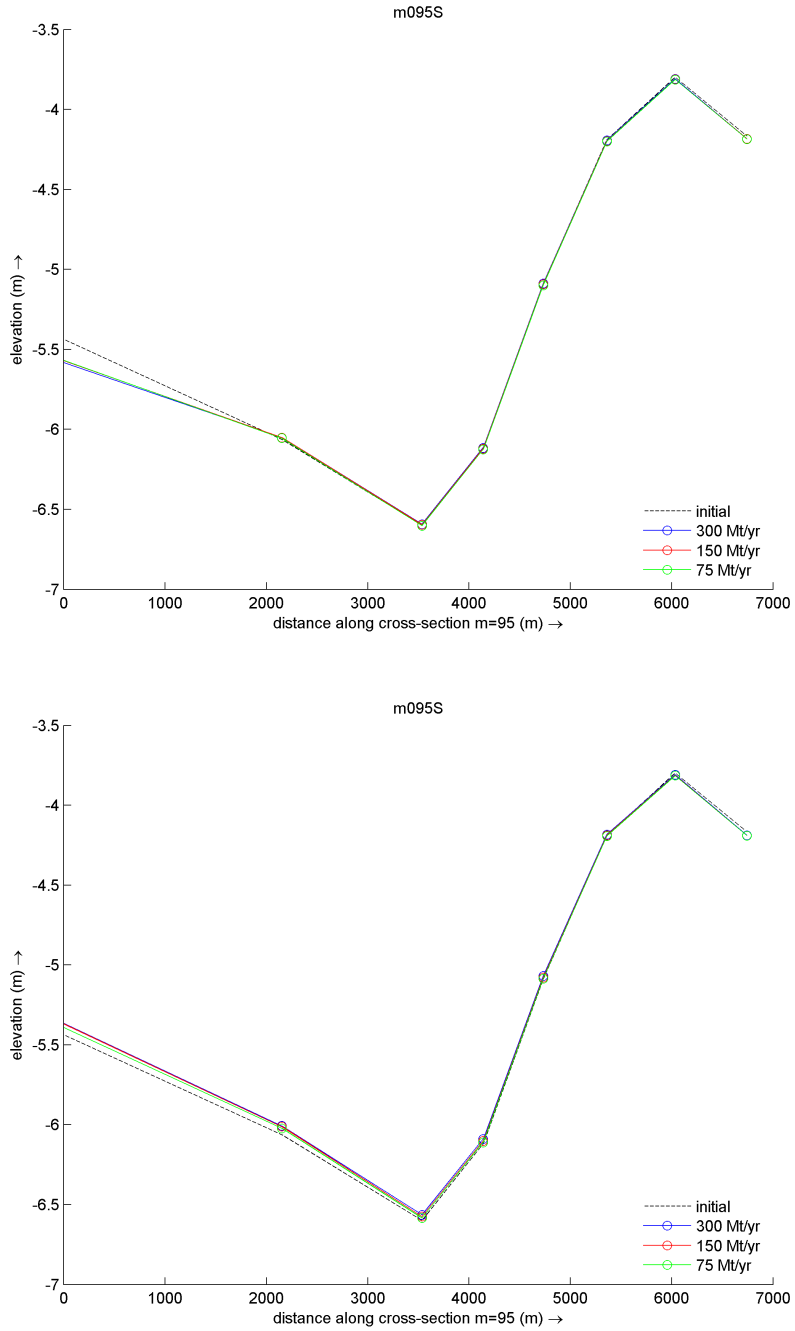

(a)

Figure 25: 1-D transect profile south to the channel p3(top panel) and p4(bottom panel)

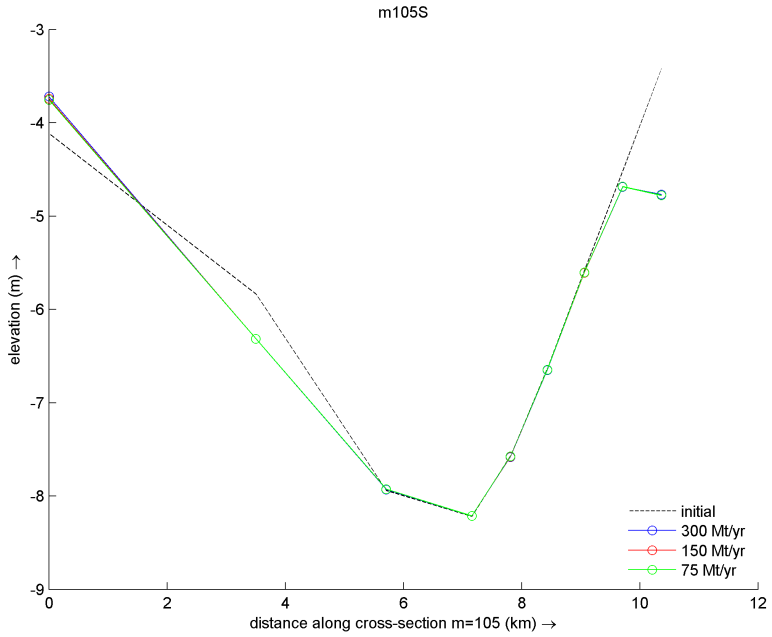

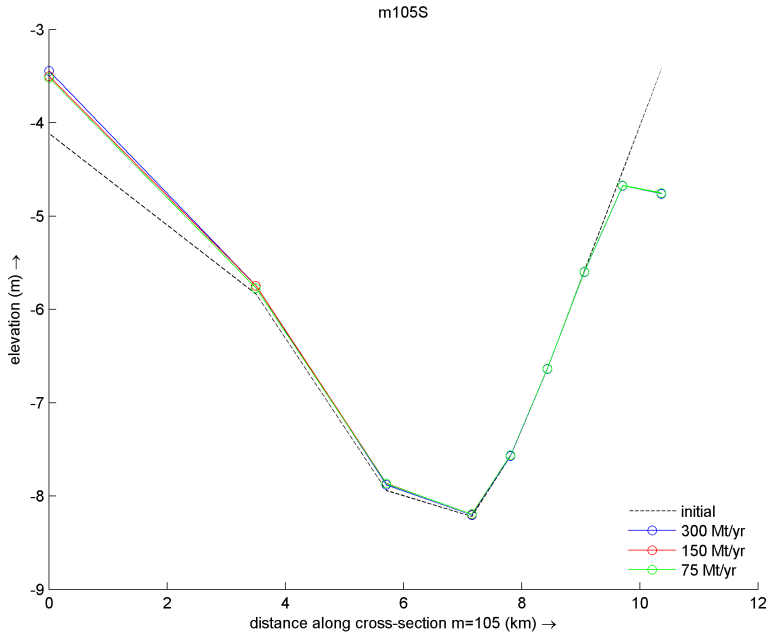

(b)

Figure 25: 1-D transect profile south to the channel p3(top panel) and p4(bottom panel)

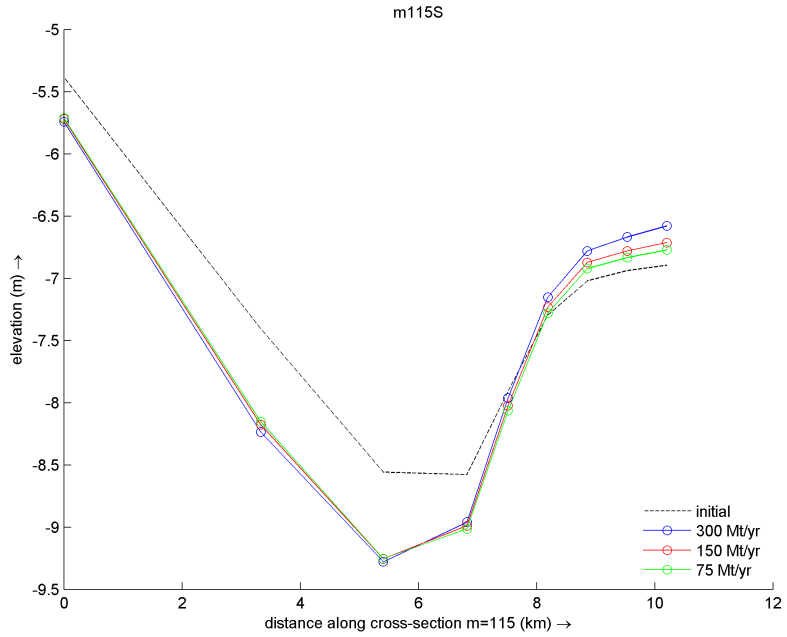

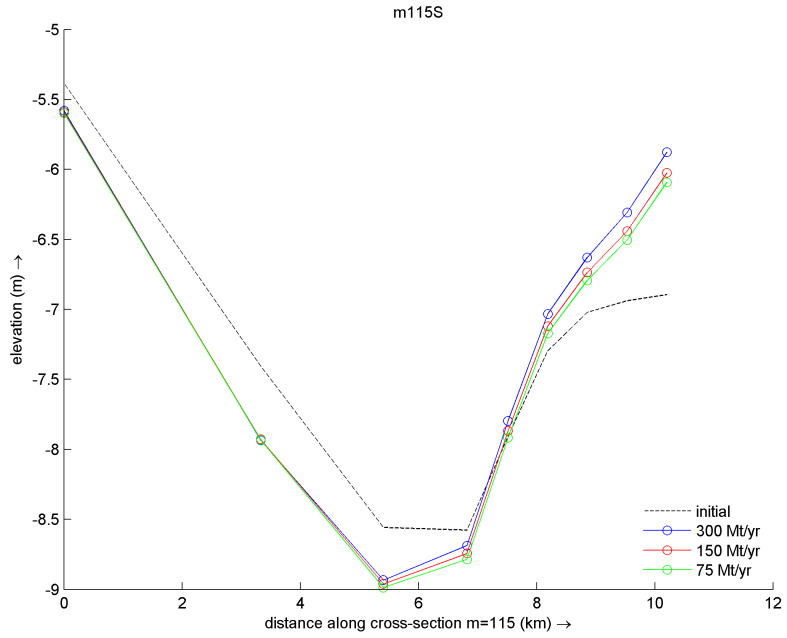

(c)

Figure 25: 1-D transect profile south to the channel p3(top panel) and p4(bottom panel)

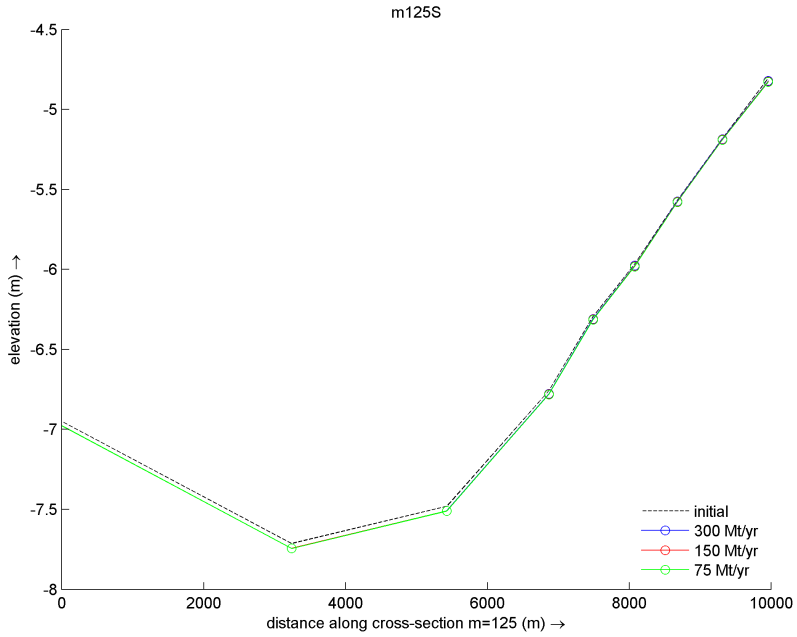

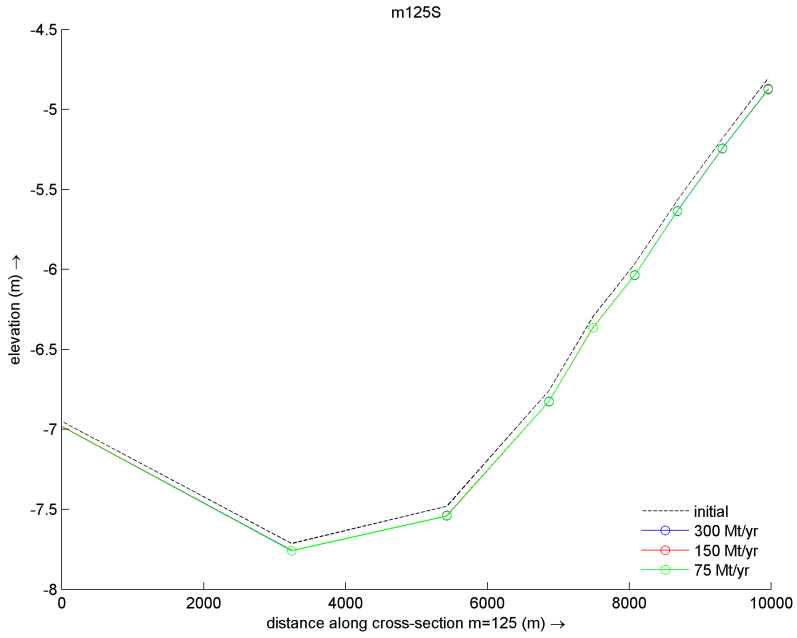

(d)

Figure 25: 1-D transect profile south to the channel p3(top panel) and p4(bottom panel)

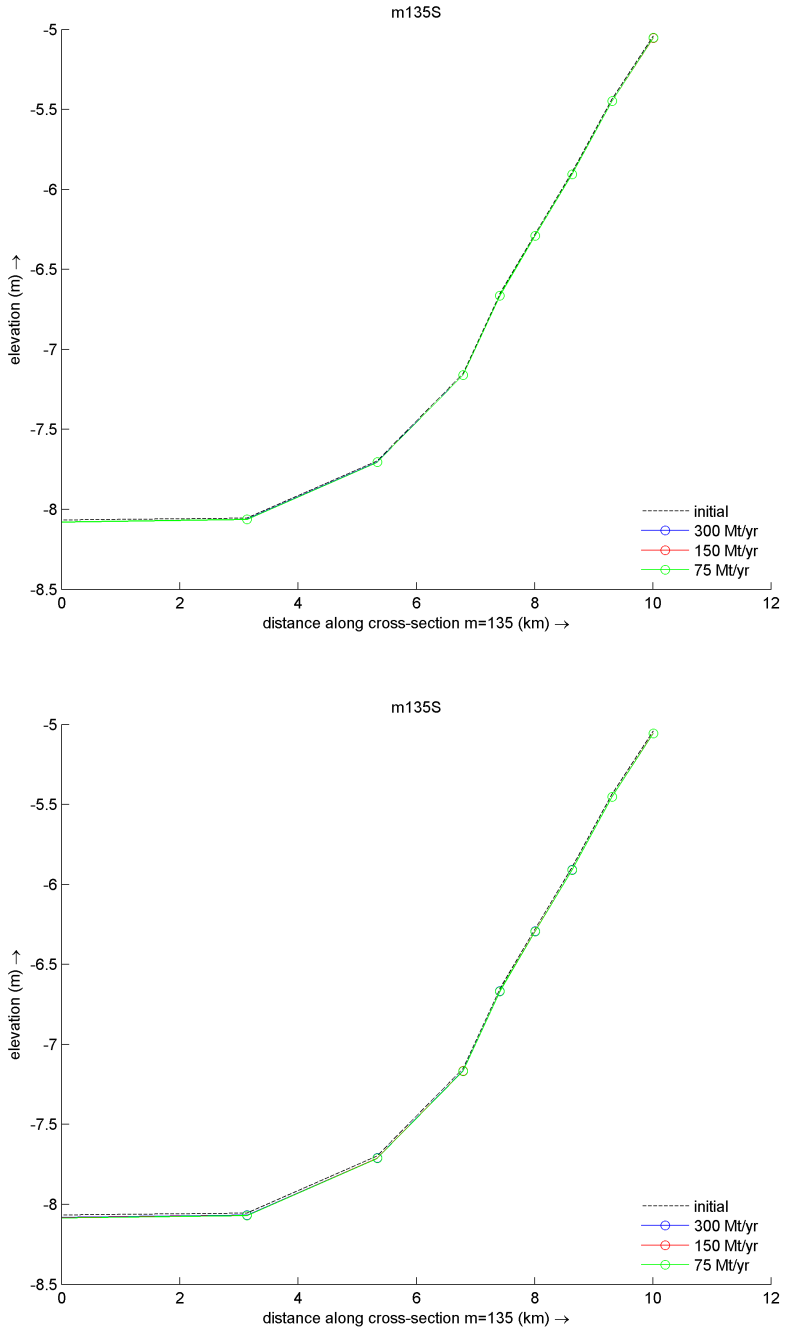

(e)

Figure 25: 1-D transect profile south to the channel p3(top panel) and p4(bottom panel)

4.2.1 Cumulative erosion/sedimentation map

Fig.10a, Fig.10b and Fig.10c show the comparison between cases with and without the jetties.

Several phenomena can be seen from the results. First, in cases without the jetties , there is a deposition center around the lower part of Jiuduan island and with the increase of the sediment flux, the deposition in this area will be larger. Second, in cases with the jetties, the sediment will be redistributed due to existence of the jetties. Inside the channel there will have more sediment deposition especially locations near north jetty switching from erosion without the jetty to deposition with the jetty, while south to the channel, there will be less sediment deposition. The deposition center in the previous cases without the jetties will have less deposition with the jetties.

Besides the comparison in the DNC region, results north to the DNC (box3 and box4 in Fig.12) are shown in Fig.11a, Fig.11b and Fig.11c. Similar to the results observed in DNC region, local sediment distribution here is also changed due to the jetties. Near the location of the north jetty, there is severe erosion in p41 (bottom panel in each figure), but in the same location it switches to sedimentation after the jetties were constructed in p31 (up panel in each figure). However, upstream to north jetty, more sediment is deposited in p41 than p31.

4.2.2 Sediment mass per area in given boxes

Fig.26-Fig.30 show the results of the sediment mass per area in each box (box location shown in Fig.12). In Fig.26, sediment mass per area increases about 330 kg/m^2 for p31, while for p41 this value decreases 70 kg/m^2. This agrees with the cumulative erosion/sedimentation map shown in Fig.10a that inside the channel there are more sedimentation with the jetty. In Fig.27, sediment mass per area decreases about 330 kg/m^2 for p31, while for p41 this value decreases 90 kg/m^2. This also agrees with the cumulative erosion/sedimentation map shown in Fig.10a that south to the channel there are more erosion with the existence of jetty. In Fig.28, sediment mass per area decreases about 35 kg/m^2 for p31, while for p41 this value dramatically decreases 570 kg/m^2. This is consistent with the results in Fig.11a which shows north to the channel there is less erosion with the jetty in p31. In Fig.29, sediment mass per area for p31 and p41 are both increased, but the differences are large: 1490 kg/m^2 and 2770 kg/m^2 respectively. This also agrees with Fig.11a that upstream to box3 there is less deposition with the existence of jetty. In Fig.30, sediment mass per area for p31 and p41 are both increased, and values are similar, 1890 kg/m^2 and 1850 kg/m^{2}respectively which indicates that DNC project will not have significant influence on the sediment transport upstream to the river mouth.

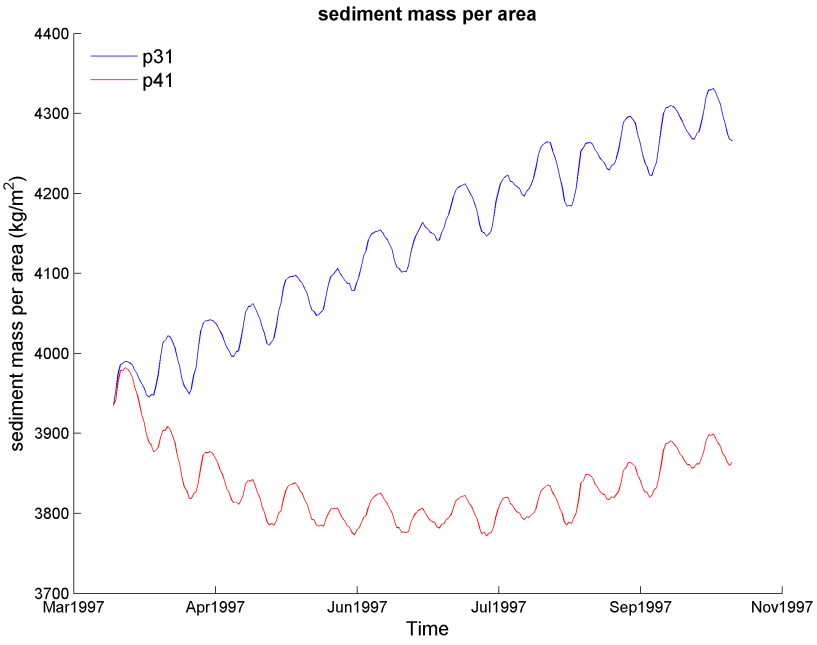

Figure 26: Sediment mass per area in box1 between p31 ad p41

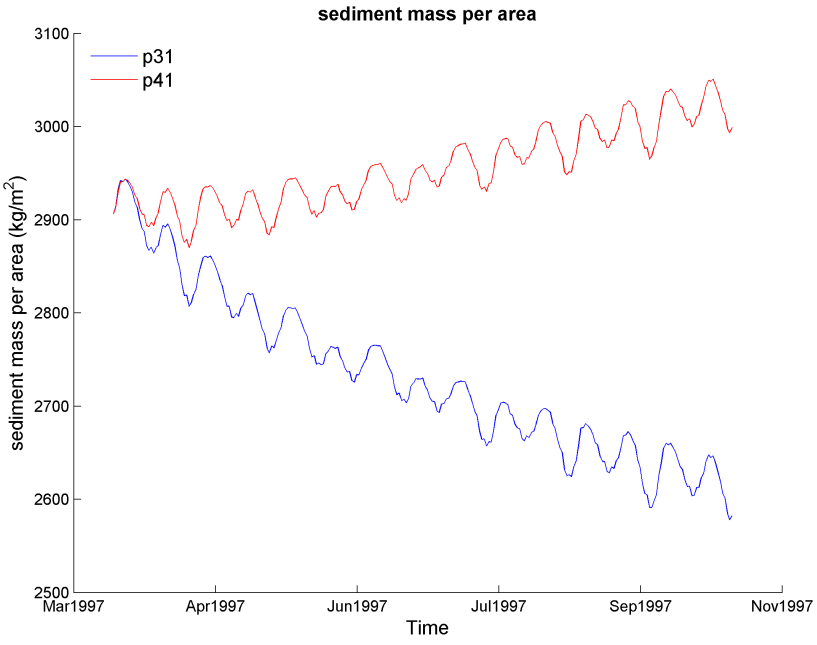

Figure 27: Sediment mass per area in box2 between p31 ad p41

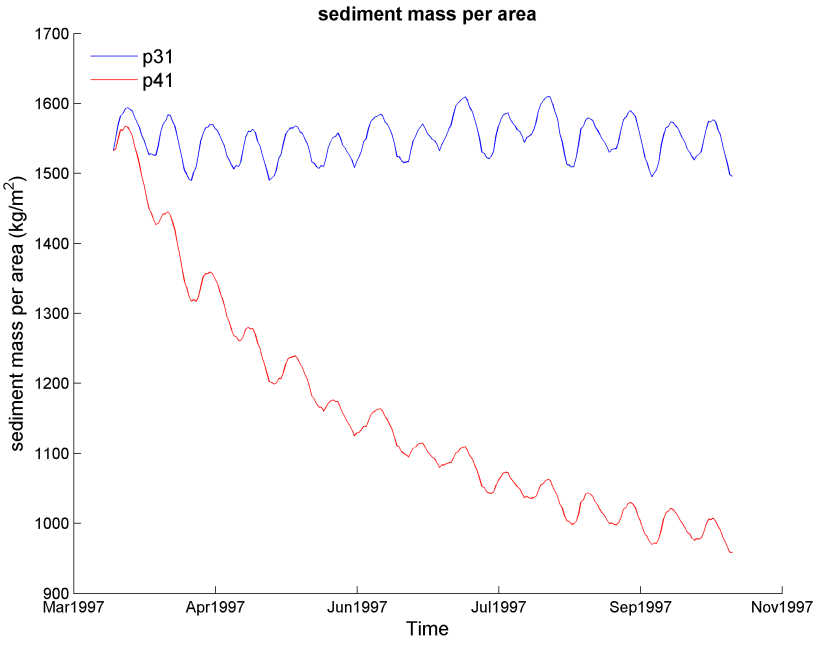

Figure 28: Sediment mass per area in box3 between p31 ad p41

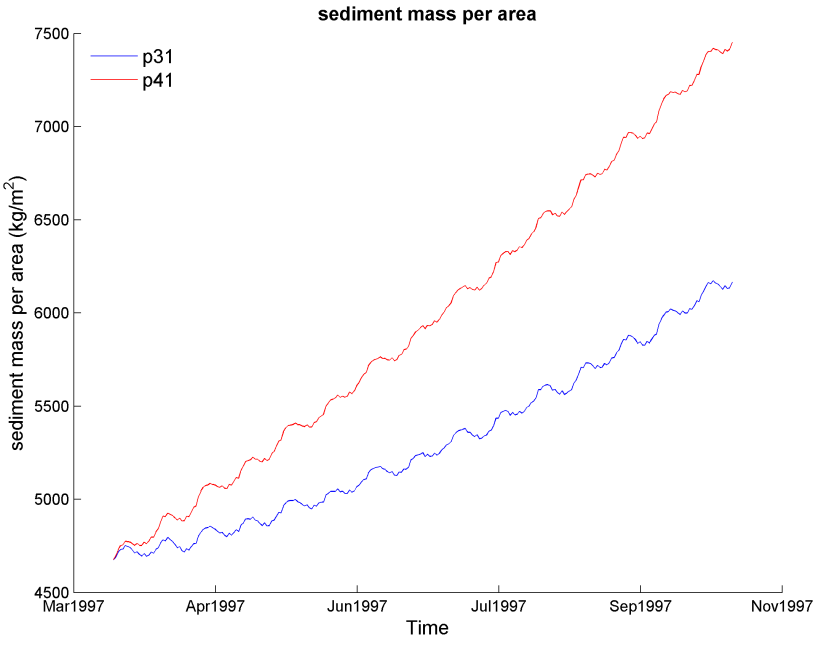

Figure 29: Sediment mass per area in box4 between p31 ad p41

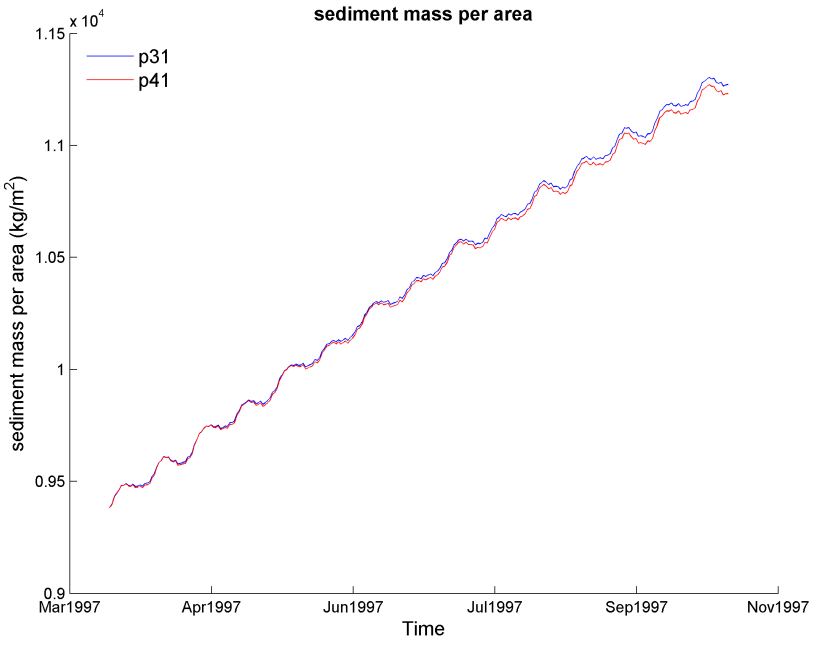

Figure 30: Sediment mass per area in box5 between p31 ad p41

4.2.3 1-D transect profile

The 1-D transect location used here is the same as shown in Fig.23. Fig.32 compares the initial bed level (p31 and p41's initial bed level are the same) with p31 and p41's bed level after the simulation for the transects across the channel. Along transect m095N (Fig.32a), bed level in p31 does not change significantly from the initial bed level while bed level in p41 decreases with more than 1m near the location of south jetty (around 1500m) . Along transect m105N (Fig.32b), bed level of p31 and p41 are similar to the initial condition except some reduction near the location of south jetty for p41. Along transect m115N (Fig.32c), the bed level of p31 rises at the two end of the profile where the two jetties locates. However, erosion and sedimentation patterns of p41 are different from places near the south jetty and north jetty. From 0 km to 6 km along the cross-section the bed level increases, while from 6 km to 12 km the bed level reduces especially in the deepest part, where the reduction can reach 2 m. Along m125N and m135N (Fig.32d and Fig.32e), the bed level is stable and there are few differences between initial conditions, and bed level of p31 and p41 after the simulation.

Fig.33 shows the transect profile changes south to the channel. Similar to the results in Fig.32, transect m95S, m105S and m115S have major bed level changes in both p31 and p41 while transect m125S and

m135S the simulation results of p31 and p42 are the same as the initial bed level. However, in Fig.32 profile lines of p31 are on top of those of p41 along transect m95N, m105N and m115N and the gap between them can be over 1 m , but in Fig.33 the scenario is opposite and profile lines of p31 are below those of p41 along transect m95S, m105S and m115S and the gap between them is smaller which can only be around 0.2 m.

Above all, the 1-D profiles correspond to the cumulative erosion/sedimentation map. Inside the channel, p31 has more deposition than p41 and the differences are large between p31 and p41. South to the channel p31 has less deposition than p41 but the difference between these two cases are not as large as those inside the channel.

4.2.4 Current

In order to analyze the current characteristics with and without the jetties in this region, results from p31 and p41 are used to make the comparison over the course of one tidal cycle (Fig.31).

Fig.34 shows the depth averaged velocity magnitude. When tide is high, the differences between p31 and p41 are small. However, when tide is low, inside the channel the velocity magnitude is smaller with the jetty and south to the channel the velocity magnitude is larger with the jetty.

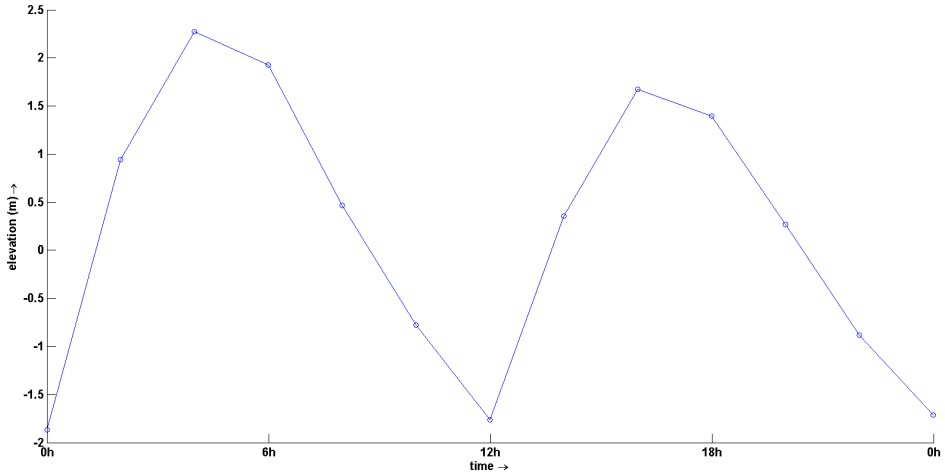

Figure 31: Water level in one tide cycle

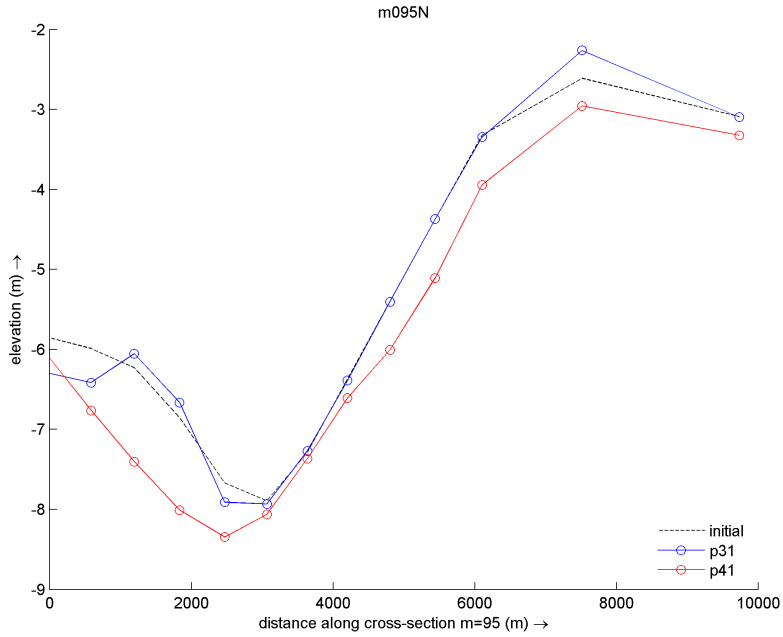

(a)

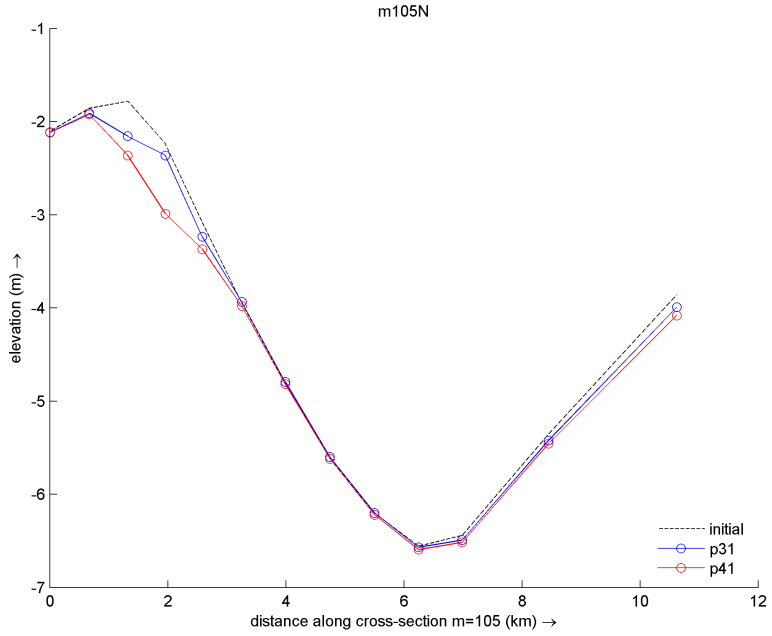

(b)

Figure 32: 1-D transect profile north to the channel between p3 and p4

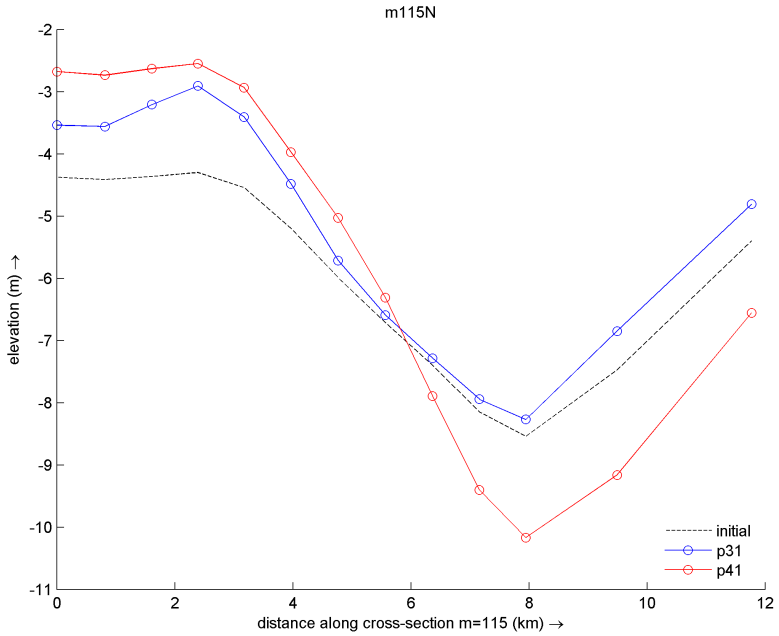

(c)

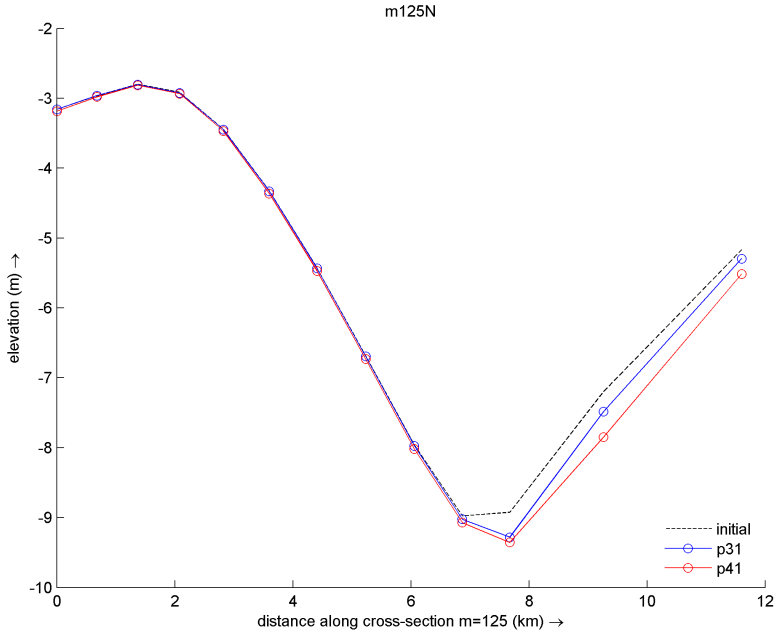

(d)

Figure 32: 1-D transect profile north to the channel between p3 and p4

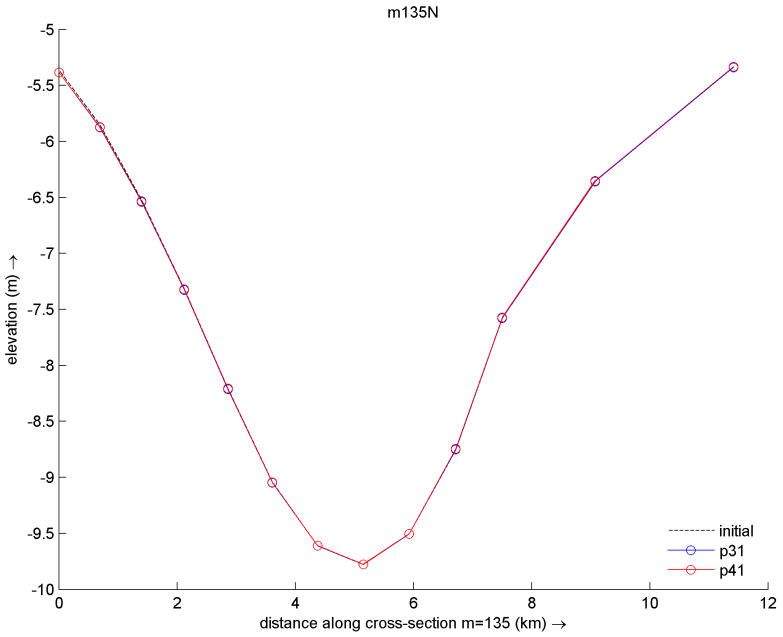

(e)

Figure 32: 1-D transect profile north to the channel between p3 and p4

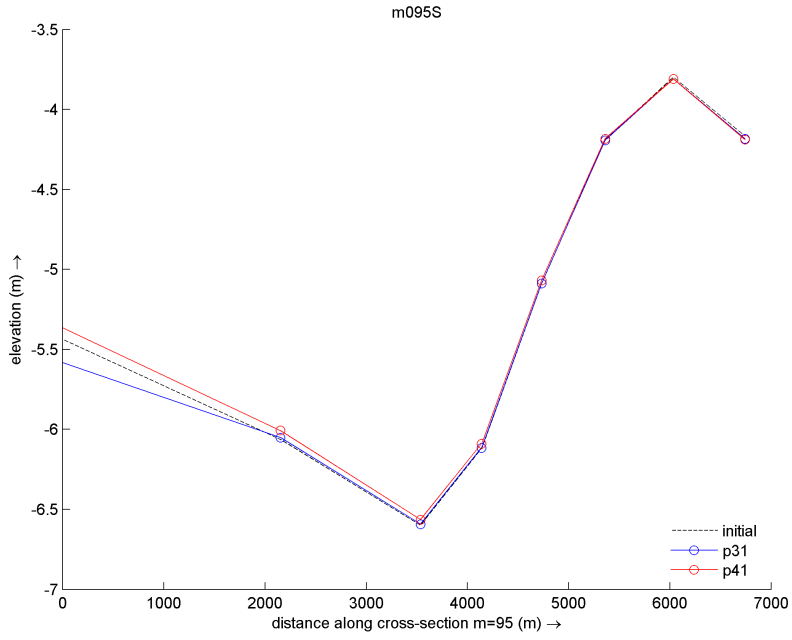

(a)

Figure 33: 1-D transect profile south to the channel between p3 and p4

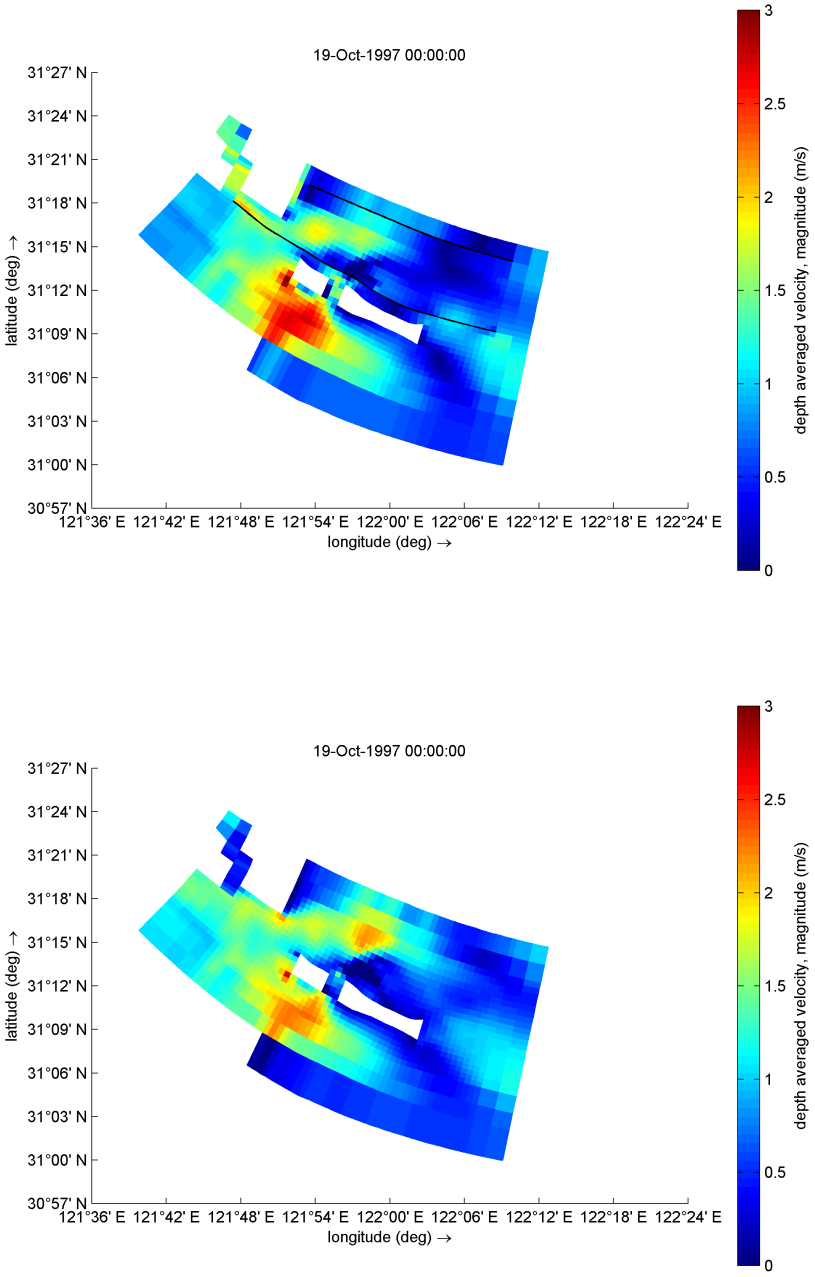

(a) Water level -1.87m

Figure 34: Depth averaged velocity magnitude in one tide cycle p31(top) and p41(bottom)

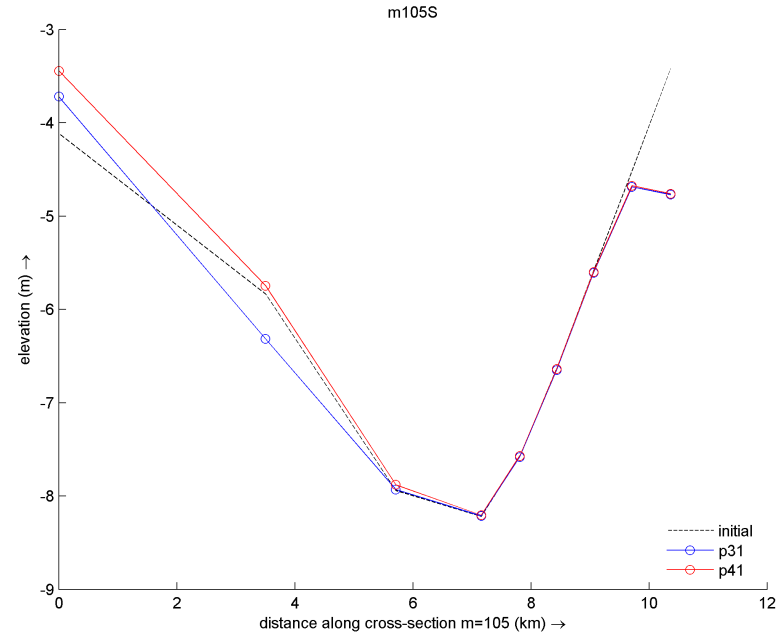

(b)

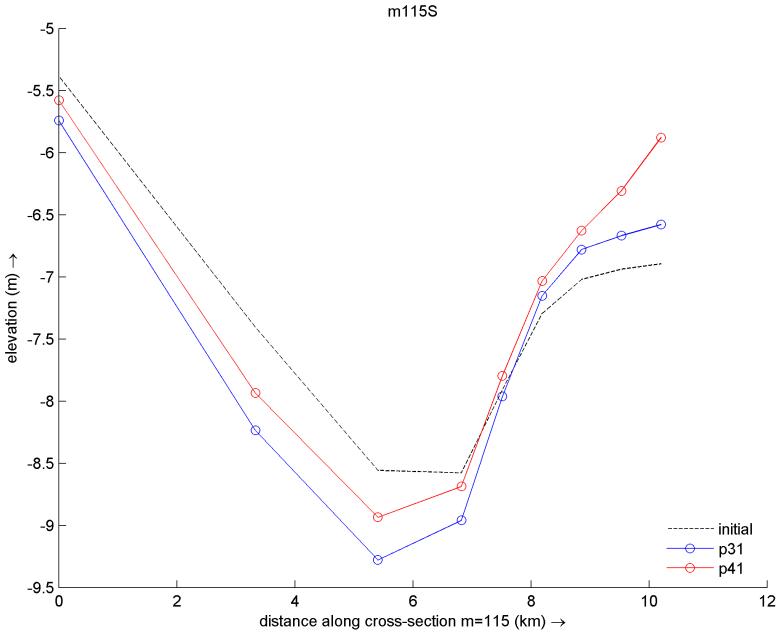

(c)

Figure 33: 1-D transect profile south to the channel between p3 and p4

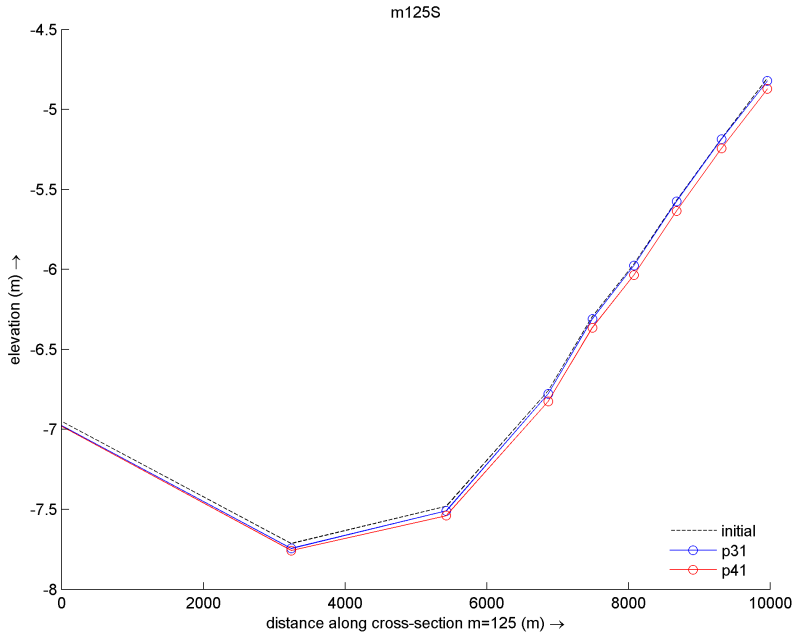

(d)

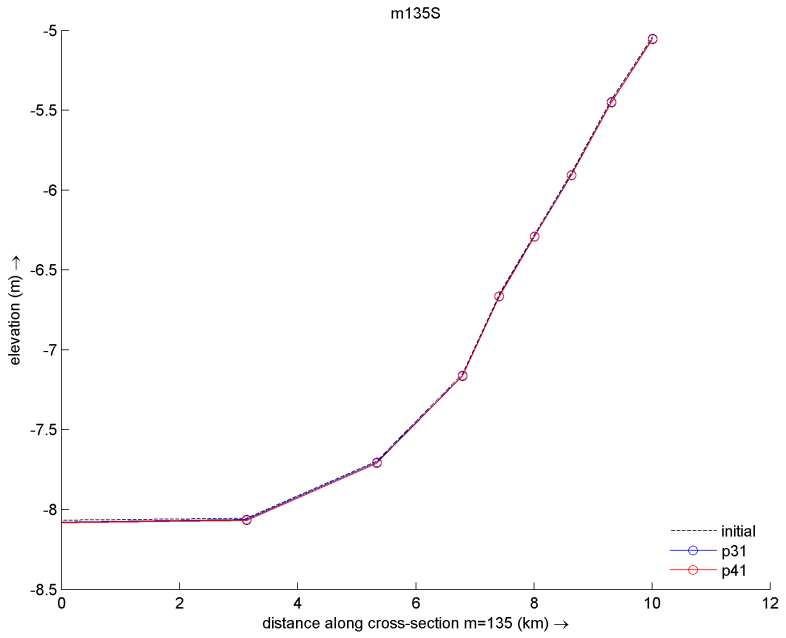

(e)

Figure 33: 1-D transect profile south to the channel between p3 and p4

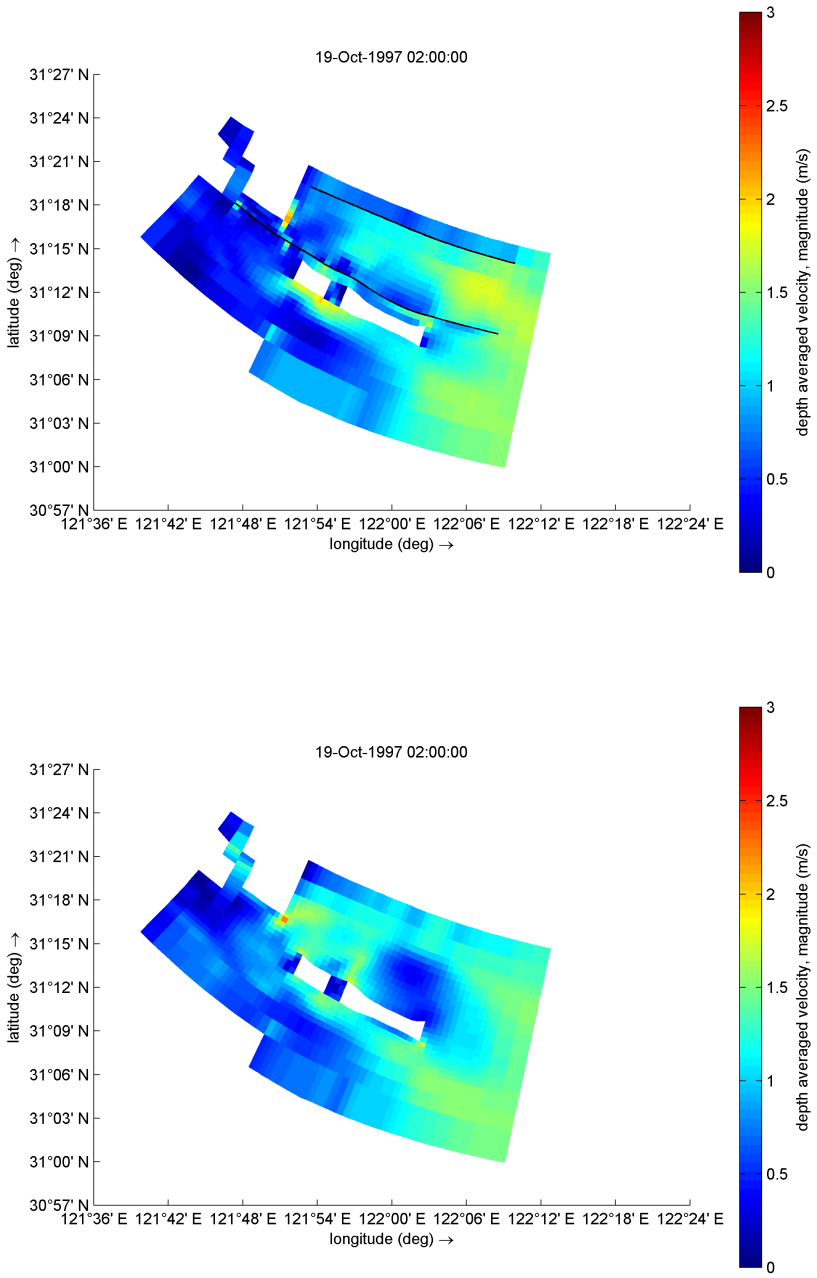

(b) Water level 0.94m

Figure 34: Depth averaged velocity magnitude in one tide cycle p31(top) and p41(bottom)

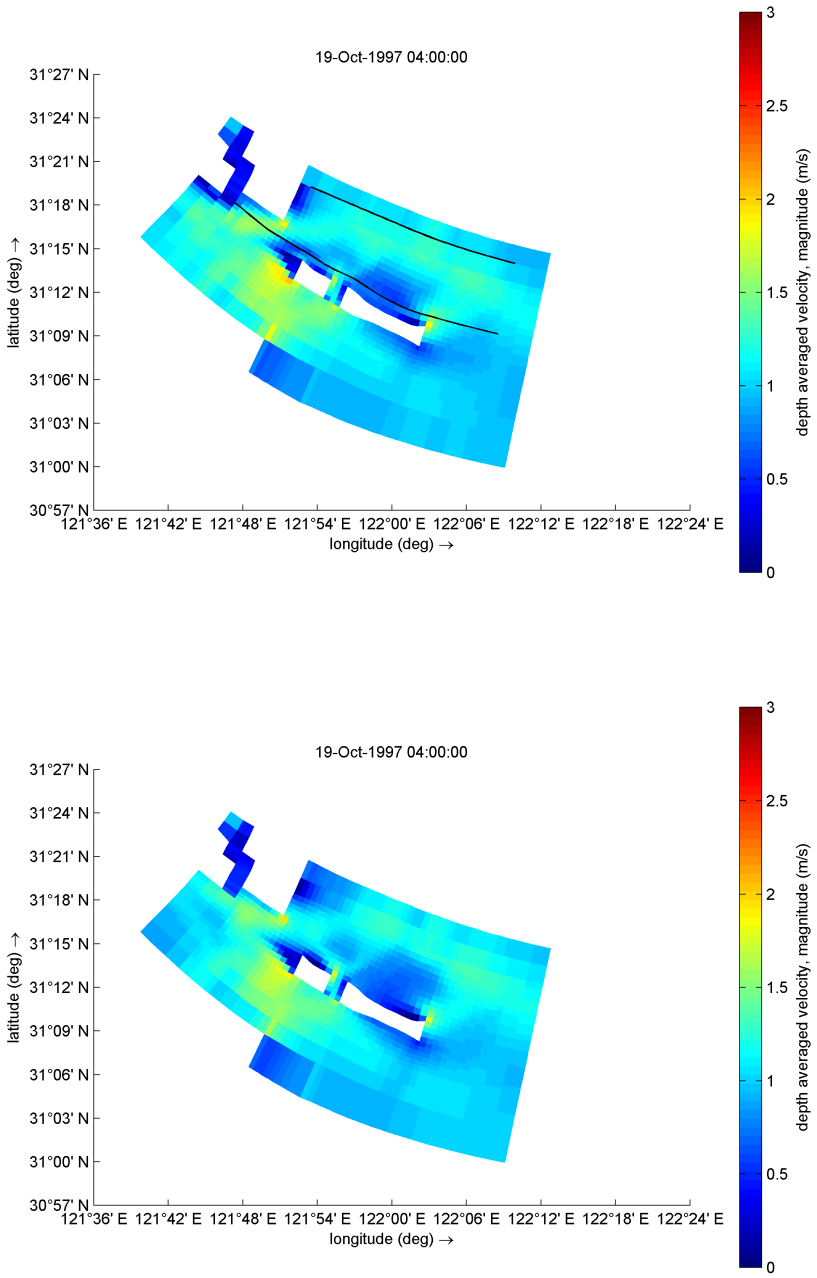

(c) Water level 2.27m

Figure 34: Depth averaged velocity magnitude in one tide cycle p31(top) and p41(bottom)

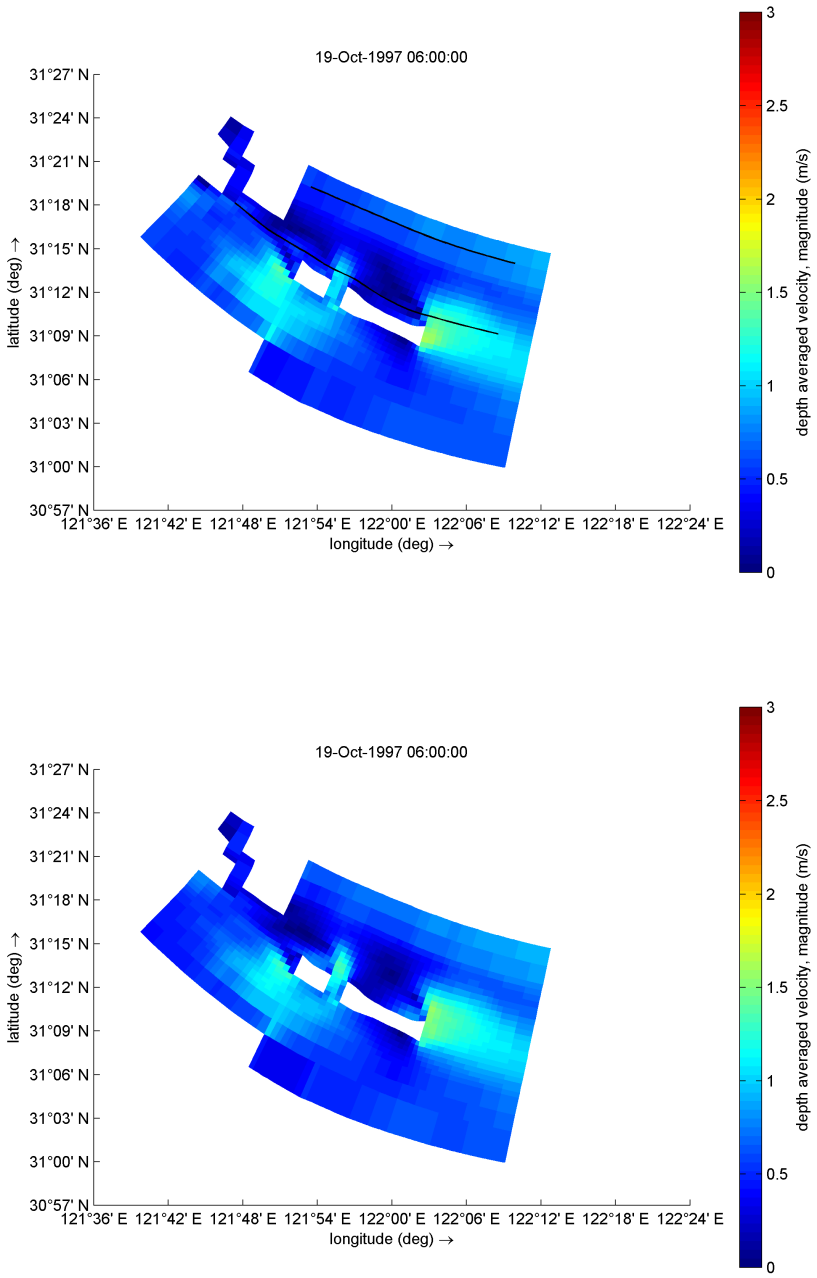

(d) Water level 1.93m

Figure 34: Depth averaged velocity magnitude in one tide cycle p31(top) and p41(bottom)

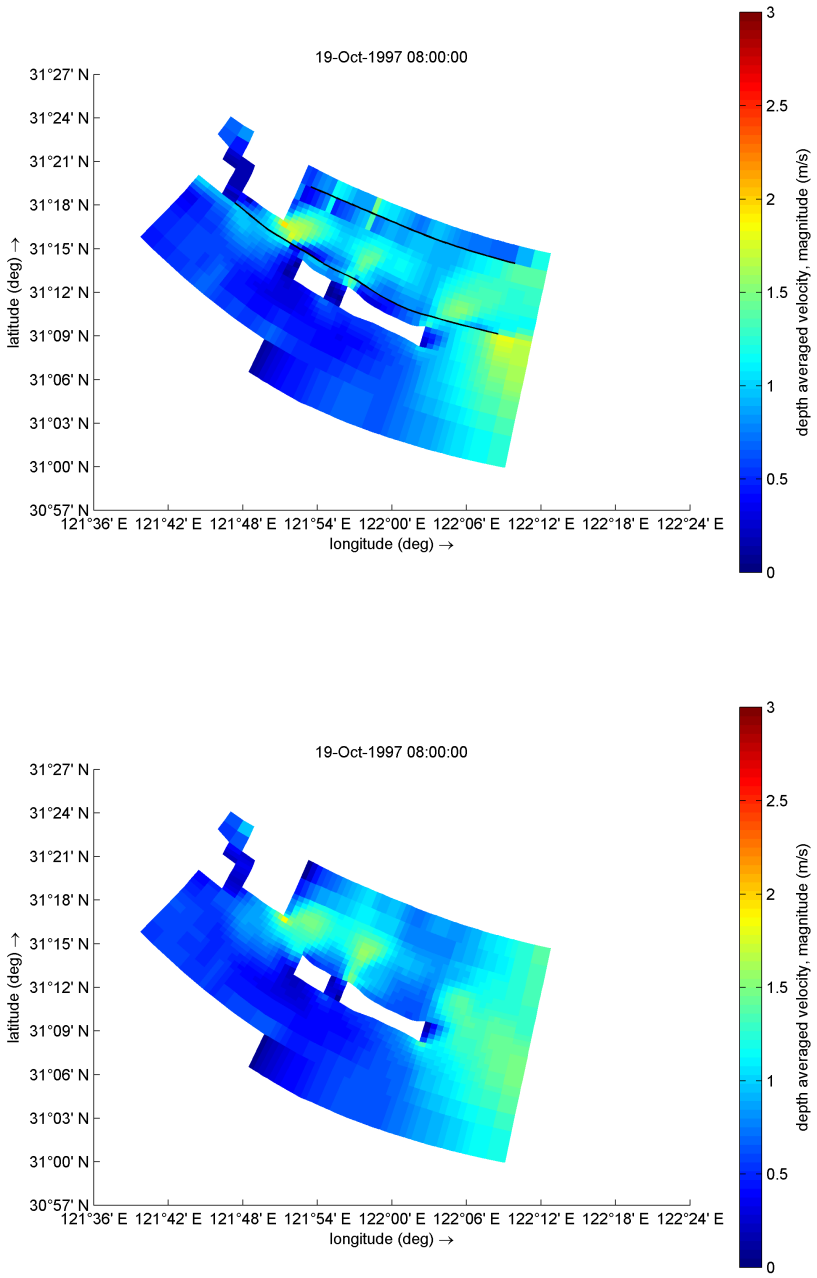

(e) Water level 0.47m

Figure 34: Depth averaged velocity magnitude in one tide cycle p31(top) and p41(bottom)

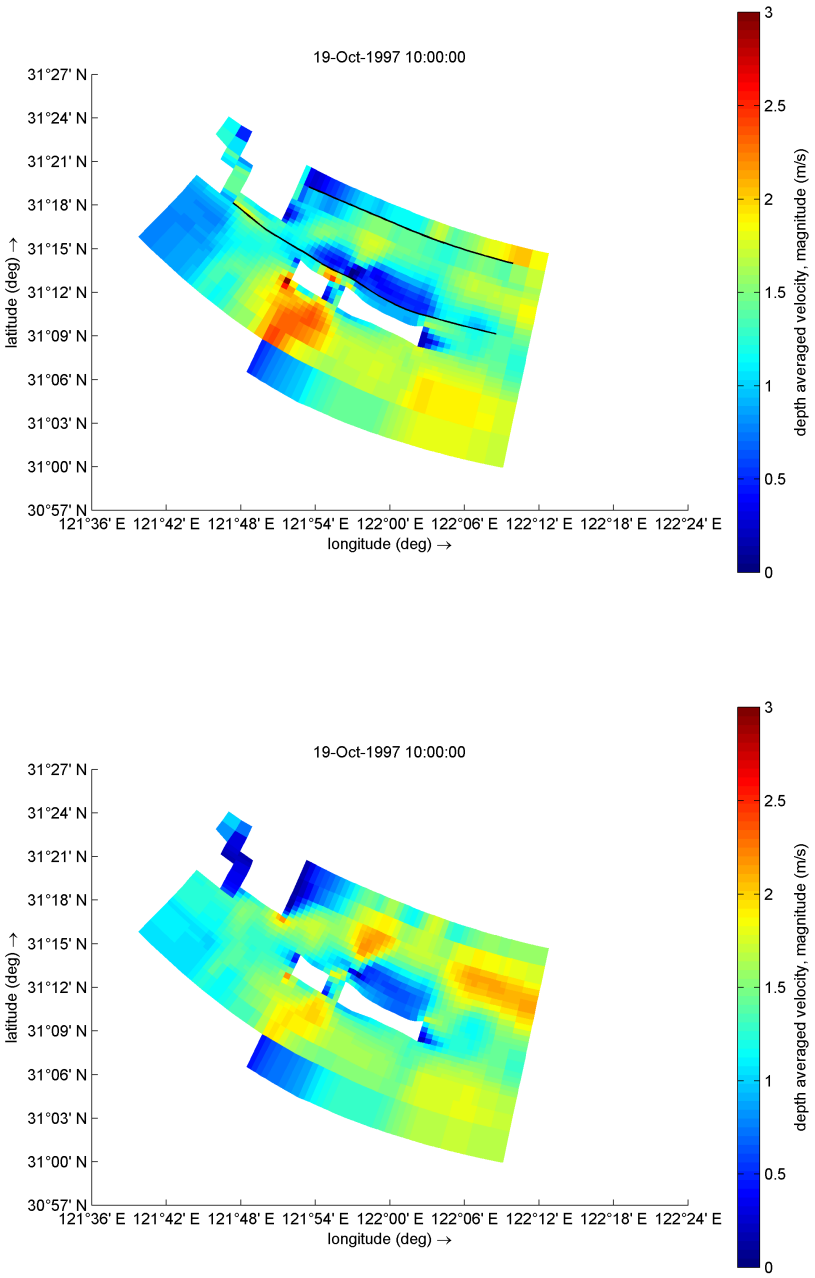

(f) Water level -0.77m

Figure 34: Depth averaged velocity magnitude in one tide cycle p31(top) and p41(bottom)

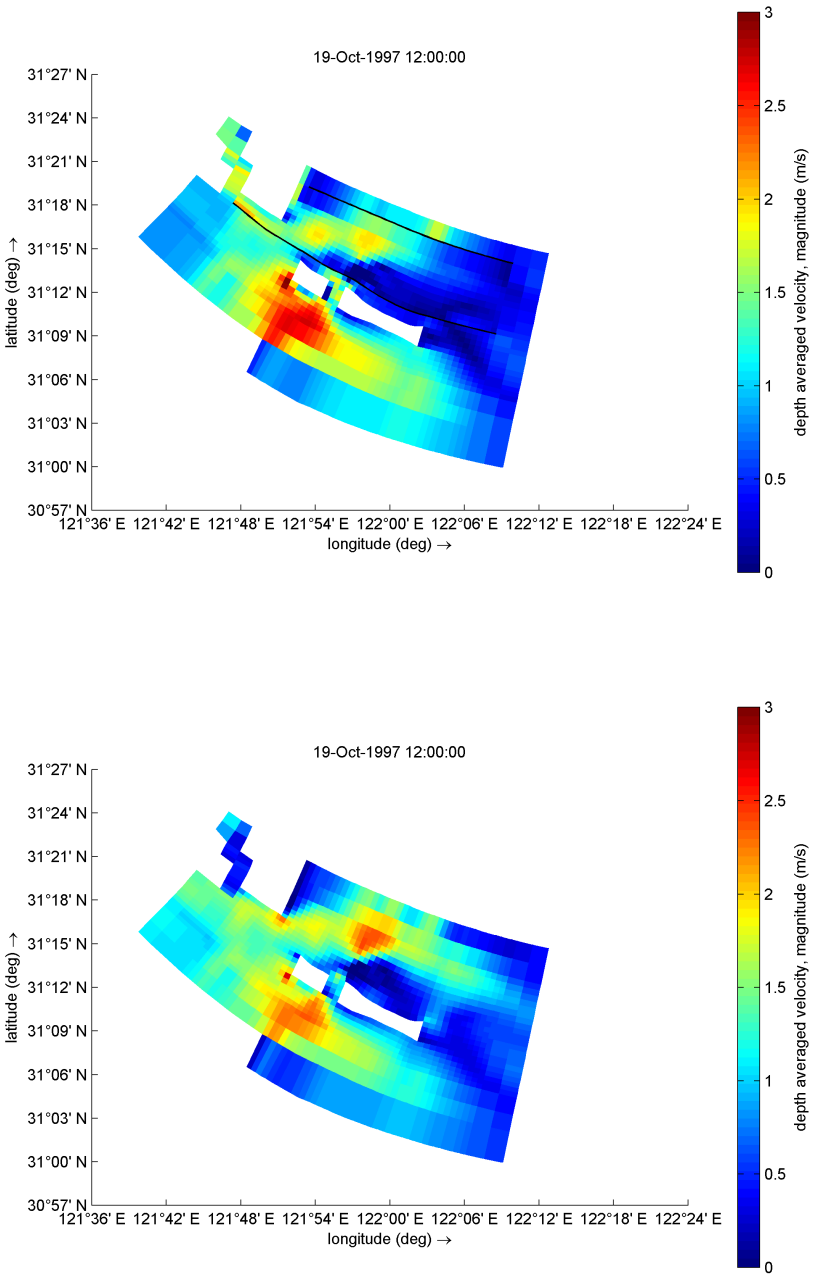

(g) Water level -1.76m

Figure 34: Depth averaged velocity magnitude in one tide cycle p31(top) and p41(bottom)

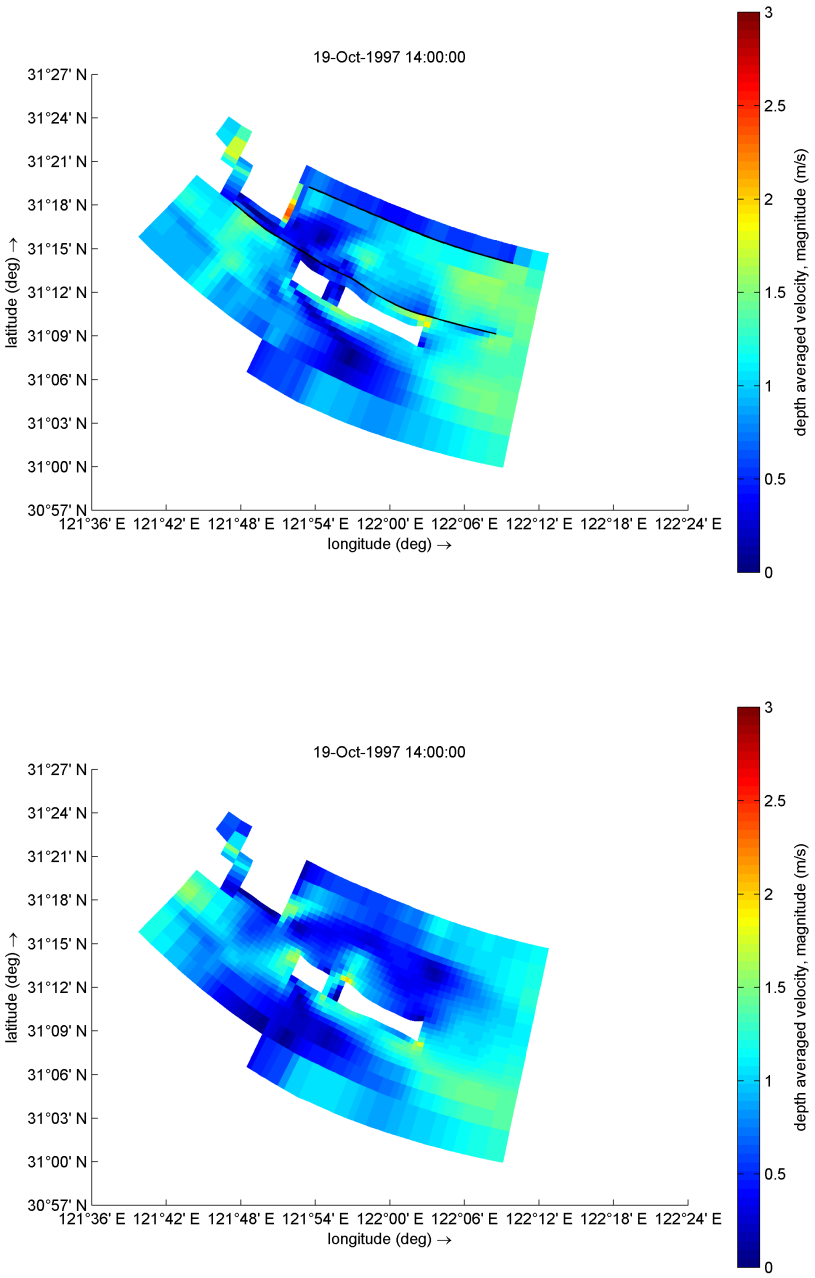

(h) Water level 0.35m

Figure 34: Depth averaged velocity magnitude in one tide cycle p31(top) and p41(bottom)

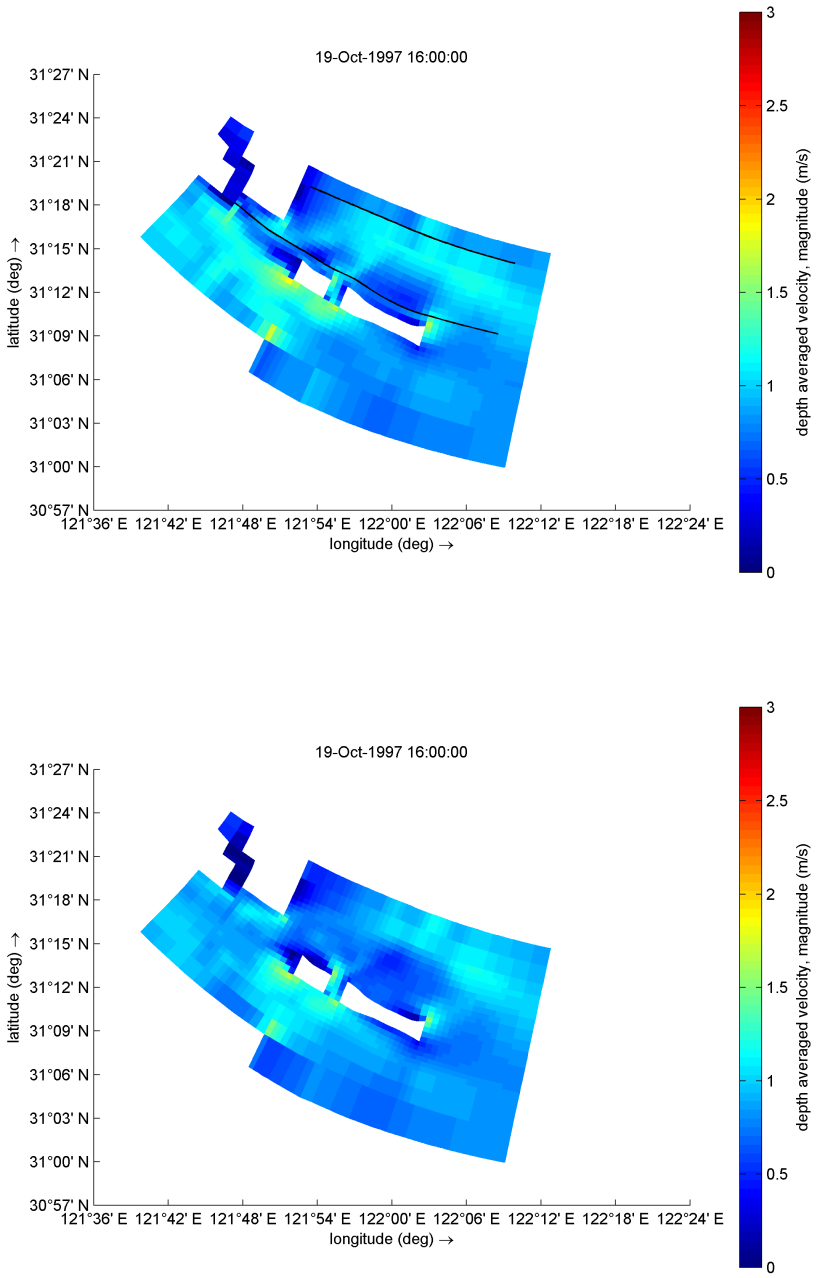

(i) Water level 1.67m

Figure 34: Depth averaged velocity magnitude in one tide cycle p31(top) and p41(bottom)

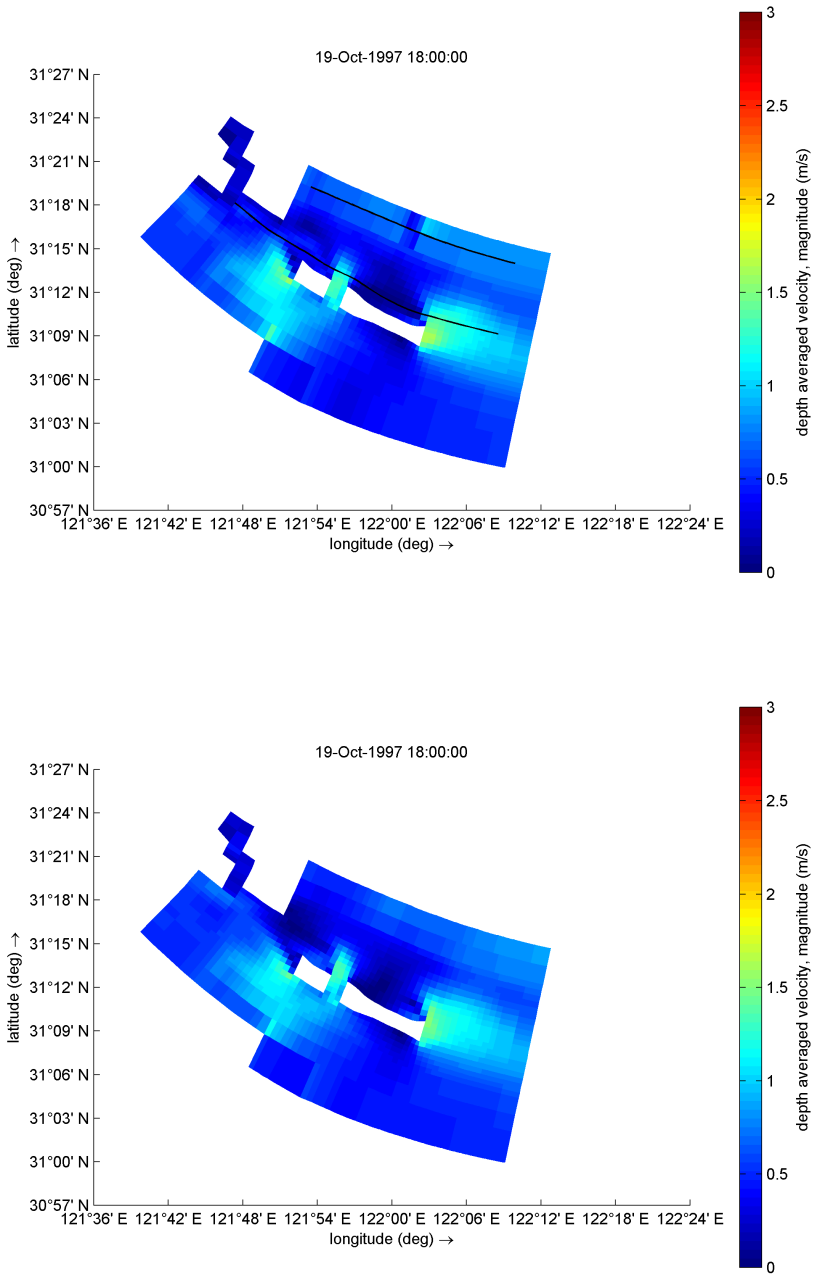

(j) Water level 1.4m

Figure 34: Depth averaged velocity magnitude in one tide cycle p31(top) and p41(bottom)

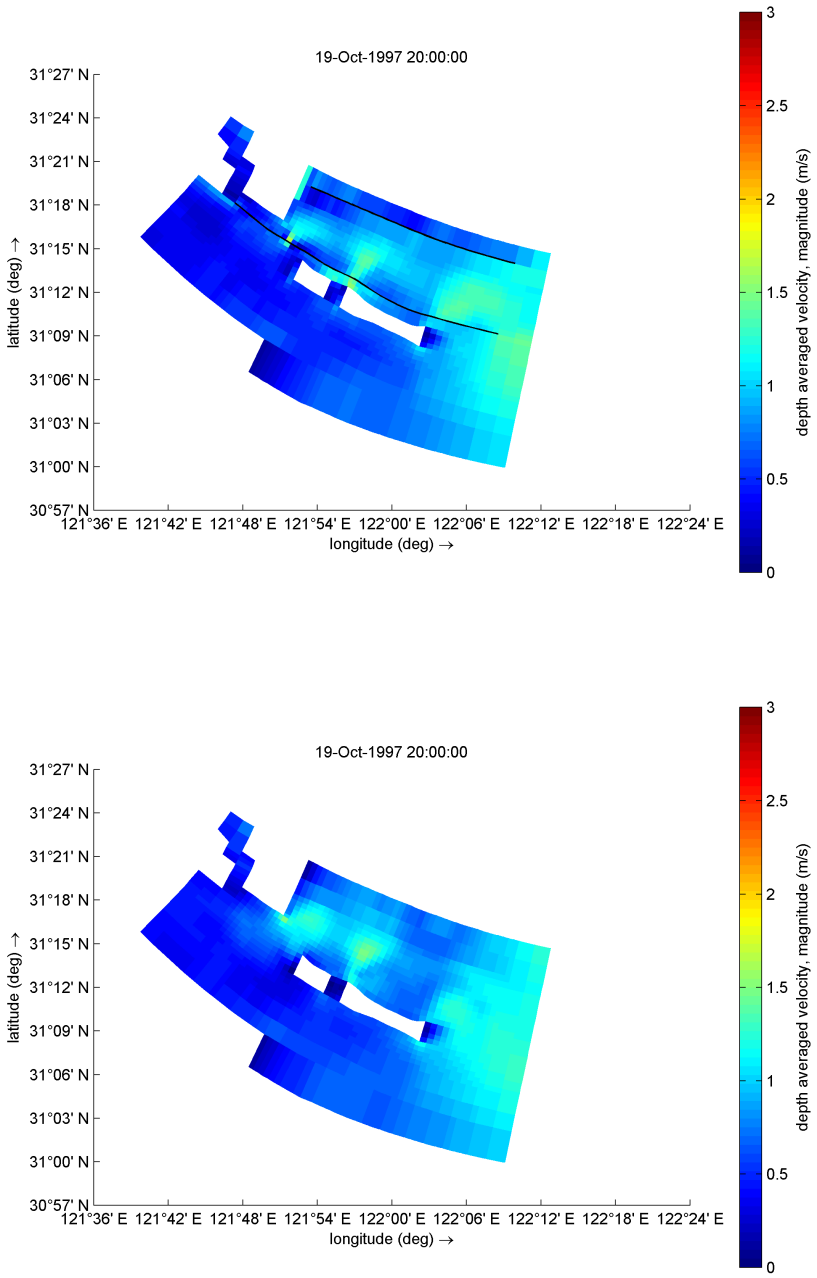

(k) Water level 0.27m

Figure 34: Depth averaged velocity magnitude in one tide cycle p31(top) and p41(bottom)

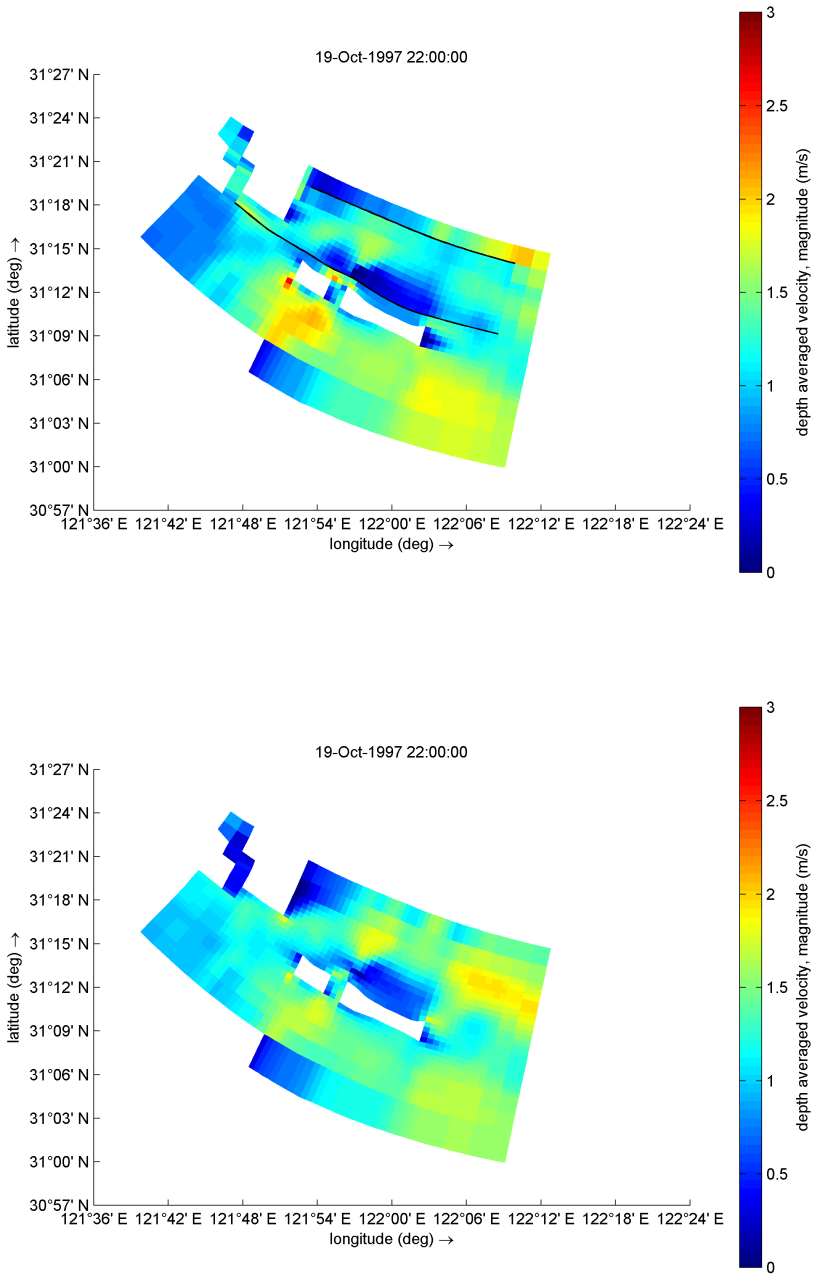

(l) Water level -0.88m

Figure 34: Depth averaged velocity magnitude in one tide cycle p31(top) and p41(bottom)

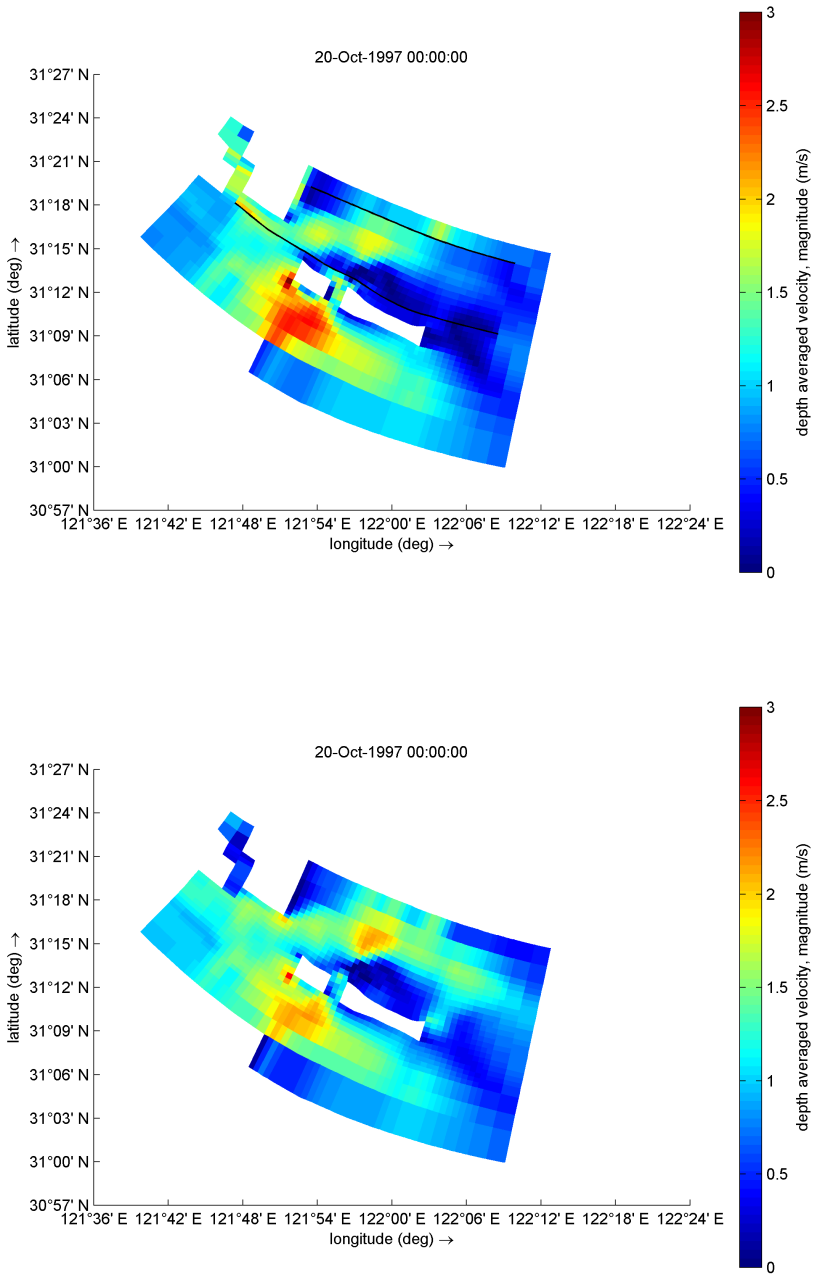

(m) Water level -1.71m

Figure 34: Depth averaged velocity magnitude in one tide cycle p31(top) and p41(bottom)

4.2.5 Daily averaged current velocity in different boxes

Daily averaged current velocity is calculated for each box in Fig.12 to analyze the correlation between morphology changes and hydrodynamic conditions. Fig.35 shows the current conditions inside the channel. It can be seen that the velocity in p41 is always larger than that in p31 especially in the peaks and troughs, which indicates that the jetties will generally slow down the current inside the channel. In Fig.36, the circumstance is reversed and the velocity in p41 becomes smaller than that in p31, but the magnitude of the differences is smaller than that in Fig.35. Fig.37 and Fig.38 illustrate the current situation in box3 and box4. Similar to Fig.35 and Fig.36, in Fig.37 the velocity in p41 is larger than that in p31 while in Fig.38 the velocity in p41 is smaller. This confirms that the jetty will reduce the surrounding current velocity while increasing the current speed in the neighboring region (box2 and box4). The velocity upstream to the river mouth is shown in Fig.39. Except for the peaks, the velocity of p31 and p41 are very close to each other.

These phenomena correspond to the results in Fig.26-Fig.30. When current velocity increases, the sediment mass per area will decrease indicating more erosion will happen.

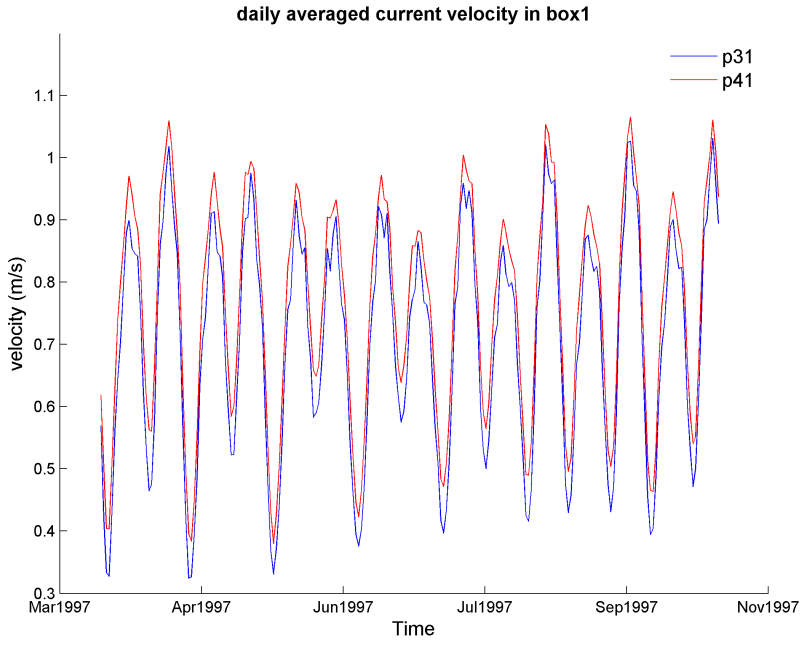

Figure 35: Daily averaged current velocity in box1

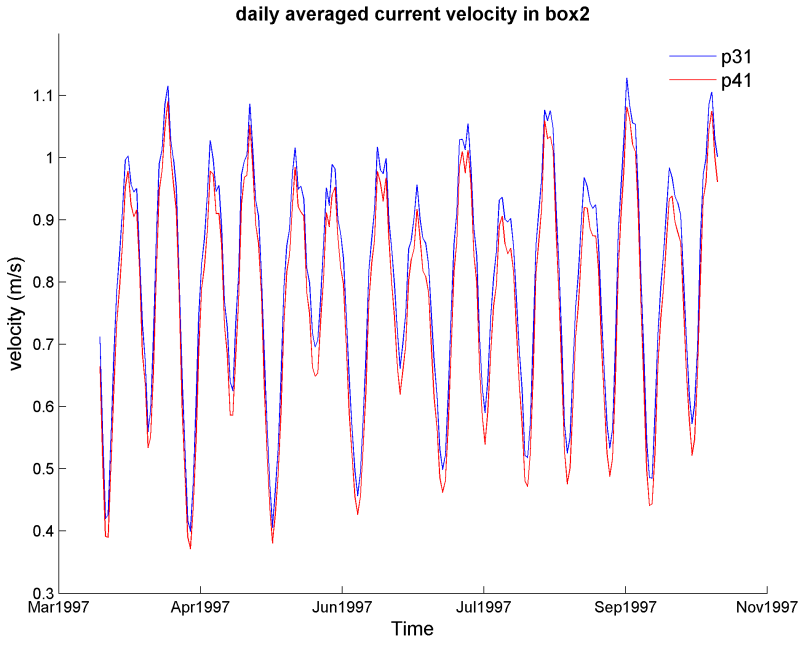

Figure 36: Daily averaged current velocity in box2

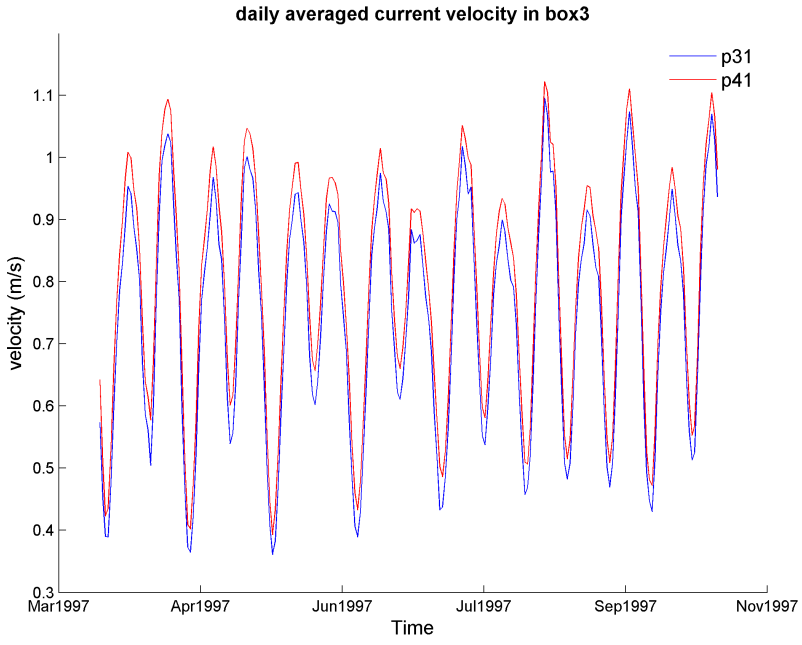

Figure 37: Daily averaged current velocity in box3

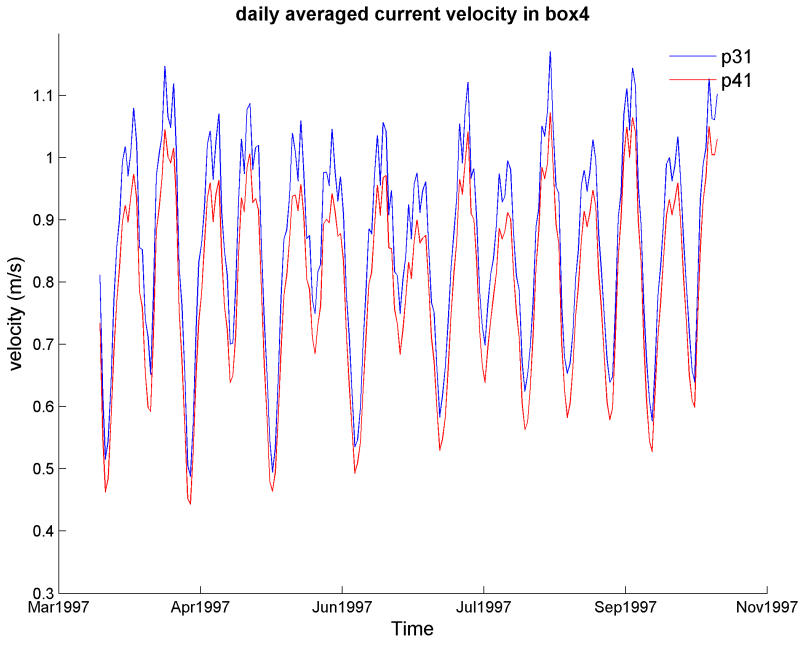

Figure 38: Daily averaged current velocity in box4

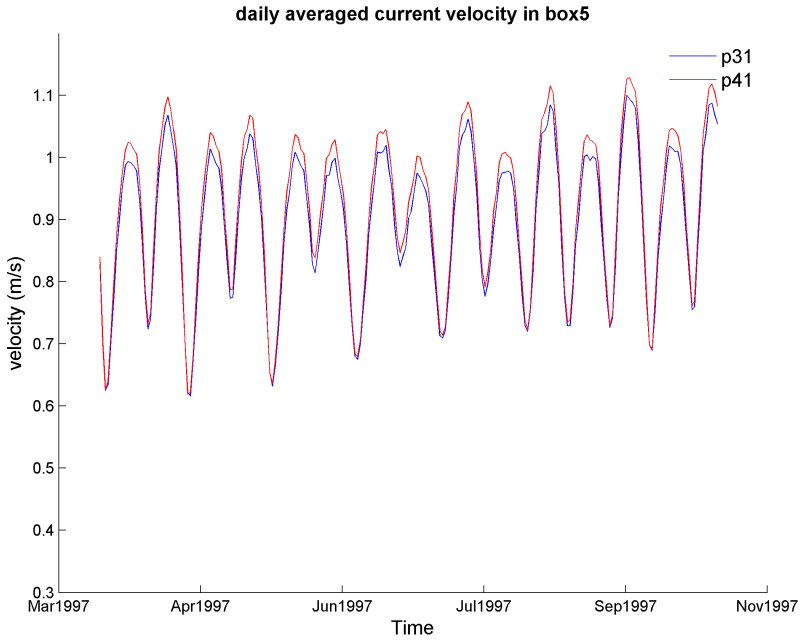

Figure 39: Daily averaged current velocity in box5

4.3 Long term trend and Prediction

To investigate the long term impact of TGD on Yangtze Estuary's morphology, results from cases p51, p52 and p53 (Table.3) are used to make the comparisons. In these cases, jetties are always included since after 2004 the jetties have already be completed and the purpose is to analyze the influence of reduced sediment flux upstream. Another point to be noticed here is that the initial condition of p5 is the same as p3, so p3 actually is part of p5 with shorter simulation time period. As a result, it is possible to compare short term and long long term effects using p3 and p5.

4.3.1 Cumulative erosion/sedimentation map

Fig.40 shows the long term erosion and sedimentation changes around Jiuduansha Island. Similar to the results in 4.1.1, distribution of erosion or sedimentation is still the same among p51, p52 and p53, but the amount differences are much larger for the long term simulation. More quantified details will be discussed in section 4.3.2 and section 4.3.3.

4.3.2 Sediment mass per area in given boxes

Fig.41-Fig.45 show the sediment mass per area results in each box (same box location for p3 and p4 shown in Fig.12) for p5 and the change values of sediment mass per area between initial condition to the end are listed in Table.6. In Fig.41, all three cases indicate increasing sediment mass per area, but for p53 (75 Mt/yr) this accretion is very small and add only 46 kg/m^2(Table.6) which is even smaller than the value 68 kg/m^2 in p33 (Table.4), while for p51 and p52 they are much larger than p31 and p32. This may due to the reason that 75 Mt/yr sediment flux rate is the flux will keep box1 area in a balanced state of sediment erosion and deposition. In Fig.42, all three cases show reduction in sediment mass per area, but for p51 and p52 the trend shows an increase after Feb 1998. In Fig.43, p52 (150 Mt/yr) is close to the sediment flux to keep the balanced state in box3 area which only increases 20 kg/m^2(Table.6), while p51 shows obvious increase and p53 indicates deduction. The location of box4 and box5 are more upstream and it can be seen from Fig.44 and Fig.45 that linear changes are the characteristics of these lines especially in Fig.45 which includes the sediment source boundary upstream.

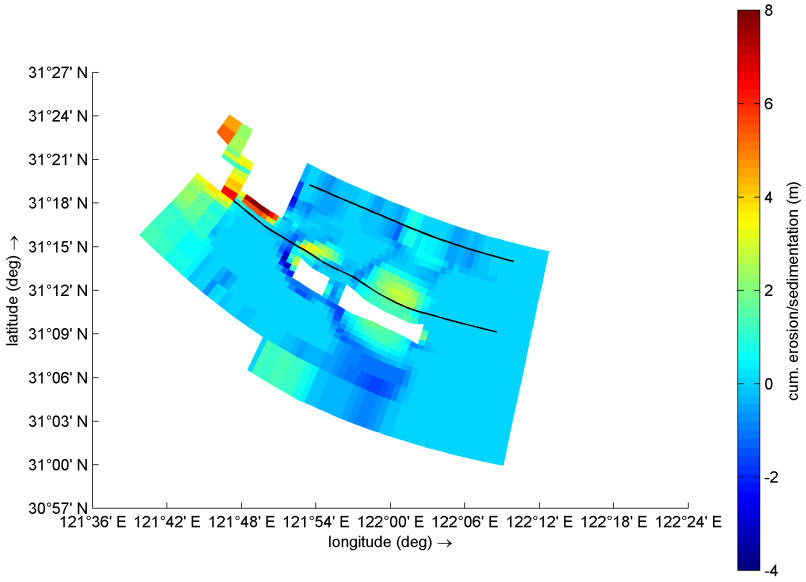

(a)

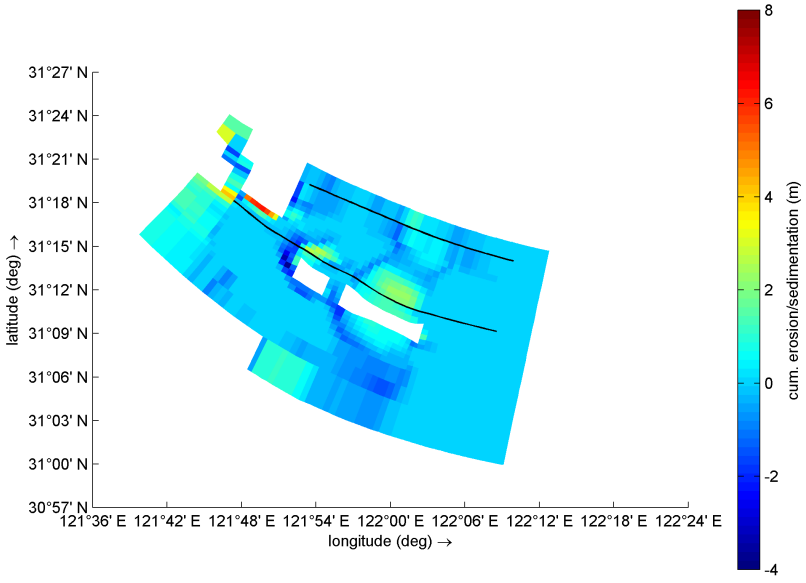

(b)

Figure 40: Cumulative erosion/sedimentation map for p7

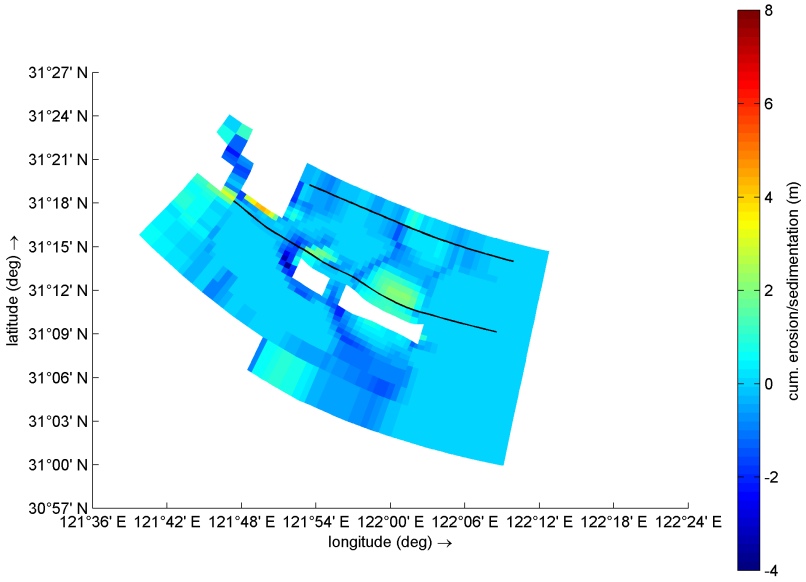

(c)

Figure 40: Cumulative erosion/sedimentation map for p7

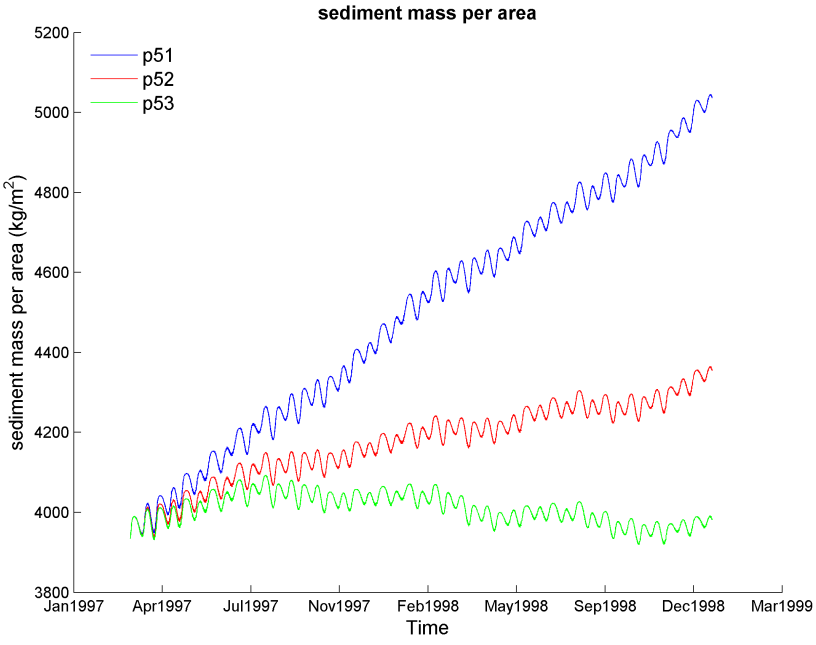

Figure 41: Sediment mass per area in box1 for p5

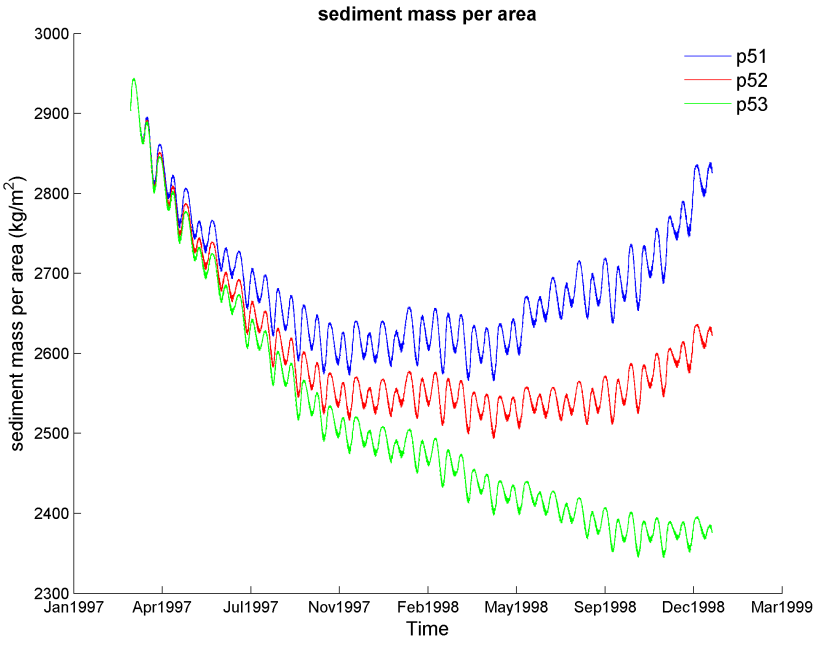

Figure 42: Sediment mass per area in box2 for p5

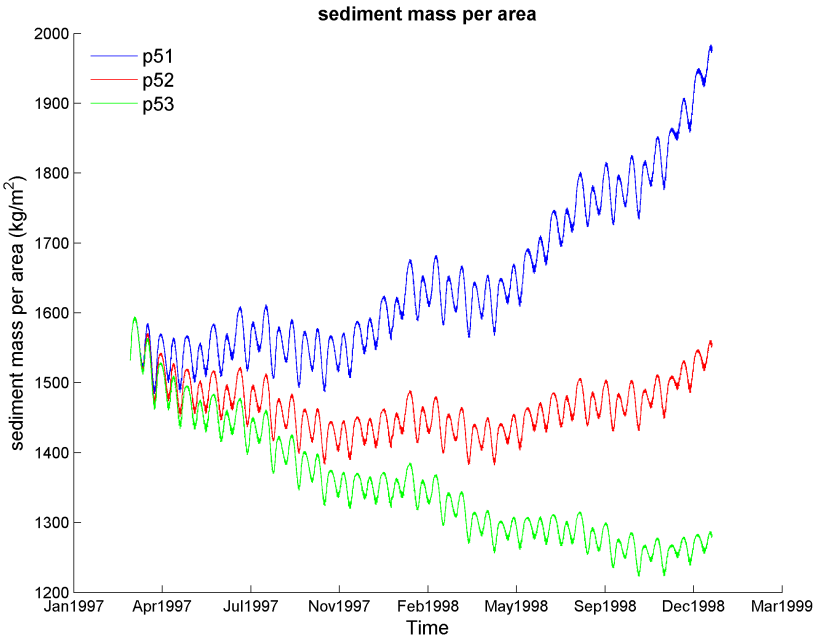

Figure 43: Sediment mass per area in box3 for p5

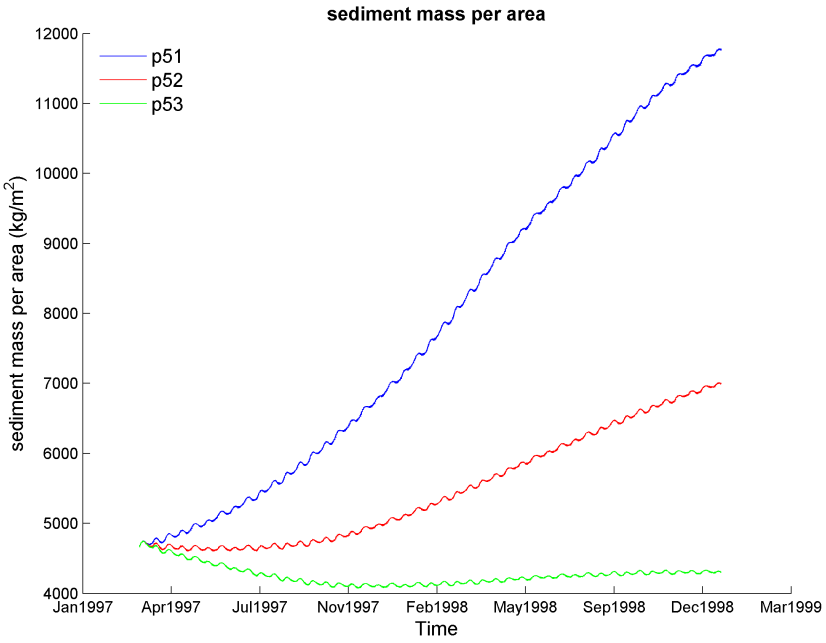

Figure 44: Sediment mass per area in box4 for p5

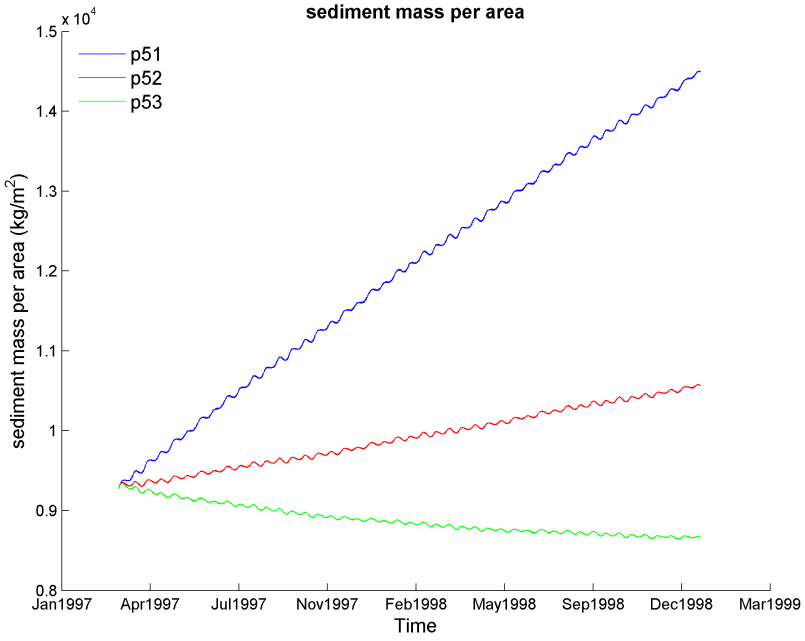

Figure 45: Sediment mass per area in box5 for p5

Table 6: Change values of sediment mass per area for p5

	p51 (kg/m^2)	p52 (kg/m^2)	p53 (kg/m^2)
box1	1101	420	46
box2	-81	-284	-530
box3	442	20	-252
box4	7092	2321	-374
box5	5218	1289	-613

4.3.3 1-D transect profile

Differences between p3 and p5 in 1-D transect profile can also be observed. The influences of two jetties in p3 (Fig.32 left panel) are reduced over time in p5 (46). For example, along transect m095N, in p3 (Fig.24a left panel) there is deposition near the location of jetties, but in p5 (Fig.46a) these deposition gets eroded and the general profile shape is more similar to p4 (Fig.24a right panel). Along transect m105N, the situation is similar, and the three lines near south jetty in 46b is more separated than p3 in Fig.24b (left panel) due to the long term flux differences. Along transect m115N (Fig.46c), more sediment deposited in 2-4 km region and more erosion occurred in 7-9 km region than the case in p3 (Fig.24c left panel). For transect m125N and m135N the profiles are also as stable as the cases in p3 and p4.

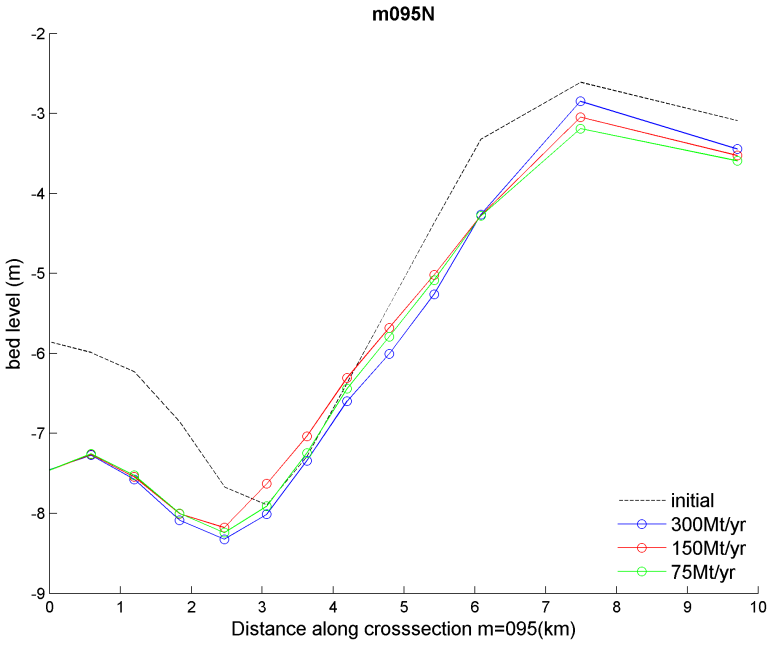

(a)

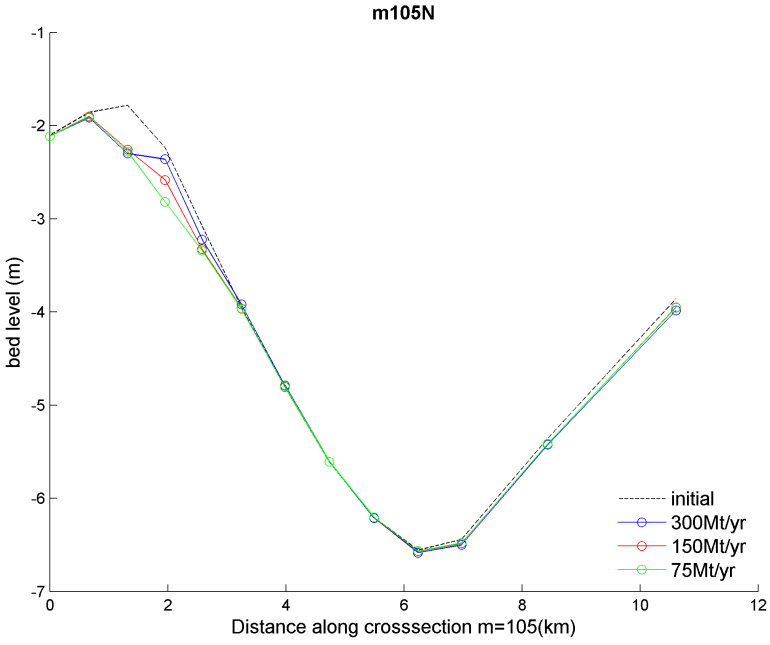

(b)

Figure 46: 1-D transect profile across the channel for p7

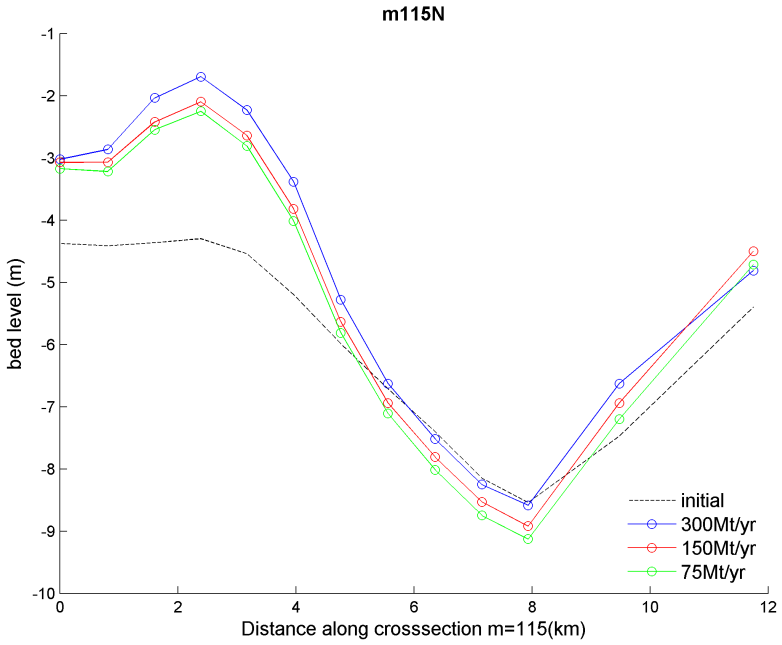

(c)

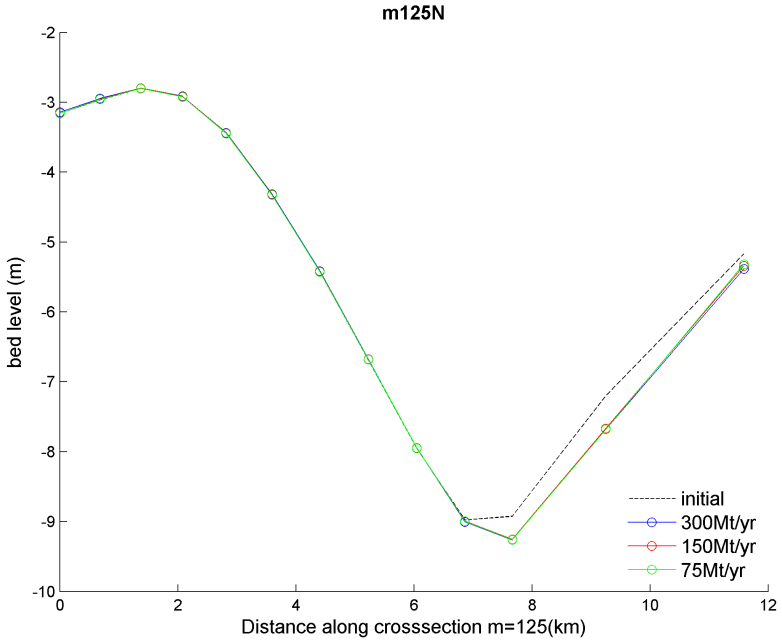

(d)

Figure 46: 1-D transect profile across the channel for p7

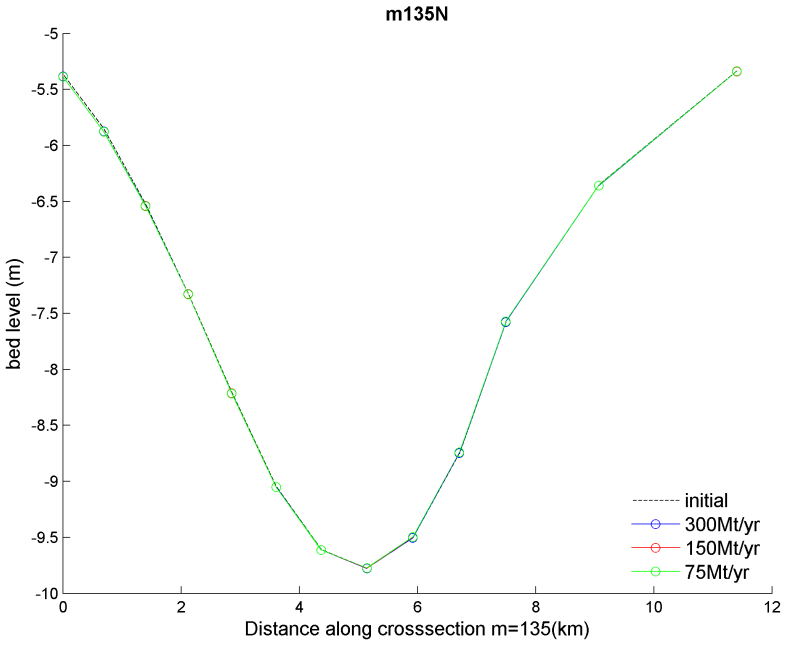

(e)

Figure 46: 1-D transect profile across the channel for p7

4.3.4 Monthly averaged current velocity

Monthly averaged current velocity is calculated for each box in Fig.47. Magnitude of the current velocity has the sequence that box5 $>$ box4 $>$ box2 $>$ box3 $>$ box1. This hydrodynamic differences is also reflected in the sediment transport. Box1, box2 and box3 are three regions in the estuary area, and from Fig.41, Fig.42 and Fig.43, sediment mass per area decreases in box2 for three cases, increases in box1 and box3 is in between. For box4 and box5, since they are close the the sediment flux source, so although the average current velocities are high in these two regions, the influences are less. More discussion about the correlation between hydrodynamic conditions and sediment transport will be shown in Discussion part.

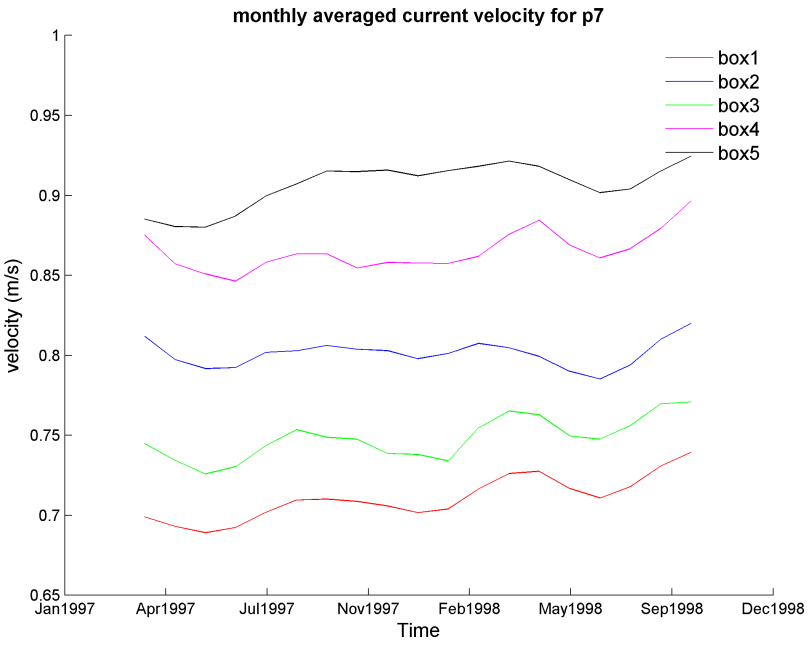

Figure 47: Monthly averaged velocity of 5 boxes in p5

5 DISCUSSION

5.1 DNC effect on current

In Fig.34, it compares the velocity magnitude between p31 and p41 in a tide cycle. It is worth noting that when the tide is low (below 0m MSL) in Fig.34a, Fig.34f,Fig.34g, Fig.34l, and Fig.34m, first, during these low tide cases, the flow velocity is usually higher than the other cases, which is caused by the large amount of water flux from the river. Due to the jetty's existence, the current pattern is changed both inside the channel and surrounding area. With the jetty, the velocity magnitude becomes smaller inside the channel. While south the the channel, the velocity is increased with the jetty. Due to low tide, less water exchange between the channel and surrounding area.

5.2 Sediment carrying capacity and the erosion/sedimentation pattern

The sediment capacity is the total amount of sediment the flow is able to transport. In Fig.12, five boxes are defined and the flow in each box has its sediment carrying capacity which can explain the erosion or deposition pattern in each box.

In section 4.2.2 and section 4.2.4, comparison between p31 and p41 are made for sediment mass per area and current velocity respectively to analyze the effect of jetties. Here, sediment carrying capacity is used to link sediment transport and current together. Due to the existence of jetties (from p41 to p31), the current velocity increased in box2 (Fig.36) and box4 (Fig.38), which means the sediment carrying capacity is also increased and more sediment will be transported. This agrees with the sediment mass per area changes in box2 (Fig.27) and box4 (Fig.29). In box2, the sediment mass per area decreases for p31 while it increases for p41, which means more sediment is eroded in p31 than p41. In box4, the sediment mass per area increases in both p31 sand p41, but in p31 the increasing rate is smaller than that in p41 which also corresponds to the higher sediment carrying capacity for p31. The other boxes such as box1 and box3 also have the same correlations that higher current velocity will have higher sediment carrying capacity and will cause more erosion or less sedimentation. The only exception is in box5. Both current velocity (Fig.39) and sediment mass per area changes (Fig.30) in box5 are very close to each other for p31 and p41. For current velocity in box5, because the location of box5 is far away from jetties comparing with other boxes, the velocity in p31 and p41 are similar to each other. For the sediment mass per area changes, the differences between p31 and p41 are also very small and the reason is that the current velocity in p31 and p41 are similar, so the sediment carrying capacity are similar.

For p5, monthly averaged velocity are calculated to evaluate the long term sediment carrying capacity (Fig.47). For the boxes in the estuary area, the sequence of sediment carrying capacity is box2 $>$ box3 $>$ box1. In Table.6, it can be seen that the change values of sediment mass per area agree with the sediment carrying capacity for the three boxes. Box1 has the lowest sediment carrying capacity, and for all the cases, p51, p52 and p53, the change values are positive. For p53 the sediment mass change is 46 kg/m^2(Table.6) which means 75 Mt/yr is close to the flux value for box1 to balance the erosion and deposition (Fig.41). Box2 has the highest sediment carrying capacity among these three boxes, and for all the cases, the change values are all negative. Even for p51 before TGD was built, the sediment mass change is -81 kg/m^2(Table.6) , which means the flux rate of 300 Mt/yr does not balance the sediment eroded for box2 and the sediment deficit in box2 can also be seen in Fig.42 where all three lines show decreasing trend. Sediment carrying capacity in box3 is between that in box2 and box1, which is also confirmed by the change values of sediment mass per area in Table.6. For p51, the sediment mass per area is increased by 442 kg/m^2. For p52, the sediment mass change is 20 kg/m^2 which is approximately a balanced value for sediment erosion and deposition. For p53, the sediment mass per area is decreased by 252 kg/m^2. So for box3, sediment flux of 150 Mt/yr will make the sediment transport balanced between erosion and deposition, while 300 Mt/yr and 75 Mt/yr will have obvious deposition and erosion respectively. This phenomena are also shown in Fig.43 where p51 has the increasing trend, p52 has the changeless trend and p53 has the decreasing trend. From the above, if sediment flux upstream reduce to 75 Mt/yr in the future, among box1, box2 and box3, box2 and box3 will experience severe erosion especially in box2, while in box1 sediment erosion and deposition can still maintain an balanced state.

From Table.4 and Table.5, when comparing the values for box1, box2 and box3, it can be observed that the erosion and sedimentation pattern has been changed due to the existence of jetties. For box1, in p4 the values in Table.5 are all negative which means erosion dominates in box1 without the jetty, while in p3 the values for box1 in Table.4 are all positive which means sedimentation dominates in box1. However, the case for box2 is just the reverse of box1. In p4 the values in Table.5 has positive (p41) and negative (p42 and p43) numbers, while in p3 the values in Table.4 are all negative which means erosion dominates in box2. For box3, in p4 the values in Table.5 are all negative, and in p3 the values in Table.4 are also all negative but the magnitude are much smaller than those in p4 which means less sediment were eroded in p3. So after the jetties was built, it triggered a new pattern of sediment transport in the local area. Much more sediment were deposited in box1 and less sediment were eroded in box3, while more sediment were eroded in box2. From the long-term view in Table.6, the influence of jetties in DNC project can still be seen there but it is

weakened by the continuous sediment flux from upstream. For example, in Fig.42, for sediment flux of 300 Mt/yr and 150 Mt/yr, the lines show incline trends after May 1998. This is different from the short term characteristics that in Fig.14 those two lines show decline trends. To sum up, the jetties built in DNC project will change the local sediment transport instantly and is the main determinant on morphology changes in the short term. In the long term, because of the continuous sediment flux from upstream, the impact from the jetties will be cut down, but the circumstance cannot go back as there was no jetties.

5.3 Long term morphology evolution in Yangtze River Estuary

From Fig.3, it can be seen that sediment flux at Datong station will be reduced below 100 Mt/yr. In the simulation cases, 75 Mt/yr are used to predict the future situation. When setting the sediment flux as 75 Mt/yr, sediment mass per area decreases in all the boxes except box1 (Table.6). Even for box1, the sediment mass per area is increased during the beginning period of p5 due to the construction of jetties, but as time progresses, the sediment mass per area is also decreased (Fig.41). As a result, Yangtze River Estuary will experience sediment starvation in the future, although there is a large number of sediment inside the Yangtze River Estuary itself (van Maren et al., 2013). Local sediment is transported between tidal flats and channels, and this is also can be observed in the simulation such as the sediment exchanges among box1, box2 and box3. Due to the existence of jetties in the estuary area, there will be more sediment trapped inside the deep water navigation channel and around the two jetties, while in the adjacent places there will be more erosion which indicates the sediment is transported in to the DNC project area. Overall, long term sediment shortage in the future together with human induced local sediment transport will switch most of the estuarine area into an erosion mode. More erosion will occur on the tidal flat and sub-aqueous delta, and shoreline of islands and tidal flats will be recessed.

6 CONCLUSION

In order to quantify the influences of two major human projects TGD and DNC, a Delft3D flow model including morphology changes has been set up. The model successfully simulates hydrodynamic condition and sediment transport in Yangtze River Estuary, and several cases are conducted to understand how TGD and DNC affect the hydrodynamic and morphological conditions in this area.

Jetties built in the DNC project will slow down the current velocity inside the deep navigation channel and will induce new pattern of local sediment transport causing more sediment deposition inside the channel. In the future, due to the completion of the TGD, the sediment flux from Yangtze River will be lower than 100 Mt/yr. From the simulation results, the reduced sediment flux will decrease the available sediment mass on the bed of Yangtze River Estuary and lead to coastline erosion of the islands and shoals in Yangtze River Estuary.

7 REFERENCES

Blumberg, A. F. and G. L. Mellor (2013). A description of a three-dimensional coastal ocean circulation model. *American Geophysical Union*, 1–16.

Booij, N., L. Holthuijsen, and R. Ris (2001). The "SWAN" wave model for shallow water. *Coastal Engineering Proceedings* (25).

Bouma, T. J., L. A. van Duren, S. Temmerman, T. Claverie, A. Blanco-Garcia, T. Ysebaert, and P. M. J. Herman (2007). Spatial flow and sedimentation patterns within patches of epibenthic structures: Combining field, flume and modelling experiments. *Continental Shelf Research 27*(8), 1020–1045.

Chen, C., H. Liu, and R. C. Beardsley (2003). An unstructured grid, finite-volume, three-dimensional, primitive equations ocean model: Application to coastal ocean and estuaries. *Journal of Atmospheric and Oceanic Technology 20*(1), 159–186.

Chen, J., H. Shen, and C. Yu (1988). *Processes of dynamics and geomorphology of the Changjiang Estuary*. Shanghai: Shanghai Scientific and Technical Publishers.

Chen, Z., J. Li, H. Shen, and W. Zhanghua (2001). Yangtze River of China: historical analysis of discharge variability and sediment flux. *Geomorphology 41*(2-3), 77–91.

Chen, Z. and D. J. Stanley (1993). Yangtze Delta, Eastern China: 2. Late Quaternary subsidence and deformation. *Marine Geology 112*(1), 13–21.

Delft3D-FLOW-Manual (2014). Delft3d flow user manual.

Edmonds, D. A. and R. L. Slingerland (2010). Significant effect of sediment cohesion on delta morphology. *Nature Geoscience 3*(2), 105–109.

Fan, D. D., Y. X. Guo, P. Wang, and J. Z. Shi (2006). Cross-shore variations in morphodynamic processes of an open-coast mudflat in the Changjiang Delta, China: With an emphasis on storm impacts. *Continental Shelf Research 26*(4), 517–538.

Galloway, W. E. (1975). Process framework for describing the morphologic and stratigraphic evolution of deltaic depositional systems. *Deltas, Models for Exploration: Houston Geological Society,Houston,Texas*, 87–98.

Gao, S., Y. P. Wang, and J. H. Gao (2011). Sediment retention at the Changjiang sub-aqueous delta over a 57 year period, in response to catchment changes. *Estuarine Coastal and Shelf Science 95*(1), 29–38.

Hu, K., P. Ding, Z. Wang, and S. Yang (2009). A 2D/3D hydrodynamic and sediment transport model for the Yangtze Estuary, China. *Journal of Marine Systems 77*(1-2), 114–136.

Jiang, C. J., J. F. Li, and H. E. de Swart (2012). Effects of navigational works on morphological changes in the bar area of the Yangtze Estuary. *Geomorphology 139*, 205–219.

Lesser, G. R., J. A. Roelvink, J. van Kester, and G. S. Stelling (2004). Development and validation of a three-dimensional morphological model. *Coastal Engineering 51*(8-9), 883–915.

Liu, G., J. Zhu, Y. Wang, H. Wu, and J. Wu (2011). Tripod measured residual currents and sediment flux: Impacts on the silting of the Deepwater Navigation Channel in the Changjiang Estuary. *Estuarine, Coastal and Shelf Science 93*(3), 192–201.

Milliman, J. D. and K. L. Farnsworth. (2010). River discharge to the coastal ocean. *Cambridge University Press,Cambridge,UK*, 384.

Milliman, J. D. and R. H. Meade (1983). World-wide delivery of river sediment to the oceans. *The Journal of Geology 91*(1), 1–21.

Shchepetkin, A. F. and J. C. McWilliams (2005). The regional oceanic modeling system (roms): a split-explicit, free-surface, topography-following-coordinate oceanic model. *Ocean Modelling 9*(4), 347–404.

Shen, F., Y. Zhou, J. Li, Q. He, and W. Verhoef (2013). Remotely sensed variability of the suspended sediment concentration and its response to decreased river discharge in the Yangtze estuary and adjacent coast. *Continental Shelf Research 69*(0), 52–61.

Song, D. H., X. H. Wang, Z. Y. Cao, and W. B. Guan (2013). Suspended sediment transport in the deepwater navigation channel, yangtze river estuary, china, in the dry season 2009:1. observations over spring and neap tidal cycles. *Journal of Geophysical Research-Oceans 118*(10), 5555–5567.

Syvitski, J. P. M. and Y. Saito (2007). Morphodynamics of deltas under the influence of humans. *Global and Planetary Change 57*(3-4), 261–282.

van Dongeren, A., N. Plant, A. Cohen, D. Roelvink, M. C. Haller, and P. A. Catalan (2008). Beach wizard: Nearshore bathymetry estimation through assimilation of model computations and remote observations. *Coastal Engineering 55*(12), 1016–1027.

van Maren, D., S.-L. Yang, and Q. He (2013). The impact of silt trapping in large reservoirs on downstream morphology: the Yangtze River. *Ocean Dynamics 63*(6), 691–707.

Wright, L. D. and J. M. Coleman (1973). Variations in morphology of major river deltas as functions of ocean wave and river discharge regimes. *American Association of Petroleum Geologists Bulletin 57*(2), 370–398.

Xie, D., Z. Wang, S. Gao, and H. J. De Vriend (2009). Modeling the tidal channel morphodynamics in a macro-tidal embayment, Hangzhou Bay, China. *Continental Shelf Research 29*(15), 1757–1767.

Xu, K. and J. D. Milliman (2009). Seasonal variations of sediment discharge from the Yangtze River before and after impoundment of the Three Gorges Dam. *Geomorphology 104*(3-4), 276–283.

Yang, S.-L., D. Eisma, and P.-X. Ding (2000). Sedimentary processes on an estuarine marsh island within the turbidity maximum zone of the Yangtze River mouth. *Geo-Marine Letters 20*(2), 87–92.

Yang, S. L., H. Li, T. Ysebaert, T. J. Bouma, W. X. Zhang, Y. Y. Wang, P. Li, M. Li, and P. X. Ding (2008). Spatial and temporal variations in sediment grain size in tidal wetlands, Yangtze Delta: On the role of physical and biotic controls. *Estuarine, Coastal and Shelf Science 77*(4), 657–671.

Yang, S. L., J. D. Milliman, P. Li, and K. Xu (2011). 50,000 dams later: Erosion of the Yangtze River and its delta. *Global and Planetary Change 75*(1-2), 14–20.

Yang, S. L., J. Zhang, S. B. Dai, M. Li, and X. J. Xu (2007). Effect of deposition and erosion within the main river channel and large lakes on sediment delivery to the estuary of the Yangtze River. *Journal of Geophysical Research: Earth Surface 112*(F2).

Yang, S. L., J. Zhang, and X. J. Xu (2007). Influence of the Three Gorges Dam on downstream delivery of sediment and its environmental implications, Yangtze River. *Geophysical Research Letters 34*(10).

Yang, Z., H. Wang, Y. Saito, J. D. Milliman, K. Xu, S. Qiao, and G. Shi (2006). Dam impacts on the Changjiang (Yangtze) River sediment discharge to the sea: The past 55 years and after the Three Gorges Dam. *Water Resources Research 42*(4).